May 2019

CM Scale Flapping Wing Of Unmanned Aerial Vehicle At Very Low Reynolds Numbers Regime

Abduljaleel Altememe
Clemson University, aalteme@clemson.edu

CM Scale Flapping Wing Of Unmanned Aerial Vehicle At Very Low Reynolds Numbers Regime

---

A Dissertation
Presented to
the Graduate School of
Clemson University

In Partial Fulfillment
of the Requirements for the Degree
Doctor of Philosophy
Mechanical Engineering

---

by
Abduljaleel Altememe
May 2019

Accepted by:
Dr. Oliver J. Myers, Committee Chair
Dr. Richard Miller
Dr. Yue Wang
Dr. Suyi Li

Abstract

This dissertation investigates the CM−SCALE Flapping Wing of Unmanned Aerial Vehicle (FWUAV) that can accommodate nacelles of the scale of current Unmanned Air vehicle (UAV) designs are complex systems and their utilization is still in its infancy.

The improving design of unmanned aerial vehicle from previous teams by improving the wings and outer body of bird. So, to potentially improve wing design, a complaint joint mechanism is proposed in order to make wing flapping and provide lift and thrust needed to fly. Also, change the wing design from flat wing to airplane wing by using two different airfoils, NACA 0012 and s1223. For bird's body change the internal body to ensure to contain all internal components and give more space for flapping wings. Concurrently a redesign of the outer shell by making it smoother and lighter will be commensurate with the updated design. In addition, development of an evaluation methodology for the capability of a flapping wing to replication design loads by using computational fluid dynamic CFD by using fluid structure interaction in 2D and 3D analysis. We will investigate the design and analysis of the flapping wing. Specifically, this includes:

1. Review of cm−Scale Unmanned Aerial Vehicle Model and design
   (a) Investigate flapping Mechanism.
   (b) Investigate gear mechanism.
2. Analysis of flapping wings for MAV
   (a) Select Airfoils for flapping wing.
   (b) Analyze Flapping Wings.
   (c) Make recommendations for Tail design for MAV.
   (d) Make recommendations for the improved design of MAV body.

3. Development of Finite Element flapping wing Model

   (a) 2D computational analysis for Airfoils

      i. NACA0012 Airfoil.

      ii. s1223 Airfoil.

   (b) 3D computational analysis with different shape of wings.

      i. Relationship between critical parameters and performance.

      ii. Design Optimization.

Which is new key to make flapping wing close to the nature or real flapping wing, a new wing design inspired from nature exactly from thrush and scaled to our design. Starting from gear design by choose proper gear system. Then redesign the wings to commensurate with new bird. Computational fluid analysis also will used to replicate the loads needed to fly. This is another important area in which the literature is not offering guidance.

Addresses the lack of an overview paper in the literature that outlines the challenges of testing a full−scale flapping wing Unmanned aerial vehicle onto laminar flow test and suggests research direction to address these challenges. Although conceptual in nature, this contribution is expected to be significant given that it takes experience in the unmanned vehicle industry to determine what challenges matter and need to be addressed. The growth in testing full-scale unmanned air vehicle using a laminar flow test being recent limits the number of people who can offer the perspective needed to suggest a research roadmap.

Dedication

To the memory of my father, who passed away when I was kid.

To my mother Shamsa, my wife Sumaya, my son Ali, my sisters and brothers with all my love and respect.

Acknowledgments

First and foremost, I thank God for his countless blessings, for the favors he bestowed upon me, and for providing me with the strength, patience and enthusiasm to complete this Ph.D. dissertation.

I would like to express my deepest gratitude and respect to my dissertation advisor and chairperson, Dr. Oliver J. Myers, for his continuous guidance and support. I am extremely grateful for the friendship and monitoring relationship we developed during my time in Clemson. I thank him for believing in me and patiently teaching me innumerable lessons related to research and also for encouraging me when my research progress was slow, and for giving me the time and resources I needed . Without his thorough guidance, the completion of this work would not have been possible. I also thank my advising committee members: Dr. Richard Miller, who greatly inspired my work in the area of Computational Fluid Dynamic Analysis (CFD) and Turbulent Flow., In addition, I would like to thank Dr. Yue Wang and Dr. Suyi Li for their great support and enthusiasm about my area of research, especially Micro Aerial Vehicle Design and for their insights and valuable inputs regarding research design. Furthermore, I would like to thank them for the many opportunities provided and their support. Also, for their encouraging and constructive feedback. Special thanks also go to all the professors I have taken courses with: Dr. Richard Figliola, Dr. Yue Wang, Dr. Richard Miller, and Dr. Lonney Thompson.

I would like also to acknowledge the continuous assistance of the departmental staff for their excellent work and endless help during my study. My sincere thanks go to Ms. Gwen Dockins, Mr. Michael Justice, Dr. Joshua Summers, Ms. Poole Kathryn , Mr. Bass Stephen and Ms. Patricia Nigro.

I consider myself very lucky to have been surrounded by Iraqi friends :Firass Aldamouk, Dr. Dhia Saleem, Dr. Mohammed Abdulali, Dr. Luay Aboalarab, Dr. Mostafa Alani, Dr. Haitham

Zeddan, Dr. Saad Hussain, Dr. Wessam Hameed, Dr. Aws Ajaaj, and Dr. Omar Almahmood for bringing in the Iraqi atmosphere abroad and making Clemson feel like home. outstanding colleagues and office-mates. I thank all of them for making my journey as a graduate student a memorable one. Special thanks go to Abdulmunaam Zuhairy, Wessam Zuhairi, Hiyam Zuhairi and Ali Abdulmunaam for their great friendship and endless help and support.

Completion of this work would have been impossible without the encouragement and support of my family. My deepest gratitude goes to my parents. My father, Mr. Hussain Altememe, and my mother, Mrs. Shamsa Yassin, for their endless love, kindness, support, and continuous care. My wife, Dr. Sumaya Alzuhairy, for her limitless aid and encouragement through my graduate studies. My sister, Zainab and Sookut and bothers, Abdulwahid, Abduljabaar, Abdulkareem and Mohammed for their endless love and encouragement.

Table of Contents

List of Tables

List of Figures

Chapter 1

Introduction and Literature Review

1.1 Overview

Air vehicles remotely piloted or having an autopilot are generally defined as unmanned air vehicles (UAV). Unmanned air vehicles (UAVs) can be used both for civilian and military applications. They could have different missions according to their civil or military usage such as ground surveillance, payload or cargo carriers, traffic control, and geological surveying applications. Unmanned air vehicles, UAVs, may be considered as the future of aviation. Technological advances in aviation electronics, avionics, seem to enable the air vehicles to fly themselves with small help of human pilot. Several UAV concepts have emerged and many of them have been made operationally successful.

With the ubiquity of the UAVs, counter measures for the UAVs have been taken. Increased counter measures decreases the effectiveness of the UAVs, preventing the mission from being accomplished. As with all military technology, the offensive weapons advance and the defensive measures adapt to neutralize the threats. One potential next stage in the reversing advantage of offensive and defensive technology is the Flapping Wing Micro Aerial Vehicle (FWMAV) [1].

The recent interest in micro aerial vehicles (MAVs), largely motivated by the need for aerial reconnaissance robots inside buildings and confined spaces, has galvanized the development of inch-

size flapping wing MAVs that could mimic the insect flight [2]. This is a challenging endeavour for several reasons. For instance, aerodynamics for inch-size flapping robots differs substantially from manmade fixed or rotary-wing vehicles. Moreover, sensor types and size constraints add complexity to the design of MAVs.

The main concerns dealt with the wings and their performance. In the biological sphere, the accepted models of animal flight were deemed too inconsistent and inaccurate for the use of computational and robot-based studies of flapping wings [3]. The results presented would present a problem in the computational fluid dynamics calculated in the theoretical tested because design ideas could be rejected or accepted incorrectly. This would affect the design decisions on which designs are tested because of available resources. Curtis et al. with the Air Force developed a method for testing a FWMAV using bench top testing. They used a thrust stand and six-component force balance to gather the force data for various wing shapes [4]. By following these methods, it can be seen the magnitude and direction of the forces from the flapping of the wing.

One approach to developing MAVs is biomimicry, biologically-inspired design. This may include a flapping wing MAV to replicate insect or bird flight. Flapping wing vehicles are sometimes referred to as ornithopters. The ability of biologically inspired MAVs to blend in with the environment sets ornithopter MUAVs apart from other designs in terms of stealth and anonymity [5, 6]. MAVs of this type are the focus of upper level research at universities and are of interest to military, police, and intelligence entities. Because of the complexity of aerodynamics and wing motion of ornithopters, there is much work that remains in creating a proven design.

The first Unmanned Aerial Vehicles (UAVs) took flight during World War I in the United States. From these first tests, the military recognized their potential in combat. After continuous research, UAVs command a permanent and critical position in the United States high-tech military arsenal. There is a desire for cm−Scale Unmanned Aerial Vehicles (UAVs) that are designed to be small and discrete, so small that they can take off and land in the palm of their operators hand [1]. Micro and cm−scale Unmanned Aerial Vehicles (UAVs) are designed to be the eyes and ears for modern soldiers. The MAV must be able to maneuver into small confined areas and ultimately possess hovering capabilities. Also these platforms can be equipped with cameras, microphones, and gas detectors. The main goal of these MAVs is the small size, weight, and energy efficiency.

For some time, interest has peaked in methods that change the baseline, or nominal, configuration of air vehicles. Very early in the aeronautics industry it realized that such a capability

could be highly advantageous. As early as World War II, fighters to carry on aircraft carriers were equipped with folding wings to increase their storage efficiency. Like birds, the capability to control the shape of the wing by folding is particularly important for small-scale unmanned and micro aerial vehicles to extend their flight envelope. MAVs and UAVs are already proven to be valuable instruments in many research and industrial applications such as agriculture, parcel delivery, aerial inspection and mapping [7].

The proposed platform can potentially be equipped with microphones, cameras, and gas detectors, but the development to construct cm−scale Air Vehicles that can fly at low Reynolds number aerodynamics is big challenge. The flapping flight of birds, bats, and insects has been the focus of many researchers in various fields such as biology, zoology, aerodynamics, and electronics because of their highly efficient maneuverability and aerodynamic benefits especially in low Reynolds numbers flight regime. For many centuries, numerous efforts have been made to mimic natures fliers in order to make artificial flapping wing vehicles. It is well known that most of the early trials for flying machines adopted flapping mechanism for generating thrust and/or lift [8, 9].

One of the goals of Unmanned Air Vehicles (UAV) development is to reduce the risk and time needed to collect the data in combat and reconnaissance situations. Army combat operations have placed a high premium on reconnaissance for Unmanned Aerial Vehicles (UAVs) and Micro Air Vehicles (MAVs). UAVs and MAVs provide situational awareness that will shape the decisions of the squad command, such that these platforms are designed to be the eyes and ears for the soldier. One approach for accomplishing this mission is to develop a biologically inspired Flapping Wing MAV (FWMAV) that can maneuver into confined areas and possess hovering capabilities.

The propulsion through flapping of wings has long been a compelling subject for bio-inspired and biomimicry research. This has become true, particularly with the advent and desire to create systems that mimic bird-flight in the cm−scale Unmanned Aerial Vehicle (UAV) community. The most crucial step is the analysis and design of airfoil which will produce minimum drag with maximum lift. Flapping airfoils are crucial for better aerodynamic performance and design because the primary mode of flight propulsion in the animal kingdom [10]. For example, birds such as the hawk shown on Figure 1.1, have mastered the art of wing flapping. The theories that are concerned with how the typical lifting surface can be oscillated for the production of both lift and propulsion are their origin in unstable aerodynamics, which began to develop in the 1920s, on an event primarily for the purpose of understanding aeroelasticity [11], rather than pushing through throbbing. This

Figure 1.1: The Hawk.

last topic was explored as a means of understanding how birds can achieve flight flight [12] and [13], and by those interested in the geometrical horizons of ornithopters [14].

While much progress has been made in understanding the basic mechanisms involved in propulsive flapping, practical ornithopters have not been developed for various reasons. The most obvious of these is the severe mechanical challenge associated with building a flapping wing. Even if this challenge could be overcome, the efficiency afforded by the propulsion system (the obvious choice for low-speed propulsion) has not been improved upon by oscillating airfoils in any theoretical or experimental study.

1.2 Flapping Wing in History

Man has always been inspired by the ease with which birds and insects fly. From early times he has observed these creatures and yearned to fly like them. It seems so natural and easy to flap the wings and be airborne. Without any other form of power than his own muscles, it was only instinctive to don feather-covered wings and flap his arms in the hope to soar like the birds. History records that this approach was doomed to failure from its outset.

As generally known, birds flap their wings in order to harness thrust when flying. When a bird changes the position of its wings, it forms an angle of attack that creates the lift force. Whereas, an aircraft harnesses power from the engine for thrust and the angle of attack is formed by the flap/aileron shape to provide for the lift. During landing, a bird changes the position of its wings for drag, whilst its tail that acts as a rudder to maneuver and decreases its mid-air speed. On the other hand, an aircraft changes the positioning of landing flap on its wing to increase drag thus decreasing the thrust. The aircraft tail is used as to maneuver and to provide for stability ([15] ; [16]).So, the tail end structure is a vital part for landing, and this is similar with how a bird uses its tail to decrease its speed. This structure is later named ornithopter by da Vinci [17].

Within the wing performance realm, the flapping mechanism played a major role in the literature review. Many have one stage flapping like Curtis et al. Another example of the one stage flapping is Yang et al. using a Watt mechanism. In the Watt mechanism, the gears are stacked vertically and linkages provide a behavior that is similar to a crank slider. The flapping from the Watt mechanism has a flapping angle of 30 [18]. A case study by Burgess et al. examined the flight of a gull. In the paper, they present a 4 bar linkage model. The 4 bar mechanisms go through three stages of extension, mid-position, and retraction in flight. The point of having the four bar linkage is to decrease the inertia and energy necessary to sustain flight [19]. By doing so, flight for FWMAVs can last longer and provide less strain on the energy source, a necessary requirement for the research being conducted.

Wing flexibility can profoundly affect the flight performance of natural [20] and engineered systems. For example, an experimental study of the hawkmoth Manduca sexta, [21] showed that a flexible wing was able to generate more lift-favorable momentum flux than a stiff wing. In addition, Barannyk et al 2012 [22] showed that flexible airfoils outperform rigid ones. In addition, several studies have shown that flight performance can be optimized at certain levels of flexibility, beyond which flight forces and/or efficiency decrease [20].

The first attempt to flight by using flapping wing was registered as early as 843 B.C. when the ninth king of Britain, Bladud, was killed when he attempted to fly in Trivanatum (London) using wings covered with feathers. Between this time and the first record by Marco Polo in the 14th century of man becoming airborne on kites in Cathay (China), numerous experimenters must have been killed just like King Bladud when their attempts to fly failed.

In 9th century Muslim Spain, more than a thousand years ago, on a hill in Cordoba, Abbas

bin Firnas, Father of the Flying Machine boldly set out to do what no man had done before. He was ready to test the first flying machine in recorded history. He constructed wings with a span that is estimated between four and five meters. Striving to keep the flying machine strong and light enough, he manufactured a light wooden frame, probably using bamboo, which is hollow like the bones in a birds wing [23].

Gliding without engine was successfully further expanded by the Wright brothers until their invention of engine powered aircraft flew 260 meters. The Wright brothers are well known today for their first attempt to fly on 1st December 1903. Since then, they have gained fame and the field of aviation has been developing rapidly with the integration of engine to the aircraft. Wilbur Wright's key to this is by studying how birds fly similar to what Ibn Firnas had done 1,000 years ago. Wright realized that a bird maintains its stability mid-air or when veering left or right by changing the positioning of its wings. Prior to building the aircraft, the Wright brothers used gliders in order to avoid any mishaps. They invented a kite with a similar function in order to confirm the effectiveness of the method [24].

Theodorsen [11] first brought to general attention the problem of fluttering in 1934. In his paper a mathematical model was given subject to the unsteady forces acting on a flat wing section performing infinitely small oscillations in pitch and plunge in an inviscid fluid with an undisturbed uniform flow. Expressions for lift and moment were derived which have been used extensively for the study of unsteady aerodynamics and aeroelasticity for many years.

Larger-scale mechanical models that mimic the kinematics of a flapping wing have been built to allow measurements that help more fully understand the underlying physics of flapping wing-borne flight [25]. Applying the existing knowledge base of conventional, linear, small disturbance quasi-steady aerodynamic theory to understand the physics of flapping-wing flight is fundamentally inadequate, despite some recent reattempts and claimed successes [26].

The capability to analyze the problem is important because direct prototyping, although not extremely expensive, can be significantly time consuming and error prone. The problem requires the capability to address structural dynamics with significant geometrical nonlinearity, mechanism modeling capability to take into account the actual flapping and pitch mechanism, and consistent fluid-structure coupling. Multibody System Dynamics (MSD) represents an ideal modeling environment to address this type of problems, since it allows to directly consider sophisticate structural dynamics and mechanism modeling. At the same time, the analysis can be consistently coupled to

external solvers for the Computational Fluid Dynamics (CFD) part of the problem [27].

By simulating insect flight several flapping wing design cases have been done in recent years [28, 29, 30, 31, 32, 33]. By employing new techniques and advanced materials the wing mass can be kept rather low and at the same time strong enough. The flapping wing models are mostly micro air vehicles that simulate insect flyers with limited wing span of 150mm. The current design of MAV the system is composed of an electric motor, a transmission system, and two wings. Powered by the electric battery plunging motion is achieved to generate lift and propelling force in low speed. In the last several years micro air vehicles have been well developed in flying performance and power transmission. However there had been no successful large flapping wing ornithopter available until 2003 when Sandra Mau [34] first built a large ornithopter with one pilot in Canada. For the large scale wing the major problem is that the wing cannot provide enough lift and thrust even with large plunging amplitude and steady sustainable flight has never been achieved. In his work a unique wing was designed for the tests. From the tests, some interesting results were found. Increasing the spar torsional stiffness would increase both lift and thrust. The effect of structural stiffness is rather significant for large flapping wing aircraft.

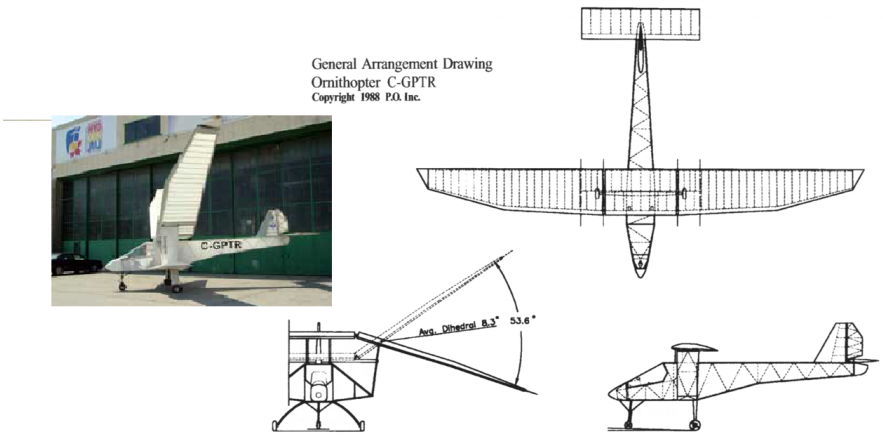

Figure 1.2: Ornithopter and General arrangement drawing of full-scale ornithopter

It is well known that mechanical wings do not provide the same efficiency and performance as biological wings. Modifications must be made in order to bring the efficiency of the wing to a point where the lift is higher than the weight of the bird. One method of this performance was researched by Jones et al. in Cambridge. One issue dealt with in FWMAVs of such a small scale is laminar separation bubbles caused in the transition from laminar to turbulent flow. Jones et

al. approached the problem by designing wings with turbulators on the front of the wings. The turbulators, or leading edge flaps, allowed for the disturbing of the air to take the wing immediately into the turbulent regime. It was found that these leading edge flaps were ineffective at high angles of attack, but they were able to greatly improve lift, even at low Reynolds numbers [35]. The final method found of manipulating the wings was to use acoustic resonance through the use of holes and channels in the wing. They took an E387 wing with 180 0.5-mm diameter holes and measured different scenarios with each row of holes. The wings with the full 180 holes performed the best with the highest ratio of lift coefficient to drag coefficient [36]. The one drawback to the experiment was that it was conducted with fixed wing tests instead of flapping wing test.

A very few models of the flight dynamics of flapping wing micro air vehicles treated the inertial/mass effects of the wings on the central body, and by extension the entire system. Many of the dynamics models present in the literature focus on the standard aircraft model and neglect the inertial effects of the mass of the wings. The standard aircraft equations of motion, to include the linearized model resulting from small perturbation theory, is extensively developed in [37]. For example, Khan and Agrawal present the modeling and simulation of flapping wing micro air vehicles based on the standard aircraft model in [38]. Simulations are presented for a hover condition by utilizing a quasi steady aerodynamic model. The aerodynamic forces generated by the wings are transformed from the wing frames to the body frame by using 2-3-1 Euler angles, but the inertial effects of the wings are neglected. An aerodynamic model is developed, based on [39], which includes rotational and leading edge vortex effects. The coefficients for the aerodynamic model are determined from a robotic flapper. The wing dimensions from the robotic flapper and the mathematical model are used to present simulations of the FWMAV in a hover condition. Many of the uses of the standard aircraft model for flapping wing flight dynamics are tied to research areas conducting control research. For example, Duan and Li developed the flight dynamics model for an ornithopter in [40] for the purpose of attitude control.

In 1997 the Wide Area Surveillance Projectile (WASP) project was commenced as a cooperative venture between Massachusetts Institute of Technology (MIT) and the Charles Stark Draper Laboratories. The focus was to improve the structural design and manufacturing of components capable of surviving launch at lightweight and remaining as durable as possible. Composite materials made up the principal materials used in manufacturing [13].

Frecker, M. et al 2014 [42], conducted a design and optimization analysis of a new contact

aided compliant mechanism. The mechanism facilitated was end and sweep compliant motion by using an angled joint. The optimization is solved by using NSGA-II a genetic algorithm. In order to achieve a bio-inspired wing gait called continuous vortex gait, the wings of the UAV need to bend and sweep simultaneously. So, this can be achieved by inserting the bend and sweep compliant mechanism into the leading edge wing of the UAV. Based on the study of the natural motion patterns of animals including humans when they approach a fixed or moving object for perching or capturing prey. The method based on tau theory, applying this theory to the trajectory generation problem of an air vehicle for perching on a target object. Tau is the action gap strategy, the tau coupling strategy and the intrinsic tau gravity, these are the three bio-inspired strategies studied for perching tasks [43].

Design and optimization of compliant spine (CS) [44], a multi-objective optimization problem with three objectives is formulated in order to perform the design optimization of the compliant spine. The goal of the optimization is to minimize the peak stress and mass while maximizing the deflection, subject to geometric and other constraints. By using a flapping wing UAV to test the accuracy of the design optimization procedure and prove the effectiveness of compliant spine design. The results from flight test proved the ability of the compliant spine to produce an asymmetry in the UAV wing kinematics during the up and down strokes.

In addition the experimental work has mainly focused on the testing of vortex passing by the wing [45, 46], lift and thrust due to the wing plunging motion [47, 48], and propulsive efficiency of flapping wing [49]. In Ebrahimis [50] research a flexible membrane wing was developed with 0.8m wing span. Wind tunnel test were conducted between 6m/s and 12m/s at frequency of 0 to 9Hz. Averaged thrust and lift were measured at 10 angle of attack. The results were used to find optimum performance of the flapping wing vehicle. Two wings with 25cm and 74cm were constructed by Sergey [51] to carry out the study of features of flexible flapping wings used in micro air vehicles. Lift and thrust generated by the flapping motion were measured to conduct the study of the required power and propulsive efficiency.

Optimization of flapping wing kinematics was carried out by Thomson [52] based on experimental results. Vertical force was measured using a load cell subject to a scaled-up hawkmoth wing. The test result was used to optimize the trajectory of a flapping wing mechanism. Jonathan Warkentin [53] designed a tandem wing flapping wing model with span of 0.72m. Lift and thrust were measured through various angles of attack and compared with the results from studies of drag-

onflies. Many experiments [54, 55, 56] have been done to conduct the design and construction of a flapping wing model. Unlike the test of fixed-wing the output results of flapping wing shows a sinusoidal manner due to the simple harmonic wing motion. Therefore the accuracy of the test results requires rather high sensitivity of the test equipment.

1.3 Birds Tail

During the course of evolution, birds have gradually lost the part of the backbone that in other animals makes up the tail, and have replaced it with feathers. The size of these feathers differs from bird to bird. Some birds like murres and puffins hardly have any tail at all. Others like peacocks and male birds of paradise have tails that are so long, they make flight quite difficult. Flight puts many restrictions on a bird's shape. For this reason, birds that spend much of their time flying almost always have lightweight, streamlined tails but other birds, have evolved tails that are shaped for uses other than flight. Some of these are used for balance, some for perching, and others others for attracting the attention of a mate [57].

1. Tail fanned on approach body held horizontally
2. Landing feet held forward to grasp perch
3. Tail closed as bird settles on perch

The importance of bird's tails are summaried below [57]

1. Air brake, When a bird comes in to land, it lowers and spreads out its tail feathers. The feathers act as brake and slow the bird's approaches.
2. A tail for balance, long tails are normally used for display, but it is more likely that they are used for balancing on the ground or clambering in trees.
3. Tail for support, some birds uses its tail to brace itself as it climbs the trunk of a tree. The tail feathers are unusually stiff so that they can support a large amount of the bird's weight as in woodpecker.

So far, the tail acts independently of the wings, but the air flows generated by both must interact. It is hypothesised that bird tails act as split flaps, tails increase the maximum lift coefficient of the

Figure 1.3: Using the Tail in landing

wings and therefore improve performance in slow, turning, and/or accelerating flight. Birds do not need a rudder because they can use the asymmetry of their wings to address yaw effects [58].

Lift and drag from the tail may also enhance stability, and the contribution of the tail is affected by morphology and posture. For example, greater drag associated with a long tail contributes to longitudinal stability. Surprisingly the horizontal tails of birds may also provide temporary yaw

stabilization, whereas pitching the tail with the trailing edge down will decrease stability. Kinematics from aerial insectivores indicates that the tail is used to vary total lift in concert with the wings rather than as an independent mechanism for controlling body pitch [59].

To understand the important of tail, first have further understanding of the aerodynamics of the bird body, it will be useful to take a broader view of the body to include the tail [60]. In many early aerodynamics researcher deals with body as a parasite upon the wings is a leftover and is misleading, because the body is also has the ability of producing lift even with the wings completely folded, as during intermittent flight (flap bounding), which are flexed-wing pauses in between flapping phases. Unlike conventional aircraft, birds able to avoid the constant drag penalty of using a vertical tail fin to provide yaw stability by twisting their horizontal tails temporarily instead [60]. So, the tail functions to reduce parasite drag it contributes to the production of lift both when the wings are not present on a carcass [61] as well as during flight in live birds. Incorporating body lift (and, by extension, tail lift) into a model of Paero reduces the estimated power required for relatively fast flight in flapbounding birds.

The ability to maneuver and the converse, controlling position to be stable in the air are of great importance to flying animals. Highly maneuverable animals may respond more quickly to perturbations, thus they are expected to be better able to maintain their path during flight in turbulent conditions [62]. Other variables besides work and power are of great importance to the biology of flying birds, including the ability to maneuver as well as be stable. Birds may therfore be able to increase yaw stability transiently by twisting their tail about its longtudinal axis. Compared with the amount of empirical data describing steady hovering and forward flight, less is known about the biomechanics of maneuvering and stability, and these subjects represent a new frontier of study [62].

1.4 Dissertation Objectives and Contributions

This dissertation builds on the current literature concerning the high frequency cm scale flapping wing of unmanned aerial vehicle at very low Reynolds Number of biologically inspired FWcm−scale UAV in two different regimes. First, it investigates a new and possibly useful application of the flapping wing of FW cm−scale UAV at laminar flow. In particular, it presents a fluid structure instruction (FSI) model, which is a flow pattern is the von Karman vortex street

that can form as fluid flows past a flapping airfoil structure and monitoring the vortices which may induce vibrations in the two dimentional (2D) airfoil and (3D) flapping wing. Second, the dissertation presents the development of a bio−inspired flapping flight system and a characterization of its performance when operating in turbulent airflow conditions. Additionally, the airfoils or wings' aerodynamic performance is comparatively analyzed between time- dependent and FSI turbulence model, discusses how these two airfoils or wings, and time-dependent FSI laminar and turbulent flow simulation results can be developed to serve the flapping flight for unmanned aerial system. In what follows, we present the Dissertation objectives in more details:

1.4.1 Objective 1: Review of cm-Scale Unmanned Aerial Vehicle Model and Design

Flapping Wings of cm−scale Unmanned Aerial Vehicle (FWUAV) that can accommodate nacelles of the scale of current Unmanned Air vehicle (UAV) designs are complex systems and their utilization is still in its infancy. This context offers an abundance of research opportunities to make significant science/engineering contributions. The first contribution of this research is the improving the design of Unmanned aerial vehicle from previous undergraduate teams by improving the wings and outer body of bird. So, to potentially improve wing design, a complaint joint mechanism is proposed in order to make wing flapping and provide lift and thrust needed to fly. Also, change the wing design from flat wing to airplane wing by using two different airfoils, NACA 0012 and s1223. For bird's body change the internal body to ensure to contain all internal components and give more space for flapping wings. Concurrently a redesign of the outer shell by making it smoother and lighter will be commensurate with the updated design. In addition, development of an evaluation methodology for the capability of a flapping wing to replication design loads by using computational fluid dynamic CFD by using fluid structure interaction in 2D and 3D analysis. The first contribution will investigate the design and analysis of the flapping wing. Specifically, this includes:

1. Review of cm-scale Unmanned Aerial Vehicle Model and design
   (a) Investigate flapping Mechanism.
   (b) Investigate gear mechanism.
2. Analysis of flapping wings for UAV

(a) Select Airfoils for flapping wing.

(b) Analyze Flapping Wings.

(c) Make recommendations for Tail design for UAV.

(d) Make recommendations for the improved design of UAV body.

3. Development of Finite Element flapping wing Model

(a) 2D computational analysis for Airfoils

i. NACA0012 Airfoil.

ii. s1223 Airfoil.

(b) 3D computational analysis with different shape of wings.

i. Relationship between critical parameters and performance.

ii. Design Optimization.

1.4.2 Objective 2: New Design and Development of Finite Element flapping wing Model

The second contribution, which is new key to make flapping wing close to the nature or real flapping wing, a new wing design inspired from nature and scaled to our design. Starting from gear design by choose proper gear system. Then redesign the wings to commensurate with new bird. Computational fluid analysis also will used to replicate the loads needed to fly. This is another important area in which the literature is not offering guidance.

1.4.3 Objective 3: The challenges of modeling a cm-scale flapping wing Unmanned aerial vehicle

The third contribution addresses the lack of an overview paper in the literature that outlines the challenges of testing a full-scale flapping wing unmanned aerial vehicle onto laminar flow test and suggests research direction to address these challenges. Although conceptual in nature, this contribution is expected to be significant given that it takes experience in the unmanned vehicle industry to determine what challenges matter and need to be addressed. The growth in testing full-scale unmanned air vehicle using a laminar flow test being recent limits the number of people

who can offer the perspective needed to suggest a research roadmap. These three contributions and related publications are deemed worthy of a PhD.

1.5 Dissertation Outline

The rest of the manuscript is outlined as follows: Chapter 2 tackles Objective 1 of this Dissertation which is concerned with review the micro and cm-scale unmanned aerial vehicle and design concepts. Details of the new design implementation of the cm-scale of Unmanned Aerial Vehicle which is inspired from nature are provided in Chapter 3, new design background and compare with previous design details of the newly proposed design are discussed. Chapter 4 tackles Objective 2 which provided computational fluid dynamic analysis of flapping airfoils at very low Reynolds number regime. Chapter 5 presents the work concerned with building a complete picture of the flapping wing of unmanned aerial vehicles at very low Reynolds number regime laminar flow. Chapter 6 investigates the numerical analysis of fluid structure interaction at low Reynolds number regime turbulent flow for flapping airfoils, flapping wings, and accuracy in the time averaged solution for various wings configurations.Chapter 7 presents the important conclusions. Finally, Chapter 8 summarizes the thesis and proposes topics that are important for future research in this area.

Chapter 2

SYSTEM REQUIREMENTS and cm-Scale Unmanned Aerial Vehicle DESIGN

2.1 Introduction

Since this UAV is supposed to be nature inspired, the idea is that the best design basis for wings should be from real birds. The basis to start off with possible include in the design that depending on the location that the UAV will be used the body and wings could be painted to look like different birds. As a baseline the FWUAV is modeled after the Warbler bird. This research must also focus on the ratio of body length to wing length as well as weight.

This section focuses on modeling part of the research work. First, an overview of the strategy used for airfoil geometry, then, using solid modeling to build the UAV body frame and particularly the flapping wing frame. Then, baseline finite element static analysis and laminar flow analysis around the flapping wing in the designs.

The design made use of previously encountered studies involving aerodynamics of small vehicles. The small length scales and low speeds that the UAV will travel at are a great benefit because any flow information could be modeled using laminar potential flows. The UAV was modeled after wildlife. The entire project is modeled in Solidworks before being analyzed further in FEA. The

Navier-Stokes equations are would be used to give a complete description of all possible flow situations. However, obtaining a numerical solution using Navier-Stokes equations is time consuming, even for the case of a laminar flow field around a wing.

The first was to design a wing that utilized the lift capabilities of an airfoil. Initial benchmarking for the airfoil used the research by Pelletier and Mueller [41]. The two were able to quantify the aerodynamics of low Reynolds number aerodynamics airfoils. The lift, drag and pitching moment coefficients in addition to the endurance parameter determines the flight parameters that are associated with the flight characteristics that determine the performance of low Reynolds numbered wings. The physical constraints of the model were designed as bird wings and were either flat bottom or featured a 4% camber. The wings had a thickness to chord ratio of 0.0193 and were selected for the ability to glide at low Reynolds number. Each wing studied was divided into 2D models and semispan aspect ratios, a dimensionless expression for relative length of the wing. Notable trends were that when higher semispan aspect ratios having higher lift coefficients and pitching-moment coefficients while having relatively similar drag coefficients for angles of attack between 0 and 10 degrees. Lift to drag ratio was highest for the higher aspect ratios as well demonstrating that longer wings will provide better aerodynamic properties. This observation was also consistent for the cambered wings that had higher lift coefficients despite also having higher drag ratios. The shape of the trailing edge was also examined as of whether a sharp trailing edge or elliptical trailing edge was better for performance. The only variable that was under the edge design was the pitching-moment coefficient, for the flat wings only. At an angle of attack of 0 degrees, there was a slight increase in positive pitching-moment from sharp trailing edges that was not well observed in the cambered models. For the purposes of gliding, the data shows that a cambered wing with a high semispan aspect ratio (i.e. large wing span with small chord length) will have the best performance [41].

The importance of the low aspect ratio again by the work of and Jacquin who examined the flapping frequencys influence on the aerodynamics. Frequencies of the airfoils were compared using the Stroudal number as the primary dimensionless parameter. The study was conducted using a NACA airfoil at a Reynolds number of 1000 and the flow field was analyzed numerically to determine the behavior of the air around the wing. From the calculated force gradients, there were definite and visible differences in the distribution of the air as the wing flapped relating to vorticity of the air. The pressure gradients on the down stroke were much higher, but on the upstroke a vortex was present that reduced pressure throughout the entire upstroke.

Relevant numerical information was the use of Stroudal values within the range of a bird in flight. Those values were below St = .5. Relevant calculations that were used to arrive at this value are all dependent on flight parameters that vary through time.

Kaplan, Altman and Ol explored vorticity was an important factor to flight even with the benefit of gliding. Wing shape with low aspect ratios are for their aerodynamics are directly related to the wings while gliding by. The selected shapes for analysis were a rectangle, elliptical and delta wing. The rectangular performed the best among the shapes in terms of generating the highest lift, but the delta wing had the strongest relative vortices. The movement of theses vortices change the pressure gradient across the wings. The airfoils movement generally changes with the vortices and the lift that is calculated is subject to those same vortices.

Combining these analyzes isolates three main design principles *i*) A thin cambered wing *ii*) the largest forces experienced on the down stroke and *iii*) a wing that compromised between a delta angle and a rectangular profile.

2.2 Very Low Reynolds Number Laminar Flow

In general, laminar Flow occurs when a fluid flows in parallel layers, with no disruption between the layers, no cross currents or eddies perpendicular to direction of flow. All fluids are compressible at high enough pressures. Since low Reynolds number flow is so slow for MAV applications, the air compression is negligible. To extremely low speeds (¡ 200 mph) the effects of air compressibility effects are negligible and the lift coefficient (CL) also contains the effects of air viscosity and compressibility. So, it will be totally inaccurate to measure a lift coefficient during a very low speed (say 5 mph) [34].

Conversely, if the incoming flow is laminar, the boundary layer often reaches separation due to the adverse pressure gradient, and the separated flow quickly undergoes transition to turbulence. Depending on the local Reynolds number, pressure gradient, flapping surface with roughness, and freestream turbulence intensity, the turbulent free shear layer can entrain enough high momentum fluid through diffusion to reattach to the surface as a turbulent boundary layer and form a laminar separation bubble [35].

Understanding the onset of separation and subsequent reattachment has considerable practical significance because they are related to the upper limit of efficiency of the lifting bodies. To

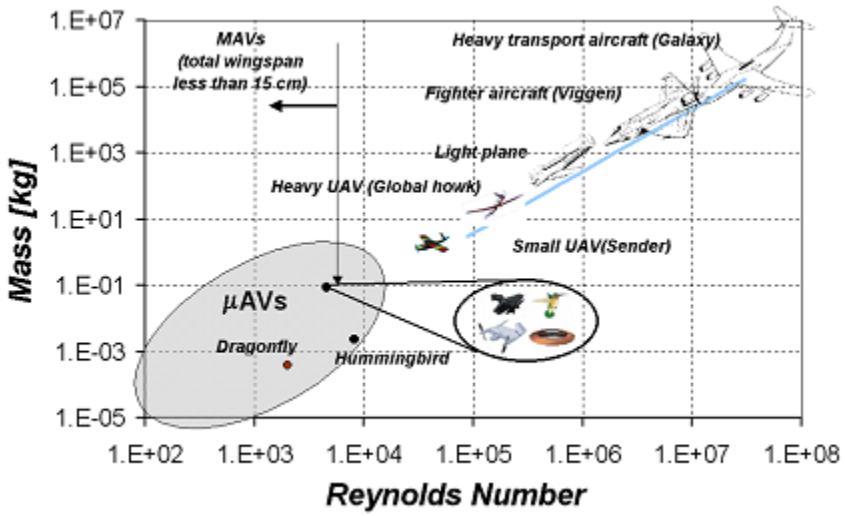

Figure 2.1: Mass Vs Reynolds Number

further illustrate the salient features of laminar separation bubble.

Flight at these Reynolds numbers is much less efficient than at higher Reynolds numbers and available power is a limiting technological factor at small scales. It is important to operate the airfoil at its maximum L/D operating point, but this requires operating close to the maximum steady-state lift coefficient. The low Reynolds number regime is significant in that it projects a fundamental shift in physical behavior at MAV scales and speeds - an environment more common to the smallest birds and the largest insects. While naturalists have seriously studied bird and insect flight for more than half a century, our basic understanding of the aerodynamics encountered here is very limited [72]. Neither the range - payload performance of bees and wasps nor the agility of the dragonfly is predictable with more familiar high Reynolds number aerodynamics traditionally used in UAV design. Since our understanding of low Reynolds number effects is limited, our ability to mechanize flight under these conditions has been even more elusive. So, in this study Laminar Regime has been considered because it is within low Reynolds number regime at which birds and small air vehicle operate. MAVs have a unique ability to fly in low Reynolds number flight regimes as shown in figure (8).

2.3 Reynolds-Averaged NavierStokes Turbulent Flow

Selecting a proper turbulence model, the structure and use of a model to forecast the effects of turbulence, is a crucial undertaking to study any sorts of fluid flow. It should model the whole flow condition very accurately to get satisfactory results. Selection of wrong turbulence model often results worthless outcomes, as wrong model may not represent the actual physics of the flow. Turbulent flow dictates most flows of pragmatic engineering interest. Turbulence acts a key part in the determination of many relevant engineering parameters, for instance frictional drag, heat transfer, flow separation, transition from laminar to turbulent flow, thickness of boundary layers and wakes. Turbulence usually dominates all other flow phenomena and results in increasing energy dissipation, mixing, heat transfer, and drag. In present study, flow is fully developed turbulent and Reynolds number Re is set to 6106. $k-\epsilon$ primarily used to model viscous turbulent model. However, these specific models are suitable for specific flow cases. Douvi C. Eleni [68] studied variation of lift and drag coefficients for different viscous turbulent model. His study shows that for flow around NACA 0012 airfoil $k-\omega$ Shear Stress Transport (SST) model is the most accurate.

K-epsilon $k-\epsilon$ turbulence model [69] is the most common model used in computational fluid dynamics (CFD) to simulate mean flow characteristics for turbulent flow conditions. It is a two-equation model which gives a general description of turbulence by means of two transport equations (PDEs). The original impetus for the K-epsilon model was to improve the mixing-length model, as well as to find an alternative to algebraically prescribing turbulent length scales in moderate to high complexity flows.

There are some limitations with RANS models as they are based on the definition of turbulent viscosity. These limitations are

1. Lack of physical description
2. Turbulence-induced secondary flows
3. Streamlined curvatures
4. Swirling flows or flows with rotations
5. Transitional flows between turbulent and laminar
6. Unsteady flows like internal combustion engines

Size	<15 cm
Weight	10-100 grams
Payload	1-18 grams
Endurance	10-60 minutes
Airspeed	5-35 mph
Range	1-5 miles

Table 2.1: System Requirements

Ability to Hover
Maneuverability
Quiet
Moderate Fly Time
Remote Controlled
Durable
Inexpensive

Table 2.2: Desirable MUAV Attributes

7. Stagnant regions in flows

2.4 System Requirements

2.4.1 Initial Requirements :

The desired system requirements are summarized in Table 2.1.

In addition to these specific requirements, there were several other desirable attributes that the system should possess if possible which are listed in table 2.2.

The design was based off these requirements, and strove to satisfy them whenever possible. So, to develop a proof of concept the research team generated conceptual designs for frame, mechanical system, electrical system, and wing mechanism. The main design tasks were to design a biologically-inspired body, utilize additive manufacturing to manufacture all the parts, assemble the electrical system, assemble the prototype, and conduct a FEA analysis [4]. Other major underlying goals were to create a MAV that utilizes the best commercially available off the shelf (COTS) parts and create a system that was highly, repeatable and inexpensive, bordering on expendable.

Motor
Battery
Camera
Radio Control
Receiver
Speed Controller
Wings
Tail
Servo
Flapping Mechanism
Gear Reducing Powertrain
Frame
Body

Table 2.3: Required Components

2.4.2 System Components and Schematic :

The original system design proposed by the prior design team had a solid foundation. Wings, motor, body, frame, camera, radio control, and battery had all been considered; however, their overall design was lacking in completeness. Steering was not provided for in the original system and must be included in the final design in order for the product to useful. Without a means to control the MAV, only uncontrolled, erratic flight would be possible which would not meet the system requirements for data collection. In addition, some of the components specified would meet the required specifications for the project; therefore, it was necessary to change the components or modify the requirement.

First step, starts with evaluation of the cm-scale UAV system by examining all of the components suggested in the original design and determining that they were still feasible. Also, looked at areas where the design was lacking and added components in those sections. Overall, a good base to build the system and spent more time refining the design rather than starting from scratch.

After evaluating the previous design, a list of the requirement components for the MAV was created and shown in table below. A system schematic was developed to gain a good conceptual understanding of the system and learn how all the components interact with each other. The diagram shown in figure 2.2 was developed to show how the system operates as a whole and serves as a guide for electrical power calculations and was used during assembly. This schematic also serves as a visual for how the electrical, mechanical, and wireless connections are attached. Throughout the design process, this schematic was viewed to ensure that no aspect of the MAV was neglected when making

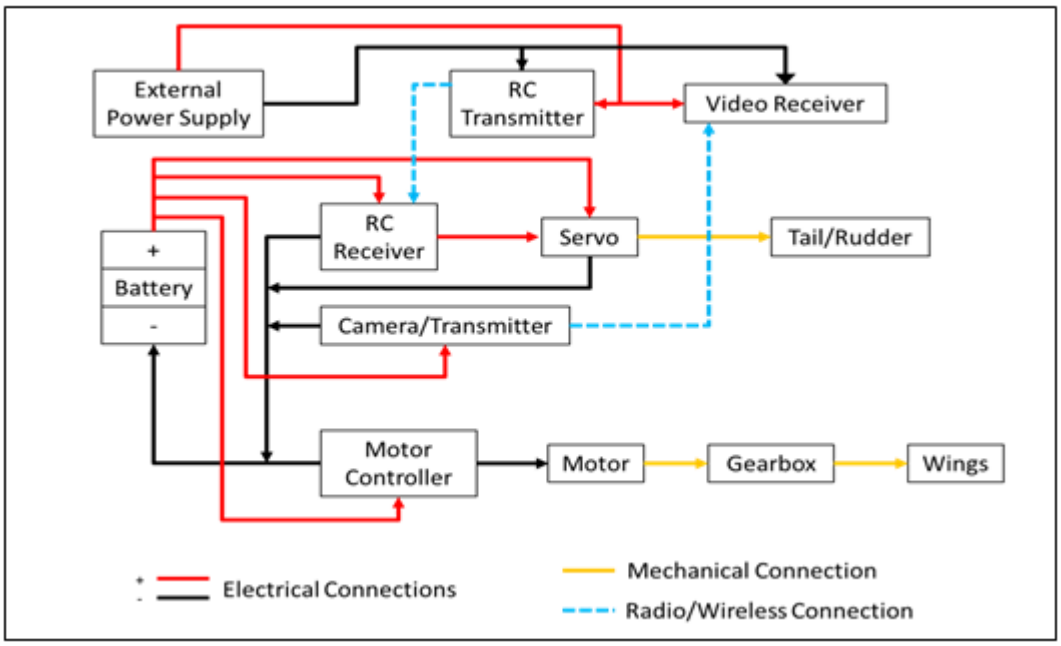

Figure 2.2: System Schematic

design changes to the system.

2.4.2.1 The battery

As the MAV is designed and expected to perform certain tasks at the highest level. Performing these tasks requires the vehicle to have maneuverability and the ability to be the eyes and ears of the soldiers operating the equipment. Batteries must be used to power the motor, actuator, and camera onboard the MAV; therefore, careful consideration must be taken to find the best available option.

So, the battery shown below in Figure 2.3 was the power source of the bird. It was a 300mAh 7.4 LiPo with a max continuous discharge current of 6A weighing 19.6 grams. The battery shown below has two connections for the charger and the speed controller.

Figure 2.3: 300mAh 7.4 LiPo Battery

Figure 2.4: Thunderbird 6 Speed Controller

2.4.2.2 Speed Controller

The purpose of an electronic speed controller is to regulate the motor speed based off an input from the RC receiver. A signal is sent from the transmitter via a joystick by the user to regulate the motor speed. In our application, the motor speed is directly proportional the wing beat frequency. So by changing the motor speed the wing beat frequency will be changed accordingly.

A Thunderbird 6 speed controller made by Castle Creations Figure 2.4 was chosen to control the speed of the motor.

2.4.2.3 The RC Receiver

Before selecting an appropriate receiver, the control requirements must be established. The minimum requirements for the MAV are motor control, servo control, and a 1 mile range. The user must be able to adjust the motor speed to regulate the flight speed of the MAV. Also, in order to

Figure 2.5: Castle Creations Berg Microstamp

steer, servo control is needed to adjust any rudders, tails, or flaps that will affect the flight motion. Therefore a receiver with a minimum of two channels is needed.

In addition to defining the requirements for the receiver, the receiver and transmitter frequency must be determined. There are several frequencies currently in use: 72 MHz, 75 MHz, 2.4 GHz, and 5.8 GHz. The 72 MHz and 75 MHz are an older frequency and simpler. The newer frequencies are 2.4 GHz and 5.8 GHz and utilized more sophisticated techniques such as frequency hopping to help reduce interference and they are more readily available; however, the newer frequencies do not have as large a range as the older frequencies. Since our requirements specify a large range, 1 5 miles, the older frequencies will be able to achieve that. Also, the camera we are considering using operates at the 2.4 GHz which could cause interference if we chose to use a 2.4 GHz system. The 72 MHz systems also seem to be more readily available than the 75 MHz; therefore, the MAV will utilize a 72 MHz system.

As mention above its function was to control the flapping speed of the wings by communicating with the remote transmitter. Therefore, it was connected to the motor and to a radio channel receiver. A Castle Creations Berg Microstamp four channel receiver shown below in Figure 2.5, controls four different components through the receiver.

Figure 2.6: Dragon Eyecam Camera

2.4.2.4 Dragon Eyecam Camera

One of the main purposes of the MAV is to provide a visual reconnaissance of an area of operation. For this purpose, the camera selection has to meet some requirements. The main concerns for the choosing the right one were the range and the weight. It is also important to remember that the camera should have a transmitter included; otherwise it will be necessary to have a separate until which will increase the weight and space required.

The next component connected to the receiver was the Dragon Eyecam camera shown in Figure 2.6. The MAV receiver acted only as a low voltage power source for the camera, as it came with its own external receiver that could be connected to any external display. The Draganfly Eyecam, which operates with a frequency of 2.4 GHz, with 300 meters range and weighs 9 grams including the transmitter. Analyzing the weight and range specifications, it is clear that the range increases proportional to the weight. Considering the low weight requirements, the Draganfly Eyecam was selected as the camera to use in the MAV. A range of 1000 feet line of sight is the maximum distance capable by the Eyecam which is less than the required range; however, it is a good system overall due to its small size, low weight and also the Radio Controls range.

The Draganfly Eyecam is comprised of the transmitter and lens in one small package and comes with a mounting bracket that could be utilized in the design of the component packaging. Some detailed information for the Draganfly Eyecam is listed in table below.

Frequency	2.4 GHz
Operating Power	$DC4.8 - 7.2$ V regulated
Power Consumption	100 mA
Size	15 $mm * 22$ $mm * 32$ mm
Antenna	Omni-directional
Transmitting Range	300 m(Line of sight)
Weight of Camera and Transmitter	9 $grams$
Weight with Mount	16 $grams$
Temperature	-10 to $+50$ C

Table 2.4: Draganfly eyecam specifications

Figure 2.7: HK-5330 ultra-micro digital servo

2.4.2.5 Servo Control

A servo was selected which would be capable of operating a tail or stabilizer. Keeping the MAV weight and size limits in mind, a small, lightweight servo was chosen for use. The HK-5330 Ultra-Micro Digital Servo was chosen and is shown in Figure 2.7. Servo was then connected mechanically to the tail rudder to control the flight.

2.4.2.6 RC Transmitter

In addition to a receiver, a transmitter is required. The transmitter must operate at the same frequency as the receiver in order for them to communicate. All the components were controlled

Figure 2.8: Remote control receiver Tactic TTX401 Transmitter

by a remote control receiver shown in Figure 2.8. The Tactic TTX401 which is a 4 channel 72 MHz transmitter and is compatible with the Berg 4L receiver.

2.4.2.7 The Motor

The Exceed RC Rocket 2205-1100kV brushless motor was selected for the design and is sized for estimated power needs. The motor was sized with a safety factor of 3 to account for friction losses in the gearing and mechanism, inefficiencies in wing design, and additional power needs for the next iteration of the project. This motor was sized assuming a wingspan of 40 cm. This motor was also selected based on its max rpm allowing a 4:1 gear ratio based on an 18Hz wing frequency. This motor, displayed in Figure 2.9, weighs 33.1 grams, has a max performance of 80W and an approximate max angular velocity of 4400 RPM without load.

Figure 2.10 below shows the basic mechanical setup for the flapping mechanism of the MAV. The motor shaft was inserted in the mechanical shaft that was connected to the gear system converting the rotational motion of the motor to the flapping mechanism of the wings. Gear design was calculated to a 4:1 gear ratio with 4 gears and 2, 2:1 ratio conversions.

Figure 2.9: Exceed RC Rocket 2205-1100kV Brushless Motor.

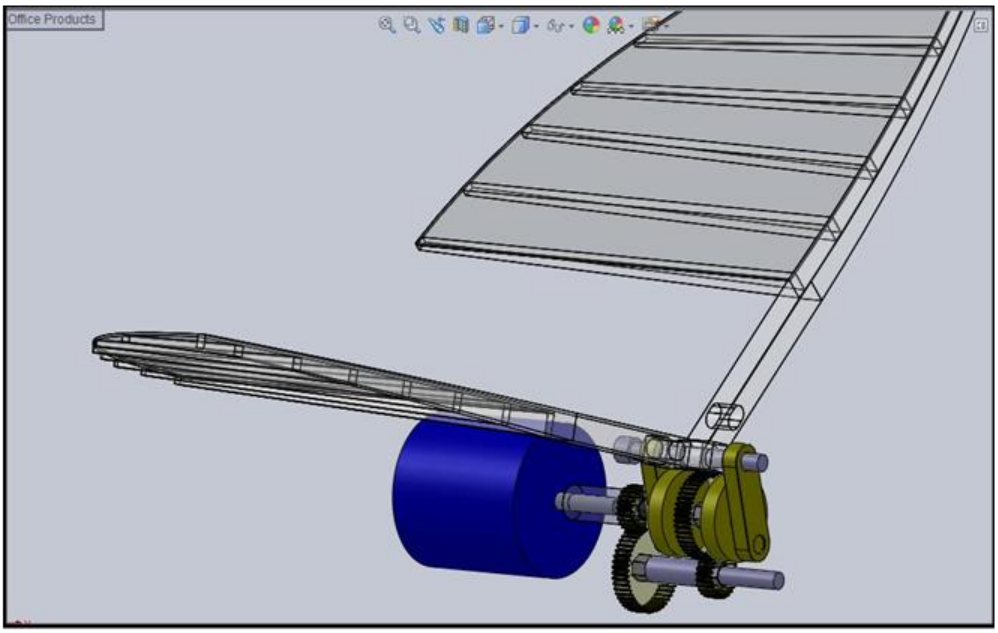

Figure 2.10: Mechanical System.

2.5 Resolved Assembly Center of Gravity

The theoretical balance point of a flying machine is the center of gravity. Lift and power calculations are conducted utilizing the center of gravity of an aerial vehicle. It was discovered that for birds, the center of gravity changes with respect to what action the bird is currently in. Birds accomplish this movement by protruding and retracting legs and feet, thus increasing and decreasing the moment arm on itself. Reproducing this complicated dynamic movement is difficult, especially

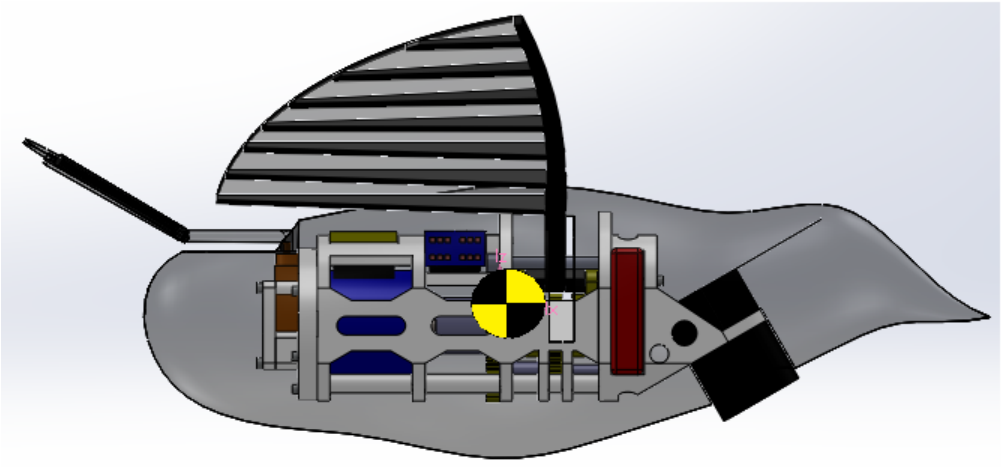

Figure 2.11: Center of Gravity Approximation

considering minimal power and space. Due to time restrictions, the center of gravity be placed at the resultant force of the wings. Placing the center of gravity here, it allows for sustained cruising flight once the ornithopter reaches appropriate speed and height. This placement gives a baseline which future design iterations can build upon.The approximated and resolved center of gravity (COF) can be seen in Figure 2.11.

In Figure 2.11, the center of gravity can be seen as the yellow and black checkered circle. The outside body is not included in the center of gravity calculations and is only for show. When the new wings and body are added to the frame, we anticipate that this will be the location of the resolved lift force of the wings. Components are symmetrically placed along the axis of the bird to allow for COF along the length to be on the axis itself.

A cavity was also designed in the new body design to house the components as shown in Figure 2.12. The locations of several components with respect to the leading edge of the wing were unable to be varied. These fixed location components included the flapping mechanism and mechanism supports as well as much of the gear train. The rest of the powertrain and the motor could be placed on one side of the leading edge of the wing or the other depending on desired shape and weight distribution. The camera needed to be located at the front of the bird angled downward. The servo and tail needed to be located at the rear of the UAV. The battery, receiver and speed controller could be placed anywhere the shape of the bird would allow. The placement of components

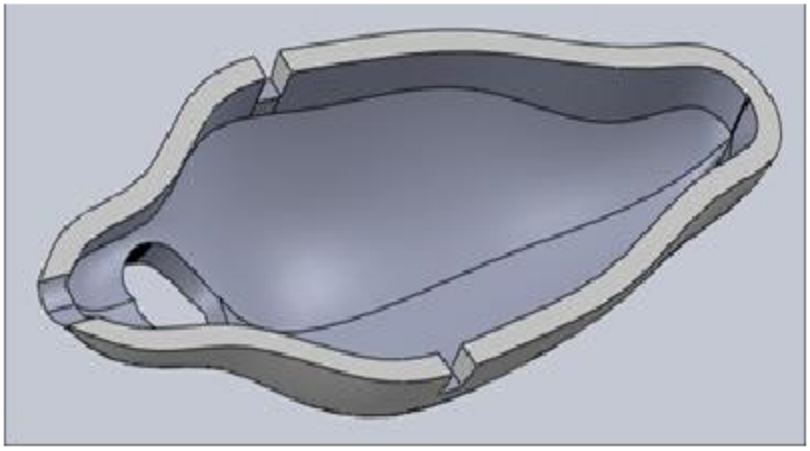

Figure 2.12: Preliminary design for Cavity for Frame.

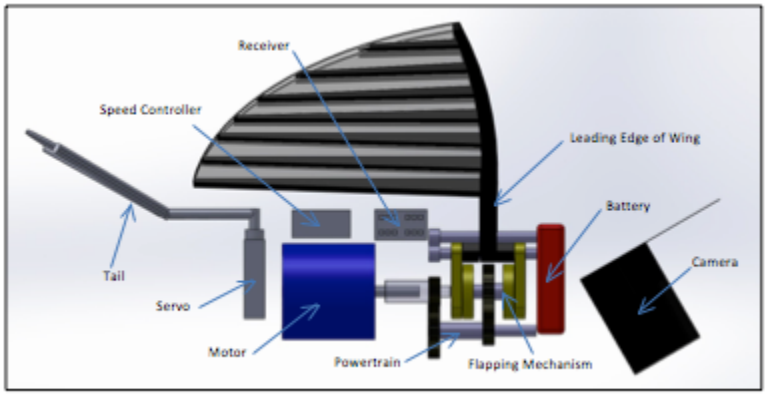

Figure 2.13: Proposed Component Placement

in the frame is displayed in Figure 2.13.

The component weights cannot be changed due that they were specified for the project requirements. Any potential weight reduction can only be applied to the frame and body concept. Low stress areas were identified and cutouts were made in these areas. Figure 2.14 shows several places where these cutouts were made

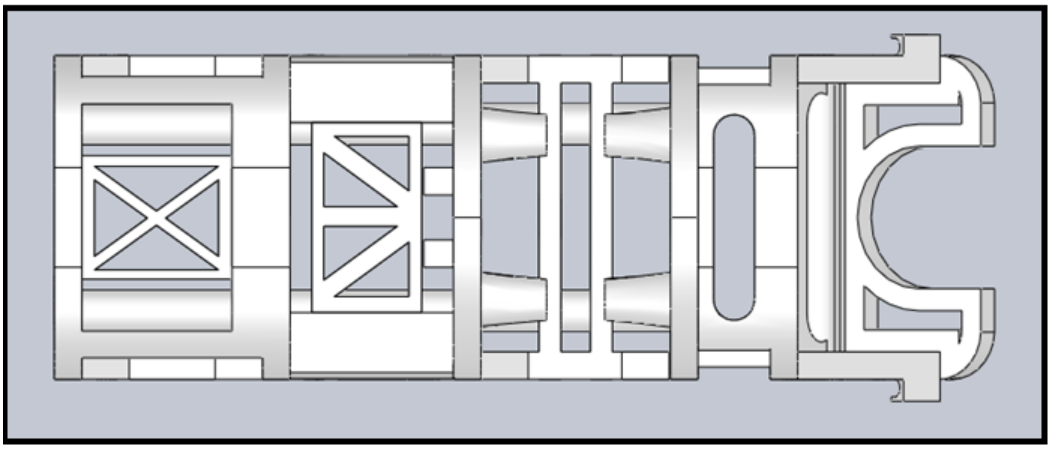

Figure 2.14: Component Housing Frame with weight reduction areas.

2.6 Proposed Modeling and wing generations

The propulsion through flapping of wings has long been a compelling subject for bio-inspired and bio mimicry research. This has become true, particularly with the advent and desire to create systems that mimic bird-flight in the Micro Aerial Vehicle (MAV) community. The most crucial step is the analysis and design of airfoil which will produce minimum drag with maximum lift. So, flapping airfoil is crucial for better aerodynamic performance and design because the primary mode of flight propulsion in the animal kingdom. MATLAB R2014b used to perform airfoil design as shown in Figure 2.15. The airfoil was designed using a standard Joukowski Transformation of a potential flow field using the equations shown below. Once the complex z was solved for, the x and y coordinates that corresponded to the airfoil were exported in a txt file that was imported into Solidworks using the Curves feature to create a workable sketch to generate an airfoil to use in the investigation.

$$\zeta = 1 + \frac{1}{z} \tag{2.1}$$

$$z = x + iy \tag{2.2}$$

Also, biological flapping wing flyers achieve flight maneuverability and efficiency in low speed flight regimes which have not perform again by human made flyers. Unmanned Aerial Vehicle (UAV) design goals are to develop flyers that maintain flight in regimes that biological flyers exceed in which includes low speeds, hovering, and urban settings. This flight is characterized by flow phenomena

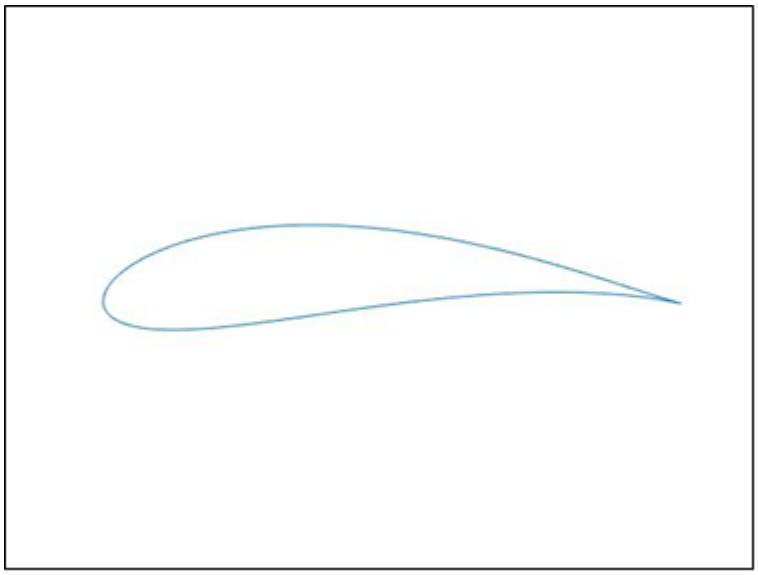

Figure 2.15: Joukowski Airfoil

that are not well understood such as, flow separation and vortical flow.

For the current study, two airfoils have been selected as shown in figure 2.16, s1223 airfoil designed in University of Illinois, Urbana Champaign and NACA0012 which is being used extensively for the wingtip in a lot of aerospace applications from the the tiny Cessna to the giant $C-5$ Galaxy. Laminar Regime has been considered because the low Reynolds number flight regime is characterized by complex flow phenomena such as: viscous flow, transition from laminar flow to turbulence, flow separation, vortical flow, etc. These flow phenomena are rarely experienced in high Reynolds number conventional fixed wing flight and have not been extensively studied. Due to the complexities of flapping flight aerodynamics, the aerodynamics are not well understood.

2.6.1 Design Methodology

One of the aspects of the MAV design is that it utilizes flapping wings instead of fixed wings. This design is different from traditional plane wings; therefore, not many off the shelf devices are usable. One research option is to design the mechanism to drive the wings and add the hinge mechanism to the wing. To increase the resemblance to natural flyers, a flapping MAV should include another mode of flight; gliding. This has proven to be a difficult objective to achieve for many researchers. A wing capable of gliding must be rigid enough to hold a steady angle of attack

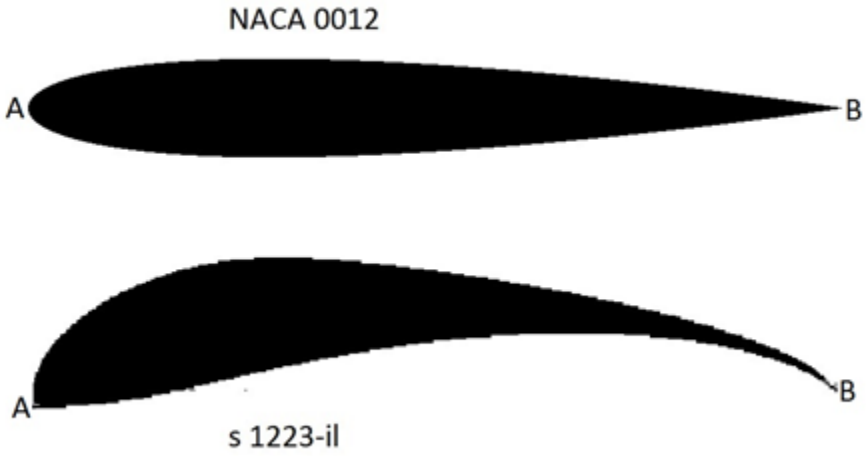

Figure 2.16: Two types of Airfoil

with a positive lift to drag ratio. This would mean locking a flapping wing in a specific place with a fixed pitch. In order to determine a possible pitch angle, an FEA analysis or wind tunnel test is needed going forward. The wing position, on the other hand, could simply be set to the top of the upstroke of the wing to prevent adding any extra weight in parts to hold the wing in place.

2.6.2 Wing Frame Design Methodology

Several aspects taken into consideration when designing the mechanism of flapping wing provided a robust foundation for design. First, it must be small and light weight that lends itself to a simple design. Then, the flap angle is assigned as a variable for optimum flight generation when creating the mechanism. Finally, the mechanism must be able to connect to gears mechanism and these mechanisms are connect to small DC motor. These three criteria provided guidelines for the design.

In order to create a wing mechanism that flapping at the proper angle, a new bend-twist-and-sweep compliant joint mechanism added to the wing frame as shown in figure 2.17. This contact-aided compliant mechanism has tailorable deflections and nonlinear stiffness in two orthogonal directions and twist about its axial direction.

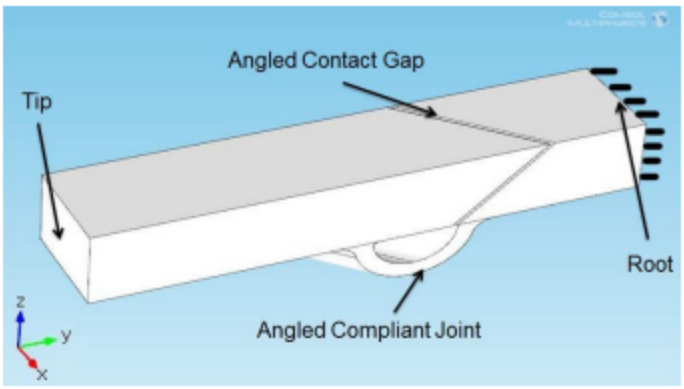

Figure 2.17: Compliant Joint Mechanism [42]

2.6.2.1 First Generation

The wing sought to emulate a skeleton with a skin placed over it to improve aerodynamics and reduce the weight of the wings. The wing frames were going to instead use an airfoil design for each rib (Figure 2.18). The gaps between the wing ribs were initially selected to serve a variable for parameter to be optimized at a later time. This portion of the wing would have to be strong enough to endure the stresses that were placed on it. This portion was then modeled with the compliant mechanism to allow for the wing to flex. The completed wing was then fitted to ensure that the overlap in the connections to the flapping mechanisms were measured correctly. With the wing dimensioned correctly, preliminary FEA test showed that the wings would be able to withstand initial static loads. The design withstood the initial loads run Simulation which indicated that it would be an appropriate design for testing COMSOL. The third stage of the first generation of wing design. Appearance does not reflect choice of material. The material used was Delrin. The discovery of design flaws using both FEA Simulations allowed failure. The first was the position of the airfoil ribs were too far forward and concentrated large moments on the wing. Despite having the compliant joint on the end and making that end taper outward, there was too much stress concentrated at the joint to withstand larger loads. The number of ribs was the second noticeable flaw as it made the wings too heavy. Adaptations in the flapping mechanism also showed that the connect joint did not allow enough movement for a proper flight pattern.

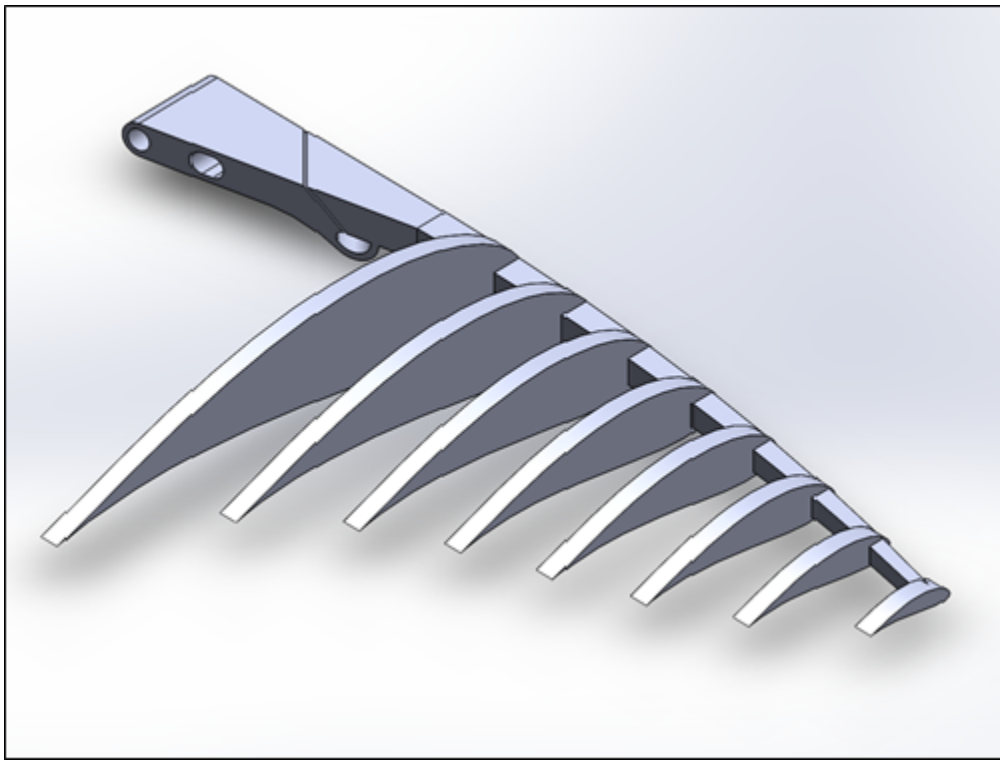

Figure 2.18: First Generation of Wing

2.6.2.2 Second Generation

As shown in figure 2.19 the second generation of the wing made up for the flaws in the first design by placing the main support beam in the center of the airfoil ribs and reducing the number of members from eight to six. While being able to withstand the static load and demonstrate the potential for a long-term use, FEA had tremendous difficulties navigating the sharp edges that were located on the wings, where the central core connected to the airfoil ribs. The slot where the wings would flap was also lengthened to improve the flapping without compromising the compliant joint. In figure 2.19 the central beam and fewer airfoils characterize the second generation of the wing design. This design featured with a fitted cover to help simulate the real model better.

2.6.2.3 Third Generation

The third generation of the wing design would solve the problem of the central core having a poor contact with the airfoil and reduce the weight by making the air profile thinner. This lower thickness to chord ratio would perform even better aerodynamically. An updated version of the

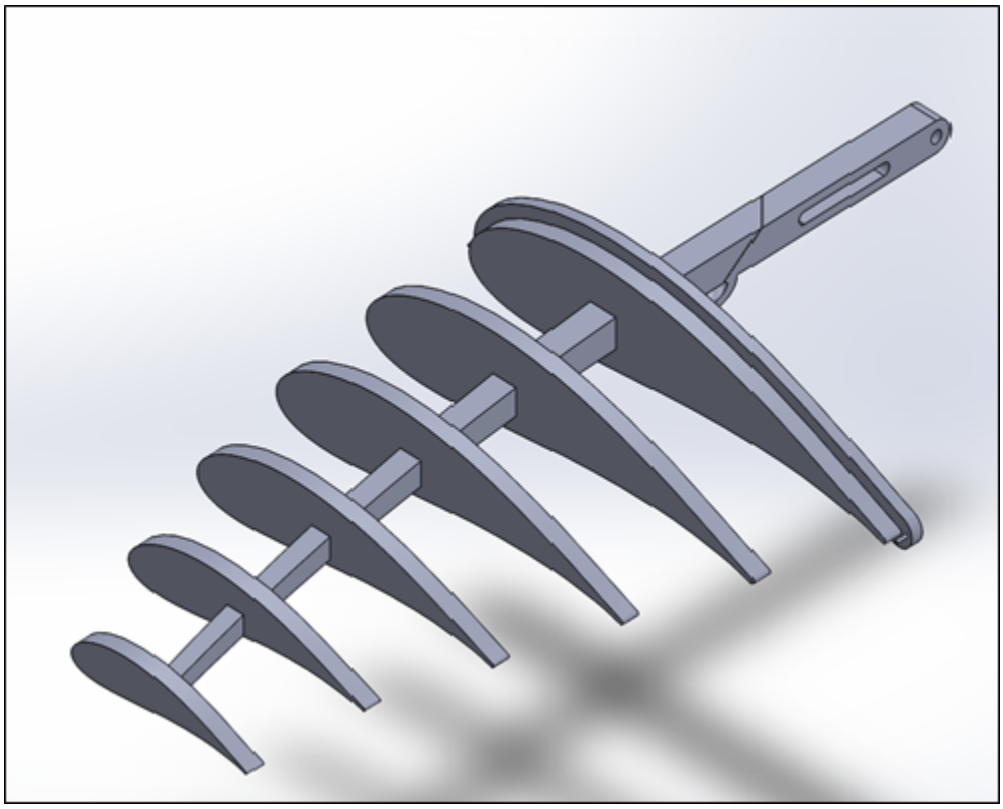

Figure 2.19: Second Generation of Wing

MATLAB code allowed for better control of the position of the splines. This made it far easier to create a series of profiles whose positions could accommodate any wing shape. This opened up the possibility of making a wing frame with a continuous volume instead of a ribbed approach. The area between each airfoil was the result of a cut operation performed after the main shape was complete. To eliminate stress concentrators between the airfoil and arm, an applied fill-in feature created a flush contact. In figure 2.20 the third generation was designed as a solid wing with a portion removed. The compliant mechanism was also parametrized to enhance the design process.

2.6.2.4 Fourth Generation

The fourth generation wing continued using the same design process as the third, but specifically featured an airfoil developed from the NACA0012 design. This design boasts a high lift to drag ratio (Islam, M., et al., 2009[63]). This meant this design had to use a modified matlab code, as it was not produced using a Joukowski transformation of a circle made in this lab. In preparation for

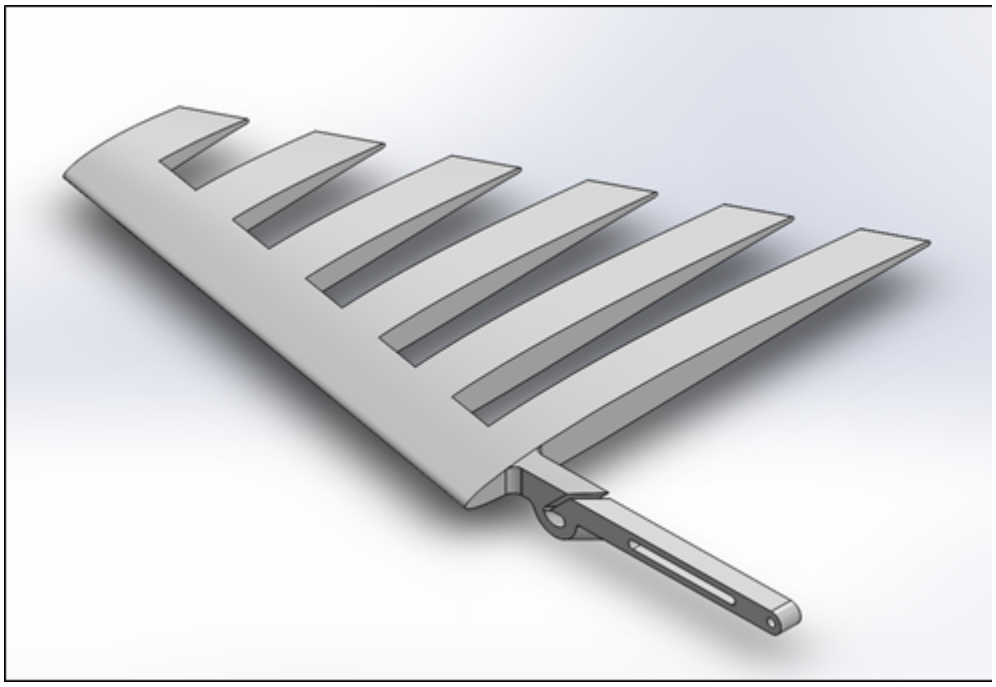

Figure 2.20: Third Generation of Wing

more varied wing designs, this particular configuration also did not include a compliant mechanism to allow for more options in flight design. In figure 2.21 the fourth generation features a much more cambered edge. This model was produced without using a Joukowski Transformation.

2.7 Wing Gear System and Frame

A few gear systems considered, but ultimately, the strength of steel gears as individual purchased parts opened up the planetary gear system as the best candidate. The wings would be pinned to the body and have extensions on them with slots. The slots in the wing would slide onto a pin on the arm that connect planet gear, in addition to that using compliant hinge mechanism in the root of the wing, and as the motor gear rotated it would cause the wings to move up and down, creating an oscillatory flapping motion.

Earlier designs of the wing mechanism had issues with the sliding joint not being long enough in the planetary arm. As the motor gear would rotate, the wings would jam and not be able to complete the cycle using a standard motor. The slot length was increased and that solved the problem. When the wing become in the upstroke, the slider pin reaches in the middle point in the

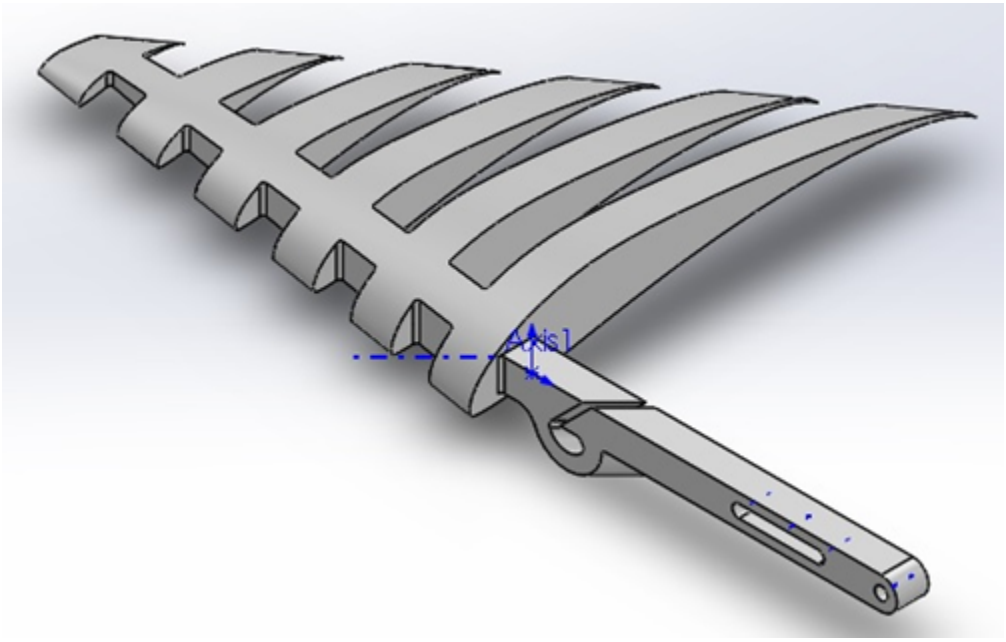

Figure 2.21: Fourth Generation of Wing

compliant joint.

All of these components are housed in a utilitarian body. The body is not intended to appear similar to a bird skeleton, but is designed for the functions the MAV will perform. The two guiding principles for production were keeping a low weight and having sufficient strength to carry equipment needed for its mission. This material includes camera, power supply and a few motors to control the various opponents.

Figure 2.22. Depicted above is the planetary gear assembly selected for the final design. The slot inside of the main arm adds a delay in wing flaps to simulate a gliding effect. The top pin is holds the wing and is held in place by a slot within the frame, transferring the rotary motion in linear motion.

2.8 Tail Design

To chose a simple design of a tail that inspired from nature and will be actuated by a servo. The tail is designed to protrude from the rear of the MAV and rotate in a circular arc. The air flow around the bird will be affected by the tail which will cause the bird to turn. Figure 2.23 shows the

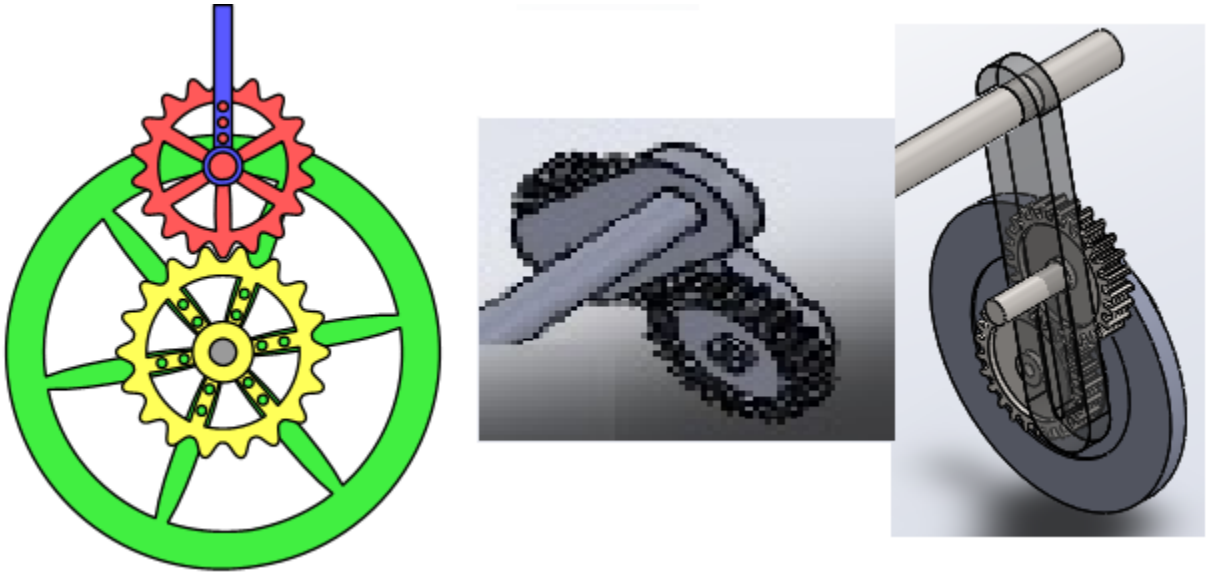

Figure 2.22: Sun and Planet Gear system

tail. Tail Design It is important to make a control for the MAV motion; therefore, it is necessary to come up with a control device inspired from birds. Since the design was based off a bird, it seemed natural to use a tail to control the flight path. In addition, several other models currently available have utilized a tail design effectively.

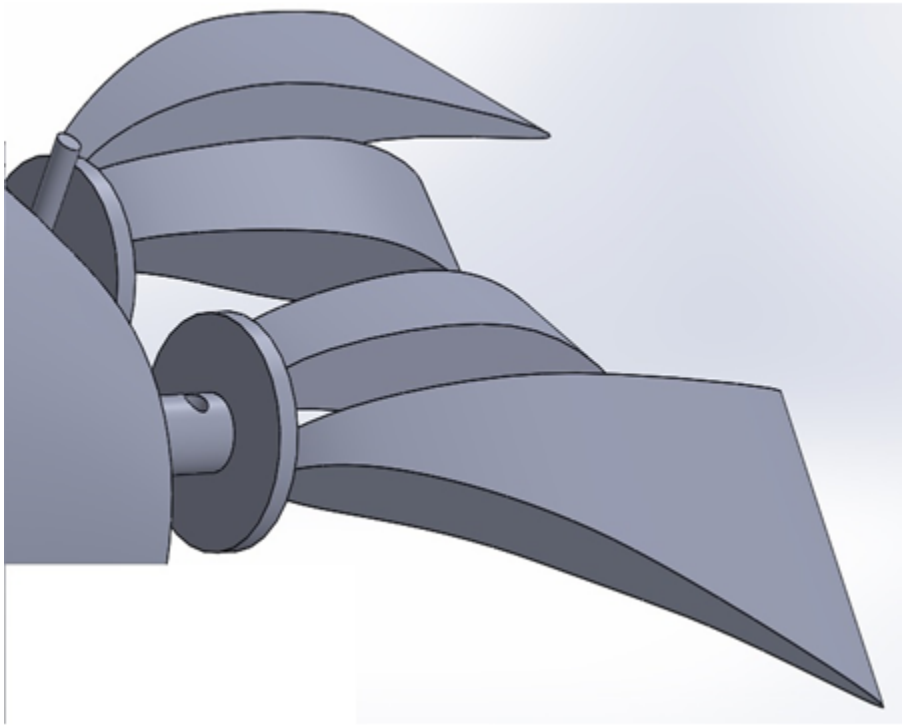

Figure 2.23: Tail Design

Chapter 3

Conceptual Physical Biological Inspired Design of cm-Scale Unmanned Aerial Vehicle

3.1 Introduction

Unmanned Aerial Vehicles (UAVs) research has increased in the past few years. Most of these efforts have been fixed wings or quad copters. Many of these UAVs are designed with military implications in mind. The UAVs present an opportunity for military forces to gather live intelligence on the ground in a more efficient and effective way than previous methods, such as scouts or planes. UAVs eliminate the risk of harm to the soldiers using them since they are isolated from the hostile environment. As the research has increased, the ubiquity of the UAVs has increased.

With the increasing ubiquity of the UAVs, counter measures for the UAVs have been taken. Increased counter measures decreases the effectiveness of the UAVs, preventing the mission from being accomplished. As with all military technology, the offensive weapons advance and the defensive measures adapt to neutralize the threats. The next stage in the reversing advantage of offensive and defensive technology is the Flapping Wing cm-scale Unmanned Aerial Vehicle (FWUAV).

The FWUAV implements flapping wings to replace rotors and other propulsion methods in quad copters and fixed wing UAVs. The flapping wings provide the lift and thrust necessary to

propel the FWUAV in the air. The flapping motion utilized in FWUAVs can be modeled using the biomimicry of animals such as insects and birds. Insects can fly through direct and indirect flight. Direct flight involves the insect flapping its wings using muscles at the base of the wing, utilized by insects such as dragonflies. Indirect flight involves the insect deforming the thorax, causing the wings to flap. Butterflies are one example of insect that uses indirect flight. Birds, on the other hand, have two methods of flight: flapping flight and gliding flight. The flapping flight comes from the up and down stroke of the birds wings to provide lift and thrust. The gliding flight involves no or little motion of the wings where no propulsion is used.

3.2 Design Concepts

3.2.1 Importance of FWMAV Research

In the context of military applications, FWUAVs is the next step of the evolution of unmanned vehicles. Although with a limited payload, the FWUAV will provide military forces with the ability to conduct surveillance and reconnaissance covertly. Other UAVs have become ubiquitous and recognizable to the counter forces of the user. With the recognition, counter forces can neutralize the UAV and prevent the gathering of intelligence. The FWUAV is a less recognizable solution that will provide high levels of intelligence to the military forces to assess and implement tactics. Better tactics will then lower the loss of life in conflict.

The research for the FWUAV sets out to design a FWUAV using 3D parts and commercially available RC components. The purpose of using these components is to make the FWUAV able to be replicable and inexpensive. One of the drawbacks of current UAVs is the expense. The FWUAV proposed will cut down on costs by creating a system that is more inexpensive to buy and replace broken parts. The 3D parts allow for replacement of broken or needed parts in a quick and efficient manner.

The FWUAV sets out to provide the intelligence needed for military purposes of increased knowledge of counter forces and decreased loss of friendly forces. The FWUAV utilizes bio-mimicry to prevent recognition, allowing for functional intelligence operation. With inexpensive replicability, the FWUAV can be used on a wide scale to widen the scope of how much intelligence can be gathered.

3.2.2 Proposed Design Requirements

The design for the FWUAV must meet certain requirements. The requirements are listed in Table 2.1 and expounded in the current section. The requirements involve the parameters of size (length), weight, flight range, payload, endurance, and airspeed. The size required is less than 15cm. The size requirement is set with the size of an actual bird in mind to replicate the shape of bird in flight to disguise the presence of the FWUAV. The weight of the FWUAV must be between 10g and 100g. With the size of the bird, the weight must be balanced. Human made vehicles and wings are not as efficient as bird wings so the weight of the FWUAV must be minimized in order to allow for flight. The FWUAV must carry a payload of 1-18g. The payload can be, but is not limited to, the camera used for the surveillance and reconnaissance purposes. Without the payload, the FWUAV becomes a device that always has to be in sight and does not provide any further information to the user.

The other requirements involve the flight of the FWUAV in the form of range, endurance, and airspeed. The range is set between 1 and 5 miles. The range of endurance allows for the user to be a respectable distance away from the area of interest and gather information for a limited amount of time. The endurance for the design is set at the range of 10 to 60 minutes. The design needs this range to show flight under the current design is sustainable over longer periods of time. It is determined by the battery size, which will create a strain with the weight requirement. The last requirement is airspeed. The desired airspeed will between 5 mph and 35 mph. The airspeed range allows for the range and endurance requirements to be met and for the FWMAV to sustain flight.

The current FWMAV project is a continuation of previous iterations. In order to improve the past design, it must first be analyzed to process its strengths and weaknesses. The primary bodies for analysis are the framing and components. The body and wings of previous are subject to analysis to be applied to future work.

3.2.3 Iteration 1 Design

The Iteration 1 design has taken into consideration the strengths and weaknesses of the previous iterations of the project. The main strengths were the size and general compartment design. The weaknesses laid in the mounting of the hardware, outdated hardware, and ineffective

body design. For the first semester of research, the primary objective was to overhaul the hardware and framing.

3.2.3.1 Hardware

Much of the hardware used in the previous iterations was outdated. The only pieces maintained in the Iteration 1 design were the motor and servo. The motor and servo were still sold commercially and fit the power needs of FWMAV. The battery, receiver, speed controller, camera, and remote control system were all changed to modernize the system so it can be used in the coming years.

The battery was updated to a Great Planes 600mAh 7.4V LiPo battery. The previous battery had a capacity to support a flight time of 5 minutes without the Draganfly camera. The camera would decrease the flight time even further. The battery was increased from 300mAh to 600mAh to reach the design requirement of 10 minutes of flight time. The drawback is that battery capacity is linear to the weight so the increased capacity almost doubled the weight of the battery.

The Berg receiver of the previous designs was updated to the Spektrum AR610C 6-CH receiver. Advances in RC technology made the change necessary. The Berg receiver used crystals that were programed to a certain frequency and channel. FWMAVs with the same crystals would not be able to fly in the same area and would malfunction and crash. The receivers have moved to a digital configuration where each receiver is linked to a single transmitter. All of the receivers and transmitters use the same frequency but have their own channel when linked. This advance in technology makes it so hundreds of FWMAVs can fly in the same area.

The speed controller was updated from the Thunderbird 6 to the Thunderbird 9. The change was made due to obsolescence. The Thunderbird 9 has an increased maximum current capacity, increasing the factors of safety for the FWMAV. The output of the battery is maximum current of 6A, so the increase in current capacity prevents failure at full potential operation.

The camera and camera system were updated since the Draganfly Eyecam is no longer commercially available. The camera was updated to the VA2500 FPV camera. The camera operates on 5.8GHz so there is no interference with the 2.4 GHz transmitters and receivers. It also has an attachment to connect with the receiver in order to receive power. The previous Draganfly camera had to be adapted for connection to the receiver. The VA2500 is compatible with the headsets, so a screen is not necessary to connect with the receiver. The headset chosen was the Spektrum

Teleporter V4. The headset provides a clear, live picture from the camera and is compatible.

For compatibility to the receiver, the transmitter was updated as well. The previous Tactic headset required crystals that transmitted to a channel, not a certain receiver. The transmitter was updated to the Spektrum DxE. The DxE links directly with the individual receiver and boasts a similar range to the Tactic transmitter.

All of the electronic hardware used is Spektrum brand. Spektrum was chosen because of its price and quality. The parts are relatively inexpensive, allowing for large scale production at a reduced price. Same brand electronics allowed for simple and efficient integration of the system to ensure compatibility. The active components are all electronic and allow for multiple FWMAVs to operate in the same space.

3.2.3.2 Frame

The previous design of the framing comprises one solid body to house all of the electronic components. The main concept of the design is the same with the effort of reducing the volume of material. The drawback is that the frame loses the functionality of the housing the components. The cavities in place were removed to save on the volume but at the cost of functionality needs redesign.

The frame for the FWMAV was designed with the component integration and assembly as the main priorities as shown in Figure 3.1. The design for the frame is segmented instead of the solid frame as laid out in the previous design iterations. The body was chosen to be segmented to make it a simple process to replace components.

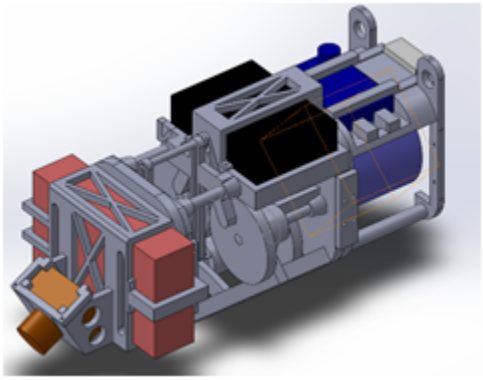

Figure 3.1: Iteration 1 Full Frame Iteration

With the Iteration 1 design, an isolated failure will not result in a complete replacement as it would have in the previous design iterations. All of the hardware components are also connected through hardware. By securing the components, vibration is minimized and the performance of the FWMAV is increased. Remform screws for plastic threading are used. The threading screws are used because of the small size of the FWMAV. The holes in the plastic are so small that the tolerances are too great for plastic threading. Plastic threads are also fragile, so there would be a larger chance of failure.

The design for the frame is broken up into three sections. The first section houses the camera and the battery as shown in Figure 3.2. There are plates that attach with the screws to the section to secure the components in place.

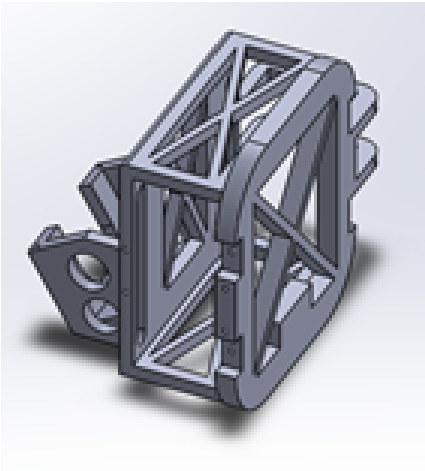

Figure 3.2: Front Section of Iteration 1 Frame

The next section houses the gearbox, flapping crank slider, and the receiver as shown in Figure 3.3. The sections connect between the front section and the gearbox section through the use of plates with 4 screw holes on each side. The panel on the front of the gearbox section and the cavity for the receiver are meant to reduce the volume of the frame. The cavity for the receiver also incorporates slots to allow for the wires of the receiver. The previous iterations treated the components are rectangles with no spaces made for the wires.

The last section houses the motor, the speed controller, and the servo as seen in Figure 3.4. The runners on the bottom are meant to create structure while minimizing the volume needed for the part. There are parts on the top to allow for the integration of the tail. The back also has

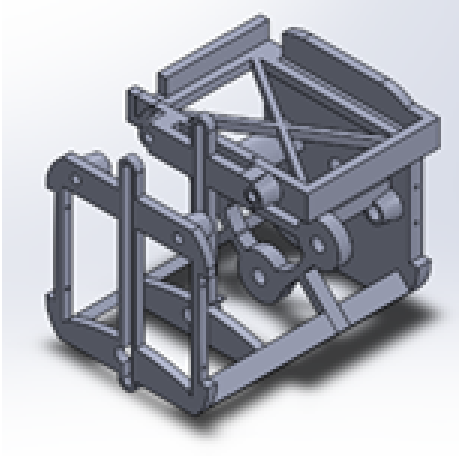

Figure 3.3: Gearbox Section of Iteration 1 Frame

screw holes to allow for attachment to the frame. By providing the connection points, the frame will not bounce around the body when in flight. The servo and the speed controller are held in place through the use of prongs that go over the speed controller and are held in place by screws that use the connection points provided by the servo. The motor is held in place through the use of the screws provided with the motor. The motor is attached through the front of the last section.

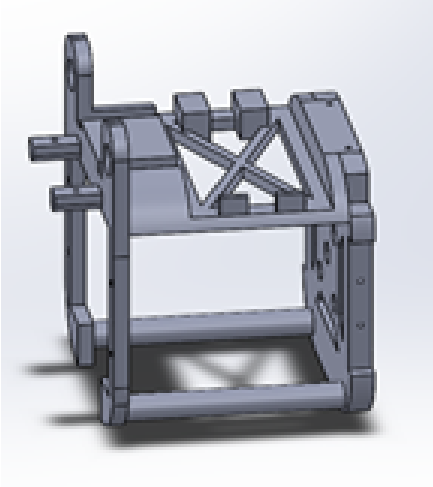

Figure 3.4: Iteration 1 Back Section of Frame

The total length of the fame is about 13 cm. The Iteration 1 design reduces the space used for the gearbox but also increases the space needed with the increased capacity of the battery.

The length falls within the design requirements, but the body is also needed to form the full bird. The design has also reduced the weight of the previous designs to account for some of the heavier elements of the Iteration 1 design, including the increased capacity of the battery.

3.2.3.3 Body

The frame for the FWMAV was designed with the components in mind. By working from the inside out, the body was designed to house the frame and its components. Each contour of the frame was considered to be a secure and attached housing. The previous designs did not allows for the frames integration but simply wanted to create an outside shape. The Iteration 1 body was created after research into the thrush body structure, size and proportions. The Iteration 1 body is a comparable size to actual thrushes but is oversized compared to the design goals. It is 24 cm long, but at the height the bird will fly the bird will not be conspicuous based on the body design. The design can be seen in Figure 3.5.

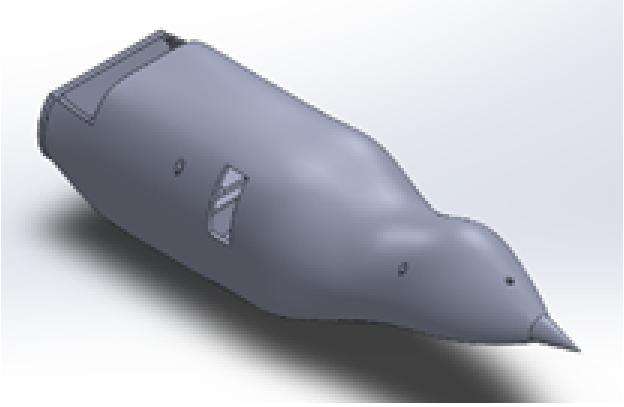

Figure 3.5: Iteration 1 Body Design

The design has connection points built in to be installed with screws. This method was chosen because the screws would result in easy installation and disassembly. The tight fit of the screws also allows for the assembly to be held tightly together to prevent the vibration of parts. The bottom is designed for the frame to be set inside.

3.2.3.4 Wings

The Iteration 1 wing design is an idea based on the flight of birds. Bird feathers change orientation during the upstroke to minimize the drag. Birds contour their feathers like a hinge to allow for the passage of air. The Iteration 1 design has three flaps to mimic the feather behavior of the birds and can be seen in Figure 3.6.

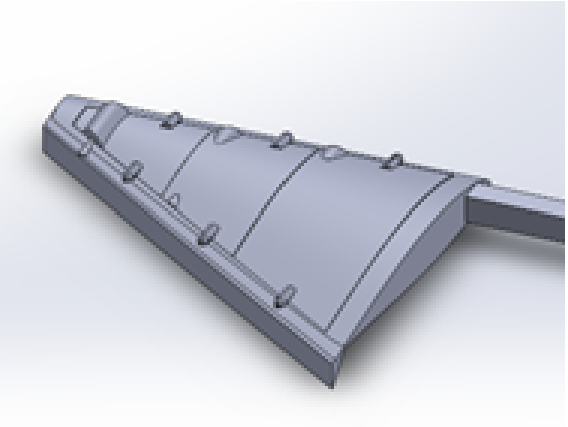

Figure 3.6: Iteration 1 Covered Wing Design

In discussion, the wings were determined to be too heavy. As large of a concern as weight is for a FWMAV, the wings failed that criteria. In the future work for the wing design, there are a few ideas that will be considered in the design. The wing profile will continue to be that of low Reynolds number applications. One idea that will be explored is holes in the wings to create channels. As stated in the Literature Review, Jones et al. designed a wing with channels and decreased the drag coefficient in a fixed wing. Another idea to be explored is the use of turbulators. The turbulators will prevent the laminar separation bubbles from forming, decreasing the drag coefficient. Each of these ideas will be investigated in tandem and separately to explore how they will affect the lift and drag of the wings.

3.2.3.5 Flapping Mechanism

The last portion of the design is the flapping mechanism. The flapping mechanism designed for the frame is similar to the first flapping mechanism in the Previous Design section. The difference is that there are two gears for the flapping motion. Each of the gears, as shown in Figure 3.7, will

have a crank for the same crank slider to ensure that the slider is working properly by creating multiple points of contact.

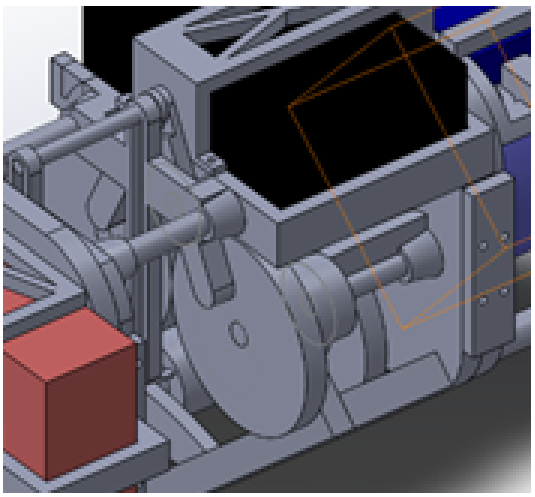

Figure 3.7: Focus on Gearbox Mechanism

The positioning for the gears was determined using the computer program MatLAB. The design wanted to test the effect of moving the long shaft with the final step gear on the other gears positions. A gear system that was strictly vertical was not possible because the gears would interfere. The results in Figure 3.8 show this. The angle was minimized in the deviation from vertical to prevent a shifting from the center of gravity and departure from the circular frame envelope.

3.2.4 Iteration 2 Design of FWMAV

Although there were merits to the design of Iteration 1, a second iteration of the design was necessary due to the inherent flaws of the original design. The first major flaw was the thickness of the printed parts. The parts were entirely too thin and were broken with the slightest pressure. They were broken so quickly that the prototype was unable to be tested. The holding areas of the parts were intact after the breakages so it could be tested as to whether they fit or not. After examination, all of the parts except for the camera fit as expected. The camera did not fit as expected due to the case that could not be removed adding to the dimensions. The tolerances on the 3D printers used also resulted in issues. The original screws that were selected were small in an effort to reduce the weight of added hardware. The tolerances in the 3D printer were too large and did not facilitate a

Figure 3.8: MATLAB Results on Gear Location Determination

possibility of using the desired screws.

A second iteration was also necessary due to simulation of the gears in FEA. The step from the motor gear to the first gear in the gear train would have resulted in failure. The selected gears were anodized metal with no given material properties, so it was modeled using the aluminum alloy properties available on the software. The maximum stress that was found was a factor of ten above the yield strength of the motor pinion gear. The gearing system also utilized the full rpm output of the FWMAV to reach the final step down. This was not an entirely realistic assumption due to the real world losses from friction and other factors such as the gears meshing perfectly. The larger gears also added weight that would need to be conserved with the large weight impact of the components already present. While the first iteration was aggressive in material reduction in order to meet the requirements in the Design Requirements section, the second iteration is more conservative to allow for bench top testing of the components to prove feasibility.

The Iteration 2 design proved to be rugged and durable, making it a good candidate because

of the nature of the use of the FWMAV. The new design also had a length of about 12.5 cm, making it a comparable size to Iteration 1. The changes would not impact the total body shape of any redesigned body.

Although time ran out for the project, the next step of the design process for Iteration 2 would have been the body of the FWMAV. The body would have been designed with minimizing the number of parts needed to complete the entirety of the FWMAV. The body would have been designed in order to encompass the frame in a way that no additional components would need to be designed to hold the hardware components in place. As listed below, the tolerances for all of the hardware were extremely tight, so all that would be needed is close support from the body to ensure that the hardware components remain in their proper places during operation.

3.2.4.1 Frame

The major changes in the design came from adjustments that were made to the frame. The major changes made to improve the design were thickening the walls between each section and replacing the panels on the side with small tabs that linked for the insertion of a screw that can be incorporated into the body of the FWMAV.

Many of the walls in the previous iteration were 2mm thick. With the capabilities of the 3D printers and materials used, this proved to be ineffective in holding structural integrity in the face of any forces. The walls were thickened to 4 mm in order to provide the required support. The added thickness provided for positive results in that the frame did not fail under the slightest pressure like its predecessor.

The tabs instead of panels were a minor change to the design that had a profound total effect. With the tolerances unable to handle holes the size of an M1 screw, it was tested to determine whether the holes for an M2 screw would have the desired effect. The holes could be formed, but the necessary screws would be much longer than the previous screws. The screws would not be able to be inserted horizontally as before as it would create interferences. The tabs were squares of dimension 5mm with a 2 mm thickness. There were a total of 3 tabs for each side of each connection so that when a nut was applied, it would provide the proper pressure in order to hold the frame parts together. The frame itself and the new tab set up can be seen in Figure 3.9. The tabs provide another advantage of reducing the number of parts that are necessary to construct the frame.

Starting from the front, there were some design changes. In the first iteration, one of the

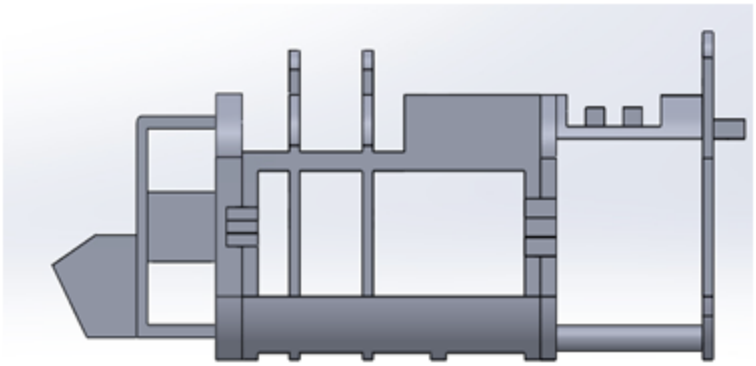

Figure 3.9: Iteration 2 Design of the Frame

prominent features was a set of prominent cut outs that would reduce the weight of part. These cut outs were removed in order to restore the structural strength of the part. In the previous iteration, these broke extremely easily and were one of the main sources of failure. The second iteration of the front section can be seen in Figures 3.10A and 3.10B. One of the advantages of the new frame is the tolerance for the battery. The battery slid into place with ease but the frame had a good hold that prevented movement. There were issues with the camera fitting into its designated slot. The distance between the supports was increased but not to the degree that was needed. This could be solved with simple steps taken in SolidWorks in the following stages of the project.

The next frame working backwards is the gearbox section. This was a serious redesign due to the simulation gearing results for the Iteration 1 design resulting in failure to a factor of 10. The first change was going from the flapping gears to reverting to a gearing system similar to the original designs. While the flapping gear set up was ambitious, it ultimately proved to be fruitless. It added unnecessary weight from the size of the gears. It was also set up to run at full capacity of the motor.

The gearing system was then adapted to reach the proper flapping frequency as outlined above while decreasing the load on the motor. The gearing was designed to utilize the motor at a three-quarter capacity so the stick could be moved to compensate for losses that are inherent in a real-life operation. FEA analysis was conducted using the capabilities above in order to test whether failure will happen. The results are outlined in Figure 3.11.

The gears were selected to be the same ratio for both of the stages, so only one set of FEA analysis had to be conducted. The highest stress that the gears faced was on the factor of 104 Pa where aluminum will fail at the factor of 108. The margin of error that would result in failure is so

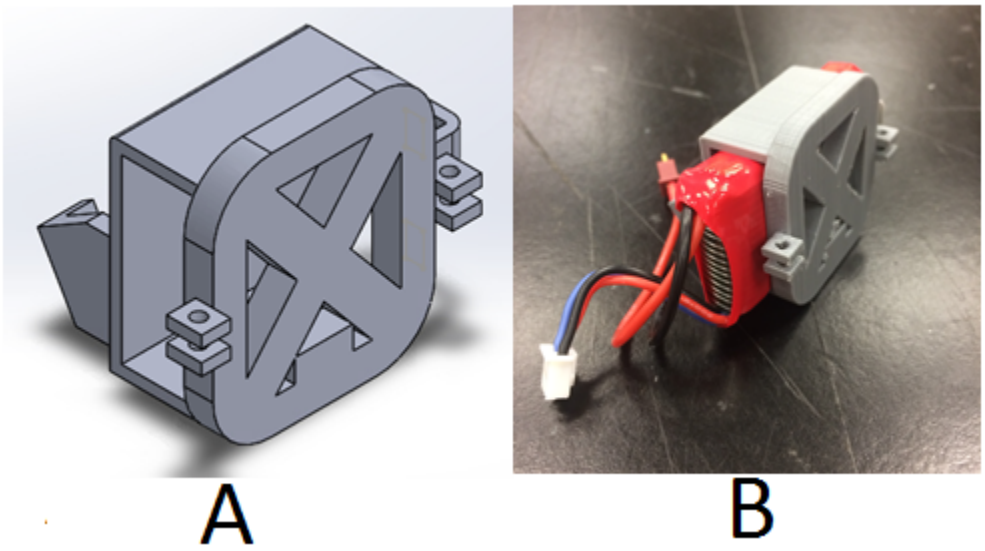

Figure 3.10: A)Solidworks Rendering of Front Section and B) Printed Part with Components

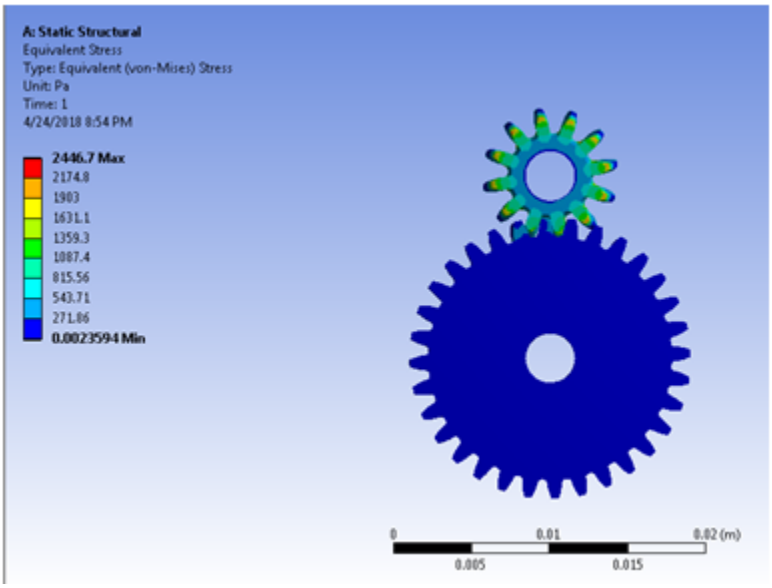

Figure 3.11: FEA Analysis of Iteration 2 Gearing

large that it can be confidently stated the new gearing system would be adequate.

Another advantage of the new gearing system comes with the crank slider system. The PLA 3D printed parts are lighter than aluminum so the crank slider wheels can be larger than the gears. Then, the size of the flaps is not as limited and can easily be adapted and controlled fort he desired

attributes.

With the new gearing system in mind, the actual gearbox was amended in order to follow through with the changes. One of the major issues with the Iteration 1 gearbox was that the slider slot was extremely thin and broke easily. The slot was reinforced to prevent this issue from happening with the Iteration 2. Parts of the gearbox also had to be redesigned to reflect the changes made in the gearing. These changes can be seen in Figures 3.12 and 3.13. Figure 3.13 also shows the printed part and the receiver inserted to test compatibility. The receiver fit inside the gearbox section with a tight fit. The receiver was difficult to remove, showing how precisely the holding area was designed and toleranced. As noted earlier in the Iteration 2 design section, the lengths of the two iterations are about the same. With Iteration 2 having thicker walls, the length had to be made up in some way. By reducing the gears from three stages to two, the added length from the thickness is removed to balance them out.

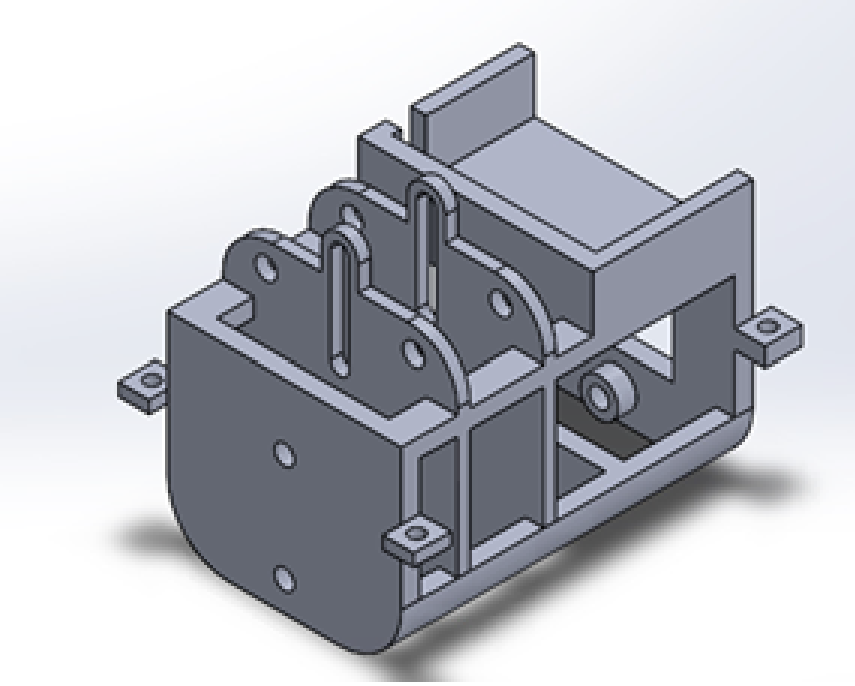

Figure 3.12: 3D Solid Model rendering of Iteration 2 Gearbox

The walls in the middle of the gear box are to hold the gear shafts in place and provide that extra support that was desired in the Iteration 2 design. The walls could be reduced further in

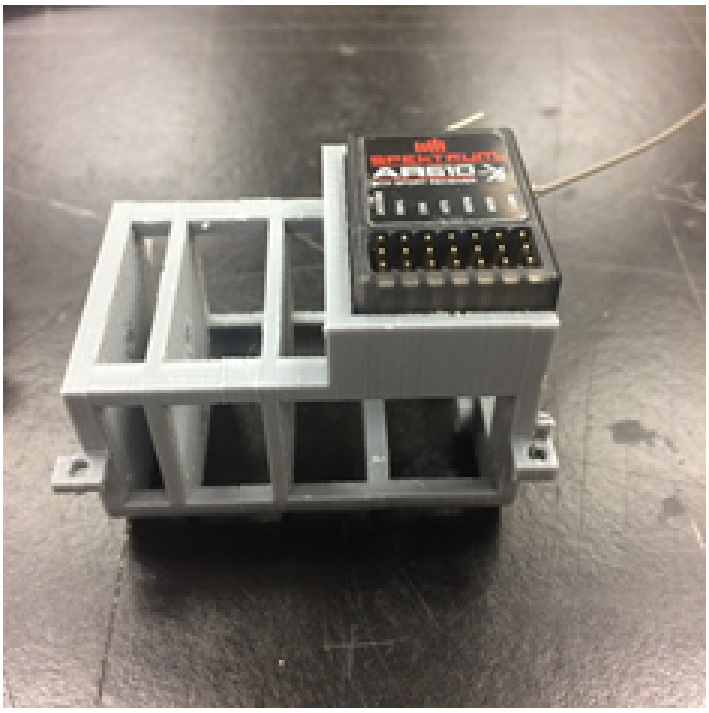

Figure 3.13: 3D Printed Gearbox with Receiver

order to reduce the weight of the part and in an Iteration 3 would most likely take place.

The final section of the frame that required redesign was the back section. The changes made to the back were minimal. The main changes simply came in the form of thickening the part that connected to the gearbox. This was thickened in order to reduce the likelihood of breakages. The hole for the motor shaft was also increased slightly because the motor shaft was unable to fit in the original hole. This was due to a tolerancing issue that was promptly dealt with. The design changes can be seen in Figure 3.14 for the SolidWorks rendering and in Figure 3.15 for the printed version. The motor fit extremely well into the proper hole, but the hole size could be increased some in order to accommodate free rotation while in operation without friction. Although not pictured in the figure, the servo also fit into its slot in the back. At the time of writing, there were no designs for the tail, so the circular holes on the very back are not proportioned to where they would accommodate such components.

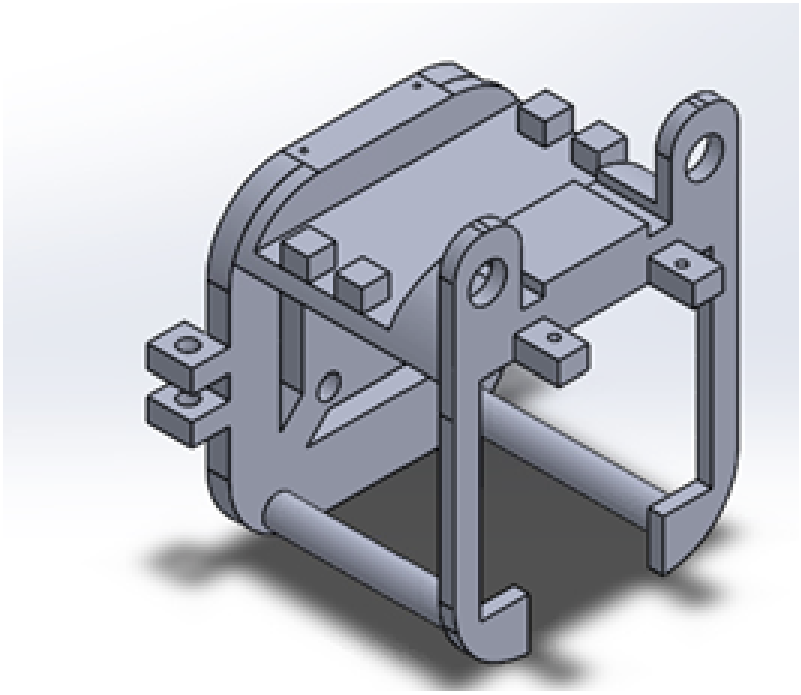

Figure 3.14: SolidWorks Rendering of Back Section

3.2.4.2 Wings

The wings were the last area of interest that were redesigned. The first iteration had wings that were much too heavy for flight and attempted to use flaps to minimize the drag on the upstroke while maximizing the area on the down stroke to achieve the lift necessary for flight. The same low Reynolds number airfoil was used for the second iterations design. The design, in simplest explanation, was the same but with the flaps taken out to yield a wing with a gap in it. This wing can be seen in Figure 3.16. This would not be the final form of the wing because it would provide no lift for the FWMAV. Instead, the wing would be covered with material. The material would drop the total weight of the wing, lowering the required lift to sustain flight while keeping the lift the same as before.

Although it has not been put into experimentation, one concept was to use bistable carbon fiber sheets to cover the wings. The hypothesis behind this decision is that the bistable material would deform on each stroke in a manner that would maximize the lift and minimize the drag. This would lead to improved results than those that are seen in the computer simulations. Overall, it

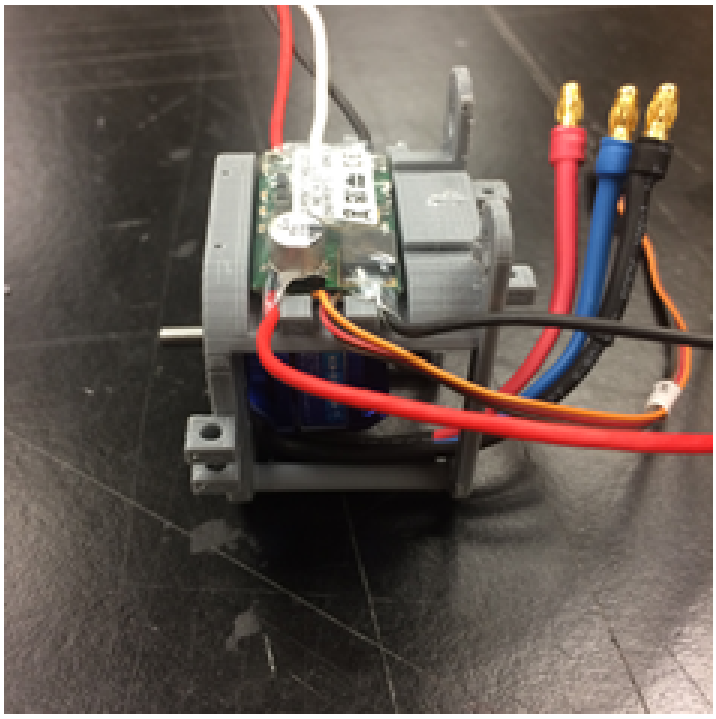

Figure 3.15: 3D Printed Model with ESC

is hoped that the wings would have the double effect of decreasing the forces necessary to achieve and sustain flight, while maximizing the flapping characteristics of the FWMAV. Future work on the project will eventually confirm or disprove this theory.

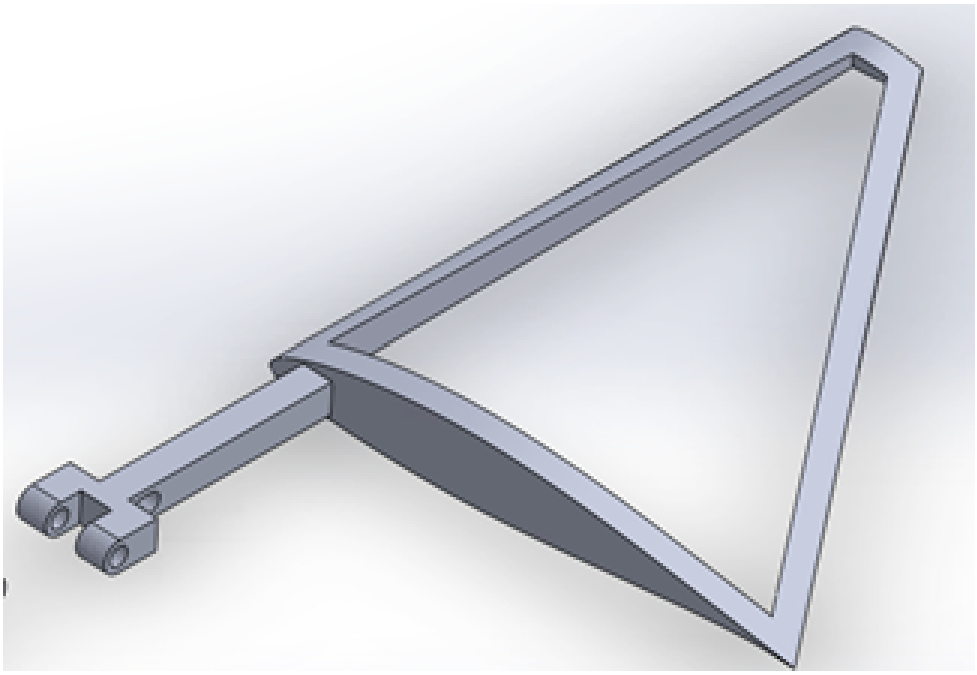

Figure 3.16: Wing Design with Cutout

Chapter 4

Preliminary Computational Fluid Dynamic Analysis for 2D Flapping Wing of cm-Scale Unmanned Aerial Vehicle at Low Reynolds Numbers Regime

4.1 Introduction

In this chapter, we present a new approach for the development of flapping airfoils of flapping wing Micro Aerial Vehicle (FWMAV) by using two different airfoils. The approach is based on applying force at trailing edge of the airfoil to produce flapping airfoil at low Reynolds number laminar flow regime. By implement fluid structure instruction (FSI), which is a flow pattern is the von Karman vortex street that can form as fluid flows past a flapping airfoil structure and monitoring the vortices which may induce vibrations in the flapping airfoil. The proposed research originated from previous studies on the response of nonlinear systems involves a fluid-structure interaction where the large deformation affect the flow path. The magnitude and the frequencies

of the oscillation generated by the fluid around the structure is computed and compared with the values proposed by (Turek et al, 2006[64]). Specifically, it was shown that, the magnitude and the frequencies of the oscillation generated by the flluid around the s1223 airfoil is better than NACA0012 airfoil.

4.2 FLUID-STRUCTURE INTERACTION

The deformation of natural wings results from the interaction between forces imposed by the fluid surrounding the wing, the wings material properties (e.g. mass and stiffness distributions), and the actuation of the wing. When an animal, such as a bird, does possess intrinsic wing muscles, these forces passively interact to produce the spatial and temporal patterns of wing movement and shape. Inertial forces result from the resistance of the wing to changes in its velocity; aerodynamic forces result from the fluid surrounding the wing; and elastic forces govern the deformation of the solid wing and connecting structure that is subject to these body and surface forces. The complex interactions between these aerodynamic and inertial/elastic forces essentially define the field of aeroelasticity [65]. However, we do not yet have a clear understanding of the principles that govern the mechanical design of flexible wings for the dual role of efficient propulsion and inertial sensing. This issue is a primary motivation for the research undertaken here.

The coupling of the inertial/elastic forces with the aerodynamic forces can in some circumstances lead to an instability that can destroy the structure (e.g. flutter), much like the famous example of the Tacoma Narrows Bridge [65]. Thus, understanding the aeroelastic nature of animal wings may not only inform the biological principles behind wing compliance but might also provide design criteria that can be applied to improve engineered systems. However, since birds have different wing flexibilities and actuation frequencies depends on wing size and speed of flapping, it can be difficult to extract the biological principles that govern the use of flexible wings in the birds flight.

In this paper we focus on fluid-structure interactions focuses on how the structural and fluid dynamics of and around a wing change with actuation frequency and airfoil flexibility. Through the development and analysis of a computational model of a two dimensional airfoil at laminar flow, we found that fluid forces do not dramatically change airfoils shape and thereby modify flight forces (i.e. the deformation in airfoil is dominated by the actuation of the airfoil structure, not the fluid loads imposed upon it).

So, considering the fluid flow around the airfoils to be compressible, the equations used by the solver are Navier Stokes equations as shown below:

$$\rho(\frac{\partial u_{fluid}}{\partial t}) + \rho(u_{fluid} \cdot \nabla)u_{fluid} = \nabla \cdot \lceil -PI + \mu(\nabla u_{fluid} + (u_{fluid})^T) - 2/3\mu(\nabla \cdot u_{fluid})\rceil I + F \quad (4.1)$$

$$\frac{\partial \rho}{\partial t} + \nabla \cdot (\rho u_{fluid}) = 0 \quad (4.2)$$

$$\rho(\frac{\partial^2 u_{solid}}{\partial t^2}) - \nabla \cdot \sigma = Fv \quad (4.3)$$

Where, the velocity field components $u_{fluid} = (u_{fluid}, v_{fluid})$ and displacement field components $u_{solid} = (u_{solid}, v_{solid})$. In general there is no a specific known analytically solution for the Navier−Stokes equations, but by using the vicinity of critical points in the flow to derive the local solutions. In other hand, the flow is characterized by low Reynolds number which is given by:

$$R_e = \frac{\rho u_{fluid} L}{\mu} \quad (4.4)$$

4.3 Simulation solution

When modeling a fluid structure interaction FSI model, we have to simplify the complexity in model to reduce the computational tax, so there are many assumptions must be settle down. To simulate the fluid structure interaction, the model includes the physics for every steps of the structure in the simulation. Therefore, the model geometry contains the airfoil inside open domain [10] as in figure 4 [64].

The dimension of open domain is (1 m height and 2.5 m long). the structure of flapping airfoil is composed of a fixed Roller (circular domain) inside the airfoil with 0.003 m radius and the center depend on the airfoil located and shape here centered at (0.42,0.5). The length of the airfoil chord is 0.1 m, both of airfoil and the roller made of elastic material as in figure 5.

On acquire the sharp trailing edge, NACA0012 airfoil is marginally modified starting with its unique shape [66].

$$y = \pm c*0.594689181*(0.298222773*\sqrt{\frac{x}{c}} - 0.127125232*\frac{x}{c} - 0.357907906*(\frac{x}{c})^2 + 0.291984971*(\frac{x}{c})^3 - 0.105174696*(\frac{x}{c})^4) \tag{4.5}$$

is used to create an airfoil between x=0 and x=1.008930411365 and (c) is the chord length. For s1223 airfoil use data file and the rescale to appropriate position . The air enter the wind tunnel as a parabolic velocity profile in the left side with mean velocity of 5 mile/hr (2.235 m/s) and assumed to be fully developed. Sometimes would require to increase the distance between the flapping airfoil and the inlet condition to prevent the effect of inlet velocity condition on the flow pattern.

$$U_o = 1.5\bar{U}\frac{y(H-y)}{(\frac{H}{2})^2} \tag{4.6}$$

where $\bar{U}$ is the wind velocity, U_o mean velocity and H is the width of tunnel Use step function for a smooth increase in velocity profile in time Eq (2) become

$$U_o = (1.5 * 2.23[\frac{m}{sec}]\frac{y(1[m]-y)}{(\frac{1[m]}{2})^2}) * step1(t) \tag{4.7}$$

The outflow condition set up in right side of the tunnel with zero pressure because it is far away from the airfoil and there is no effect on the structure. Also, assume there is no backflow in outflow to prevent the air from entering the domain through the boundary. Set no-slip condition on the upper side and lower side of the tunnel boundaries for the fluid. To make sure the inlet condition is laminar we used Glycerin but for air by using laminar flow. The properties of flapping airfoil, Glycerin and the air as in table 4.1 below:

4.4 Mesh Geometry

Meshing a geometry is an essential part of the simulation process, and can be crucial for obtaining the best results in the fastest manner. After creating a model, the mesh used in NACA0012 airfoil and s1223 airfoil to a Physics-controlled mesh, for far field required an extra coarse mesh element size. While close to the structure, the mesh is very refined to minimize singularities during the solver. The mesh generated showed that the combined mesh extra coarse and very fine mesh (structure and around structure) as shown in figure 4.2. Lowering the minimum element size in

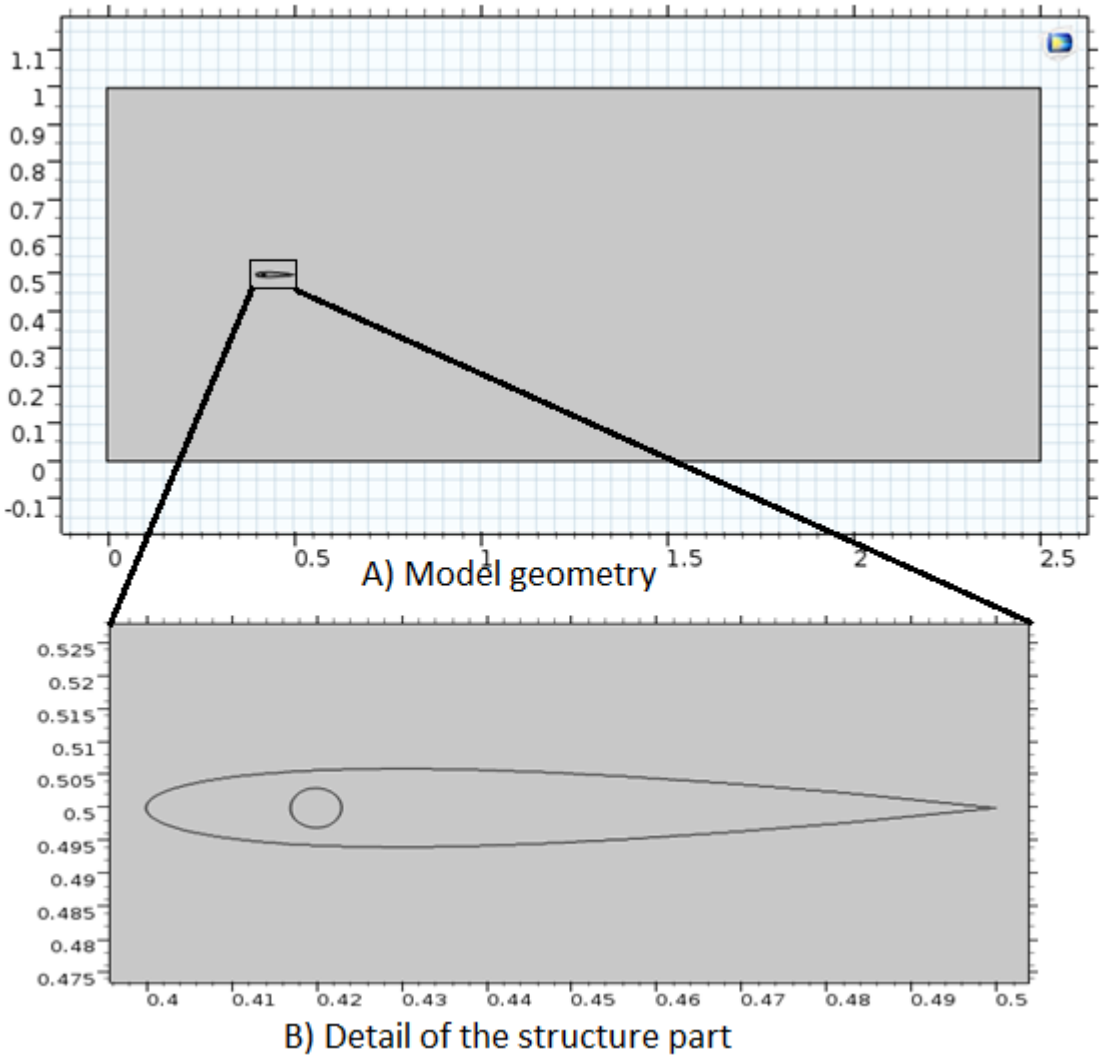

Figure 4.1: A) Model geometry and B) Detail of the structure part

mesh that is computationally taxing. The mesh for every airfoil and the tunnel as below in table 4.2.

As shown in Figure 4.3, for the structural analysis, the multiphysics aspect of the problem and the desire to simultaneously solve the fluid and structure problem proved demanding, but the fluid-structure interaction module handled these problems properly and efficiently with the default segregated solver settings, with minor modifications to the geometric multigrid solver. The fluid-structure module employs the previously mentioned Navier Stokes equations coupled with a solid stress-strain physics module. The free mesh utility had trouble dealing with some of the structures

	Value
Air	
Fluid Density	1.123 K_g/m^3
Dynamic viscosity	$1.8 * 10 - 3$ $Pa.s$
Glycerin	
Fluid Density	1260 K_g/m^3
Dynamic viscosity	1420 $Pa.s$
Airfoil Properties	
Young's modulus	5.6 MPa
Material Density	1000 K_g/m^3
Poisson ratio	0.4

Table 4.1: Fluid and Airfoils properties.

	NACA 0012 Airfoil	S1223 Airfoil
Triangular elements	9380	1398
Quadrilateral elements	532	202
Edge elements	350	131
Vertex elements	10	10
Number of elements	9912	1600
Minimum element quality	0.3322	$2.502 * 10^{-4}$
Average element quality	0.9068	0.8135
Element area ratio	$2.6438 * 10^{-5}$	$2.509 * 10^{-5}$
Mesh area	$2.5m^2$	$2.5m^2$
Maximum growth rate	2.359	2.688
Average growth rate	1.261	1.523

Table 4.2: Mesh for Airfoils and tunnel

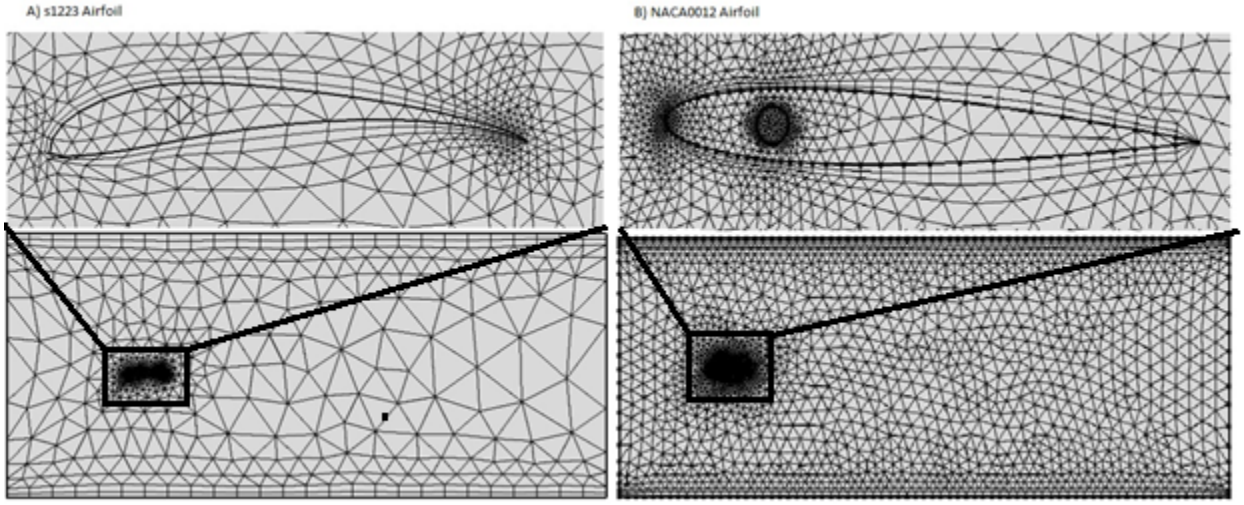

Figure 4.2: Mesh geometry around A)s1223 Airfoil and B)NACA0012 Airfoil

areas with more curvature and an automatic mesh hierarchy could not be readily achieved. This was resolved by building specific mesh cases but computing times are found to be quite sluggish for some of the geometries. The comparison between meshes types generated by COMSOL Multiphysics shows extra fine mesh best for Airfoil structure.

4.5 Results and Discussion

4.5.1 Velocity Field

In the present analysis, the velocity field are analyzed at different angle of attacks (-2, 0, 2, 4, 6, 8, 10, 12, 14 and 16) as shown in figure 4.4. In Figure 4.5 shows the von Mises stress in the NACA0012 flapping airfoil and the velocity field for angle of attack 0 at four different time. At time 2 sec the trailing edge up so, the pressure on upper side higher the lower side of airfoil that's mean the lowest lift produce at this position, another thing the leading edge at low position which help to push the fluid behind the airfoil. At time 3 sec second picture in figure 4.5 the trailing edge at low position down, so the pressure at lower side is higher than the pressure at upper side of airfoil which mean high lift and the leading edge of airfoil at high position up which help the more fluid move below the airfoil. Continue with third picture in figure 4.5 when the airfoil become at straight position, the air divide on the upper and lower sides of airfoil. And From Figure 4.5 note that the

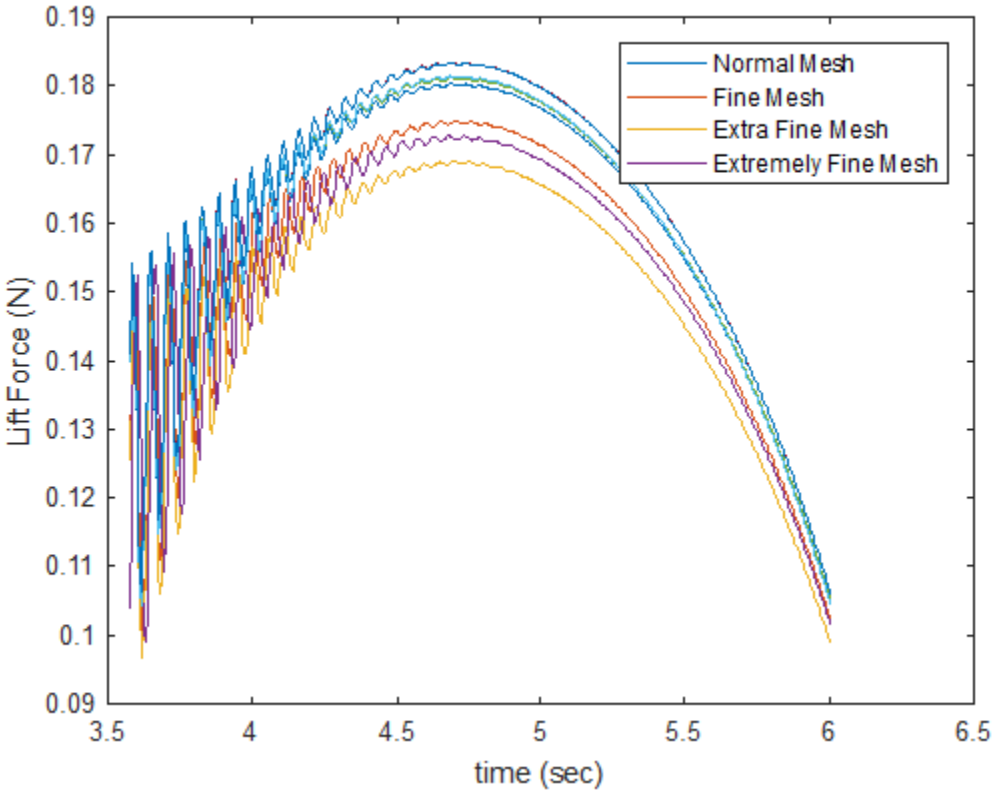

Figure 4.3: Comparison of computed force components on the airfoil using different mesh sizes

fluid wake behind the airfoil induces a large oscillations in the solid protruding from trailing edge of airfoil. In other hand, the stagnation point obviously seen on the leading edge because the flapping, the location of stagnation point change when the location of leading edge change. Also, in laminar flow there are separation and contact points but in this study, note that there is no separation point around the flapping airfoils because a laminar separation occurs closed to the leading edge which provokes a transition followed by a rapid turbulent reattachment, so, despite the relatively low Reynolds number, the flow is turbulent on the entire flapping airfoil. So, thats mean the flow cover the airfoil and the von Karman vortex street past the airfoils, which will be essentially deformed and influences those stream field. The only separation point can clearly be seen in the trailing edge as shown in Figure 4.5. In additional, observed a vortex shedding around the trailing edge of both airfoils. In other hand pressure distribution around the flapping airfoil, Max/Min surface and total displacement at different time steps. The change in pressure around the flapping airfoil produce a

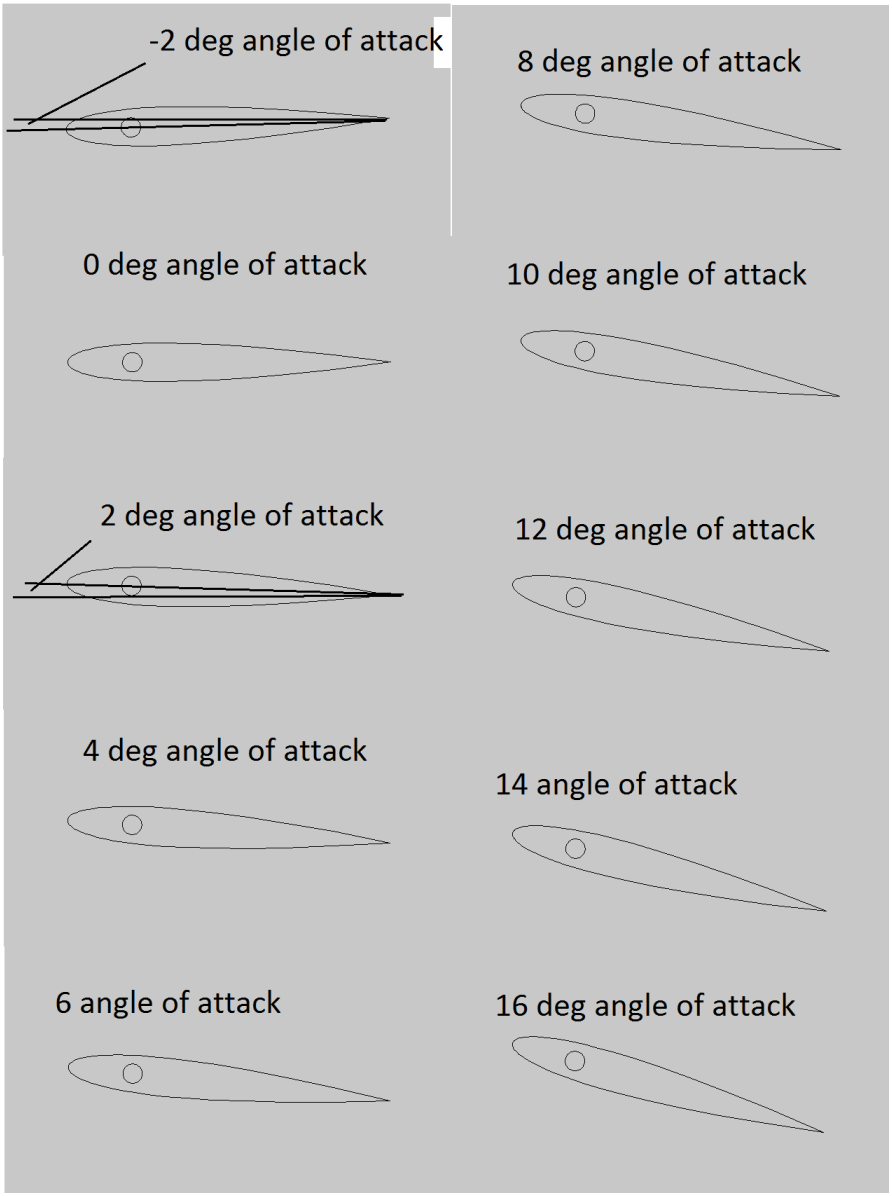

Figure 4.4: NACA0012 airfoil at different angles of attack

forces Lift and Drag. These forces evaluated by the difference between the upper surface pressure and the lower surface pressure.

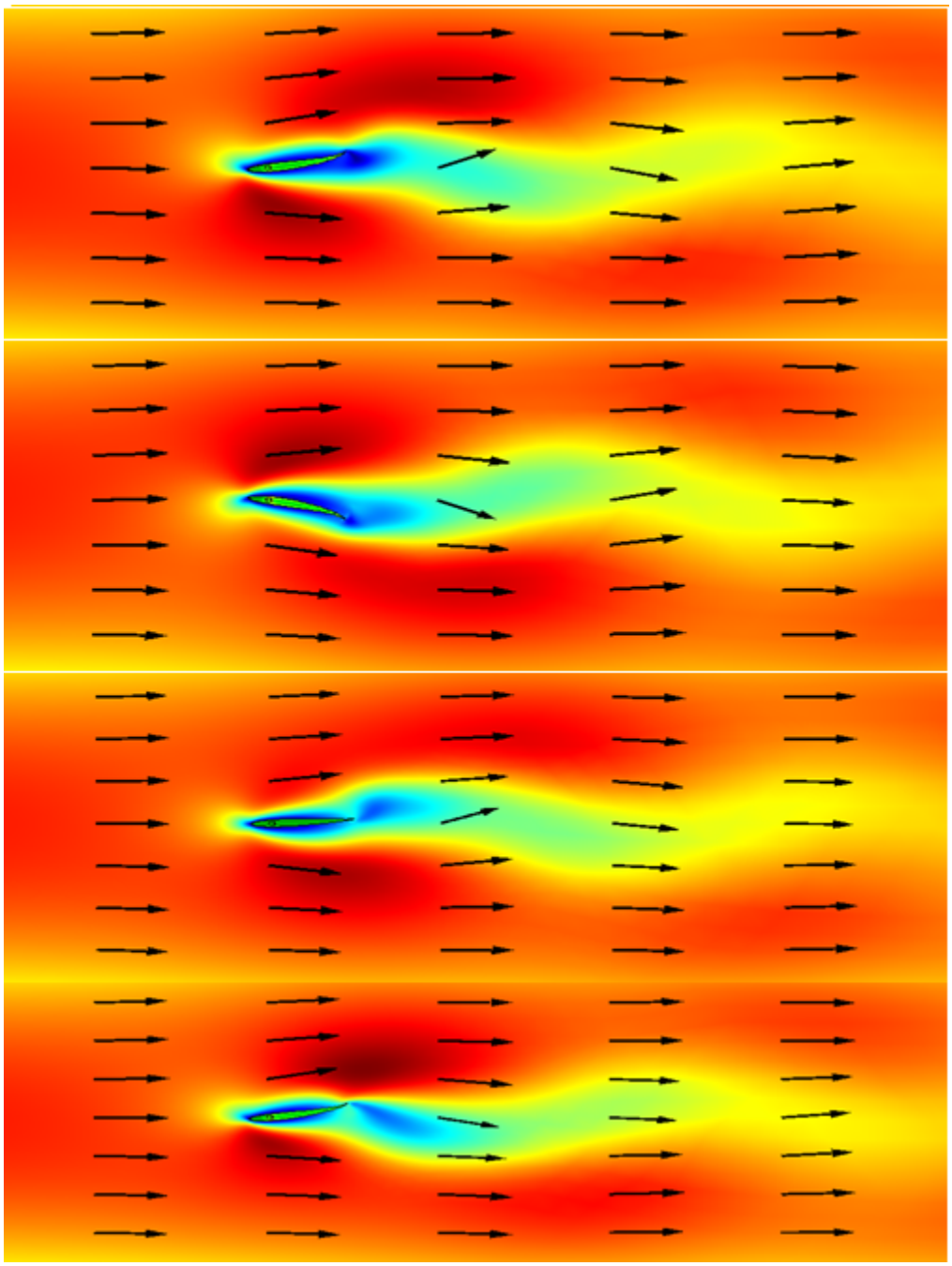

Figure 4.5: von Mises stress in structure and Velocity field in Air for four different time steps at angle of attack 0

4.5.2 Wake structure

The CFD results were used to visualize flow features. Results obtained at 5 mph at 0 angle of attack were qualitatively similar to those for (2,4,6,8,10,12,14 and 16). In Figure 4.5, a series of helicity contours are shown for each flap studied at 5 mph. Helicity values were analyzed from the instantaneous flow field for the last time step computed in the CFD analysis. Planes within each of the four flap series were taken at 0 angle of attack along the airfoil field, and were continue to be displayed behind to the trailing edge of airfoil.

An angle of 0 degrees and small movement up and down represents the leading edge of the airfoil, while trailing edge represent the top and bottom of the airfoil, respectively. At this position, we observed a clockwise (as viewed from behind the airfoil) vortex coming off of the trailing edge of the wheel, and a counterclockwise vortex coming off of the leading edge of the airfoil on flow field.

Both vortices, once separated were seen to move in a downstream direction, being carried along by the surrounding axial flow. In Figure 4.5, the flow field was moved forward to small degrees, closer to and above the leading edge of the airfoil. Again, a pair of counter rotating vortices were noted, coming off of the leading and trailing edges of the airfoil. These vortices were carried along with the forward flapping movements of the airfoil and were continually shed along the circumference of the airfoil as seen in Figure 4.5.

4.5.3 Lift and Drag Forces

As shown in Figure 4.6, the evolution of lift and drag forces for all time for both airfoils at 0-degree angle of attack, demonstrating the variation of the intensity pattern with time as the airfoil beats. Higher values indicate greater force loads, so peaks relate to apparent minimum size of the airfoil and troughs relate to when the airfoil appears at its maximum length. Airfoil beats do not include a perfect sinusoidal pattern, and the waveform contains both harmonics and noise. Glycerin as fluid used shows at t=1.5 sec NACA0012 airfoil the oscillation is fully developed but with s1223 airfoil at 1 sec. The variation of the lift and drag forces applied to the airfoils. In the Glycerin the average of the lift for s1223 airfoil is 2 N with oscillation magnitude of 320 N. In other hand the average of the drag force is about 130 N with an oscillation magnitude around 15 N. While the average of the lift for NACA0012 airfoil is 1.5 N with oscillation magnitude of 270 N. And, the average of the drag force is about 121 N with an oscillation magnitude around 6 N. The

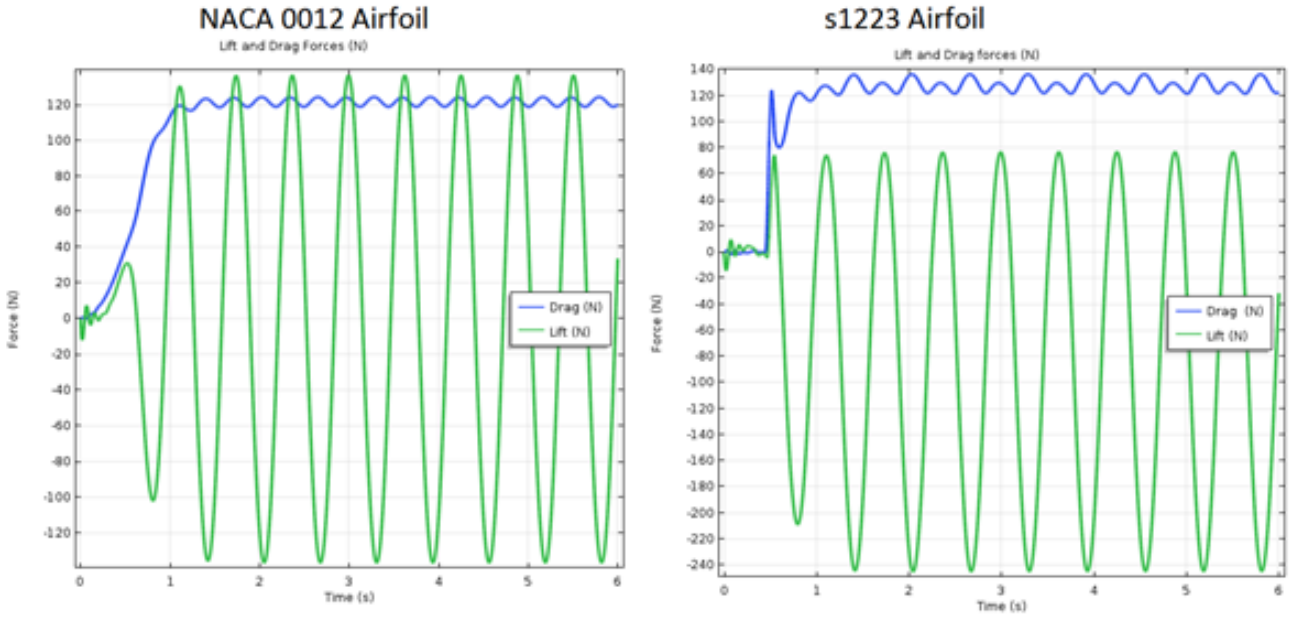

Figure 4.6: Lift and Drag Forces (N)at Glycerin and 0 angle of attack, NACA0012 airfoil (lift) and s1223 airfoil (right)

main difference between both airfoil, the drag force wave in s1223 airfoil is clear higher the lift force wave but in NACA0012 airfoil the lift force higher than drag force. In Figure 4.7 showing the fluid used is Air and the average of lift force in s1223 airfoil is 0.5 N and oscillation magnitude around 7 N while, the drag force is 1 N with oscillation 1 N but in NACA0012 airfoil the lift around 0.2 N with oscillation 2.6 N and the drag is 0.7 N with oscillation 0.5 N. Figure 4.5 and Figure 4.7 shows the drag force larger than lift force due to the viscosity of the fluid. In addition the oscillation in lift force is larger the oscillation in drag force because the oscillating in y direction is larger than x-direction. The plot Figure 4.6 for Glycerin shows that for s1223 airfoil most of the lift is generated after one second of the motion, for NACA0012 airfoil most of the lift is generated after 1.5 sec but in Figure 4.7 for NACA0012 most lift generated at one second and for s1223 airfoil less than one second. Also, when angle of attack increase both drag and lift force increase as shown in Figure 4.8 and Figure 4.9.

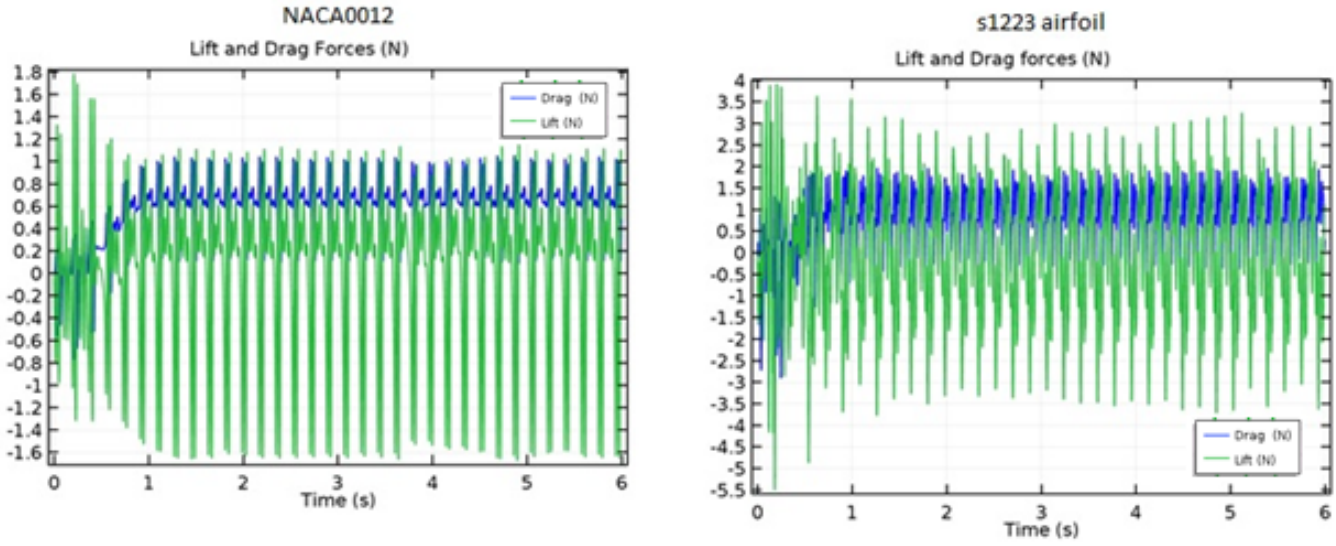

Figure 4.7: Lift and Drag Forces (N) at Air and 0 angle of attack, NACA0012 airfoil (lift) and s1223 airfoil (right)

4.5.4 Oscillation of Trailing Edge

In Figure 4.10 shows the oscillation magnitude of trailing edge displacement for Glycerin driving fluid for both direction x and y. for NACA0012 the x-displacement oscillation about 1.0 mm around the average 0.5 mm and the difference in y displacement 0.5 mm with oscillation around 7 mm. The trailing edge oscillation in s1223 airfoil completely difference because the oscillation magnitude in x displacement around 1.5 mm with average -3 mm. Also, the difference in y displacement around 2 mm with oscillation magnitude of 9 mm. Figure 4.11 shows the oscillation magnitude of trailing edge displacement by changing the fluid to Air for both direction x and y. for NACA0012 the x-displacement oscillation about 3.5 mm around the average -3.5 mm and the difference in y displacement 5 mm with oscillation around 30 mm. The trailing edge oscillation in s1223 airfoil in x the oscillation magnitude displacement around 14 mm with average -14 mm. Also, the difference in y displacement around 20 mm with oscillation magnitude of 68 mm. The huge difference between oscillation magnitudes because the trailing edge in s1223 convex but the trailing edge of NACA0012 is straight.

In addition, The fundamental frequencies are distinct, with multiple harmonic peaks shown in Figure 4.12 shows the main harmonic oscillation frequencies when using Glycerin as fluid, for both

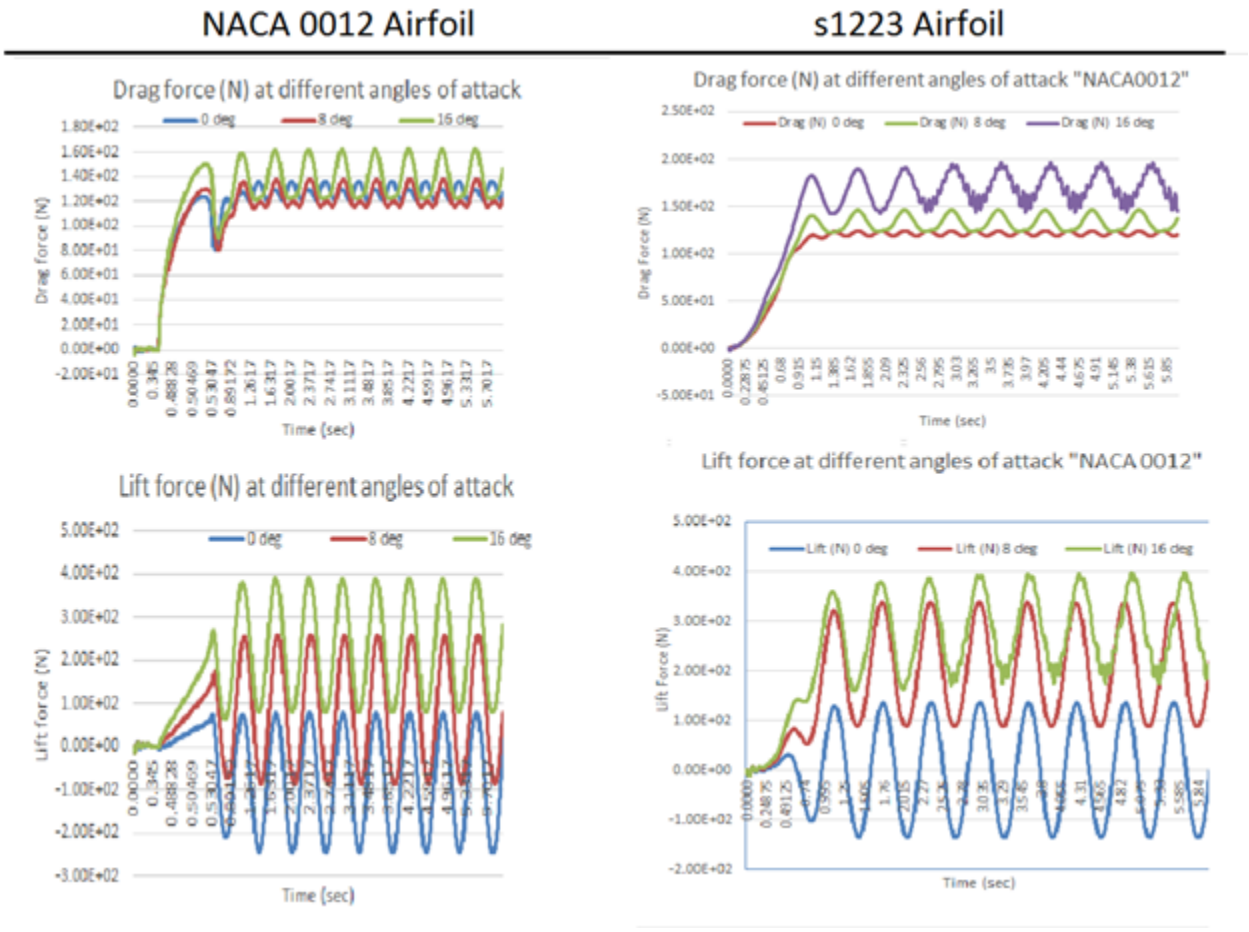

Figure 4.8: Lift and Drag Forces (N), NACA0012 airfoil and s1223 airfoil for different angle of attacks at Glycerin

airfoils NACA0012 and s1223 the frequency for x displacement is 3 Hz and y displacement 2 Hz. In Figure 4.13 also shows the main harmonic oscillation frequencies but using Air. The frequency for the x displacement is 12 Hz but in y displacement is around 8 Hz in NACA0012 airfoil. In s1223 airfoil the frequency in x displacement 22 Hz and in y displacement around 8 Hz.

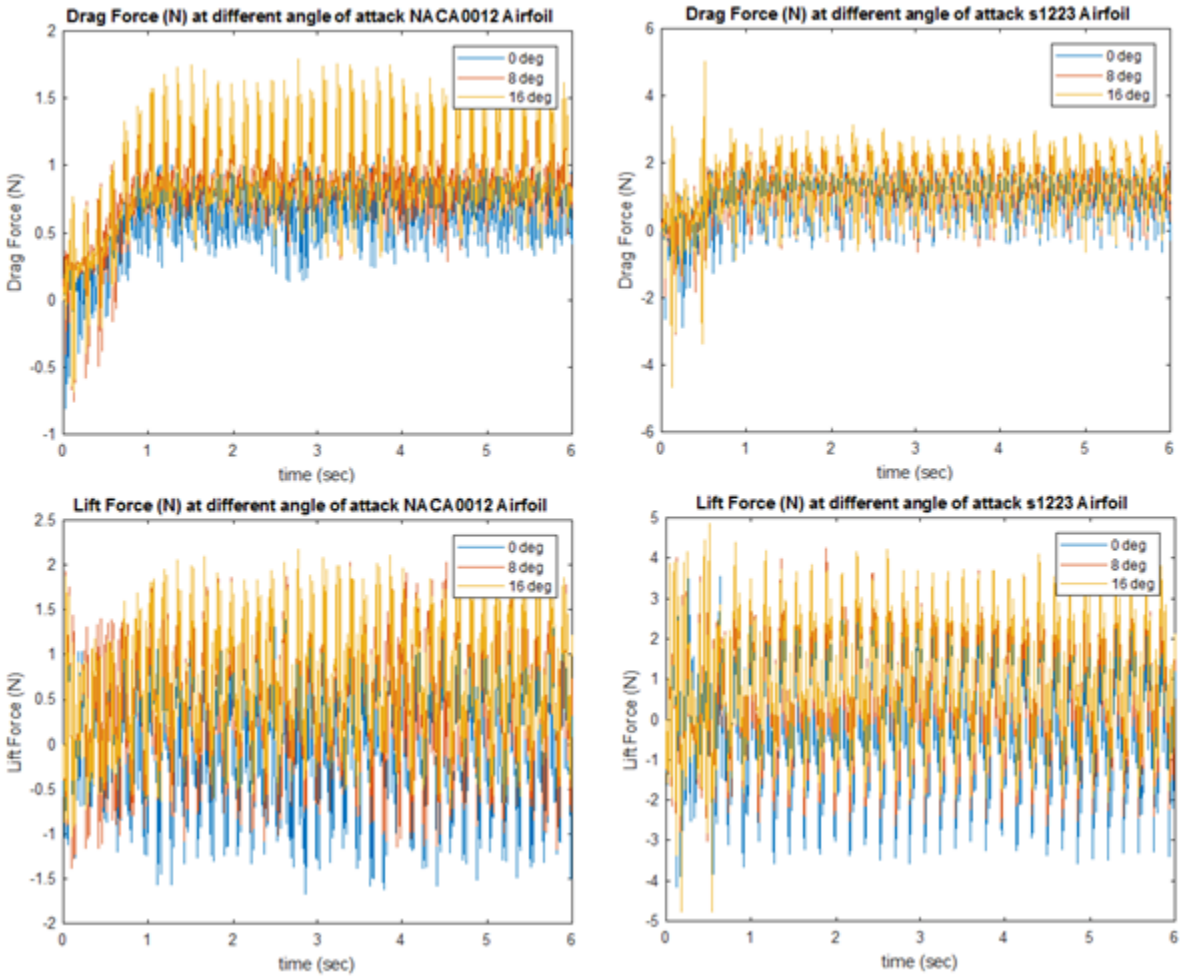

Figure 4.9: Lift and Drag Forces (N), NACA0012 airfoil and s1223 airfoil for different angle of attacks at Air

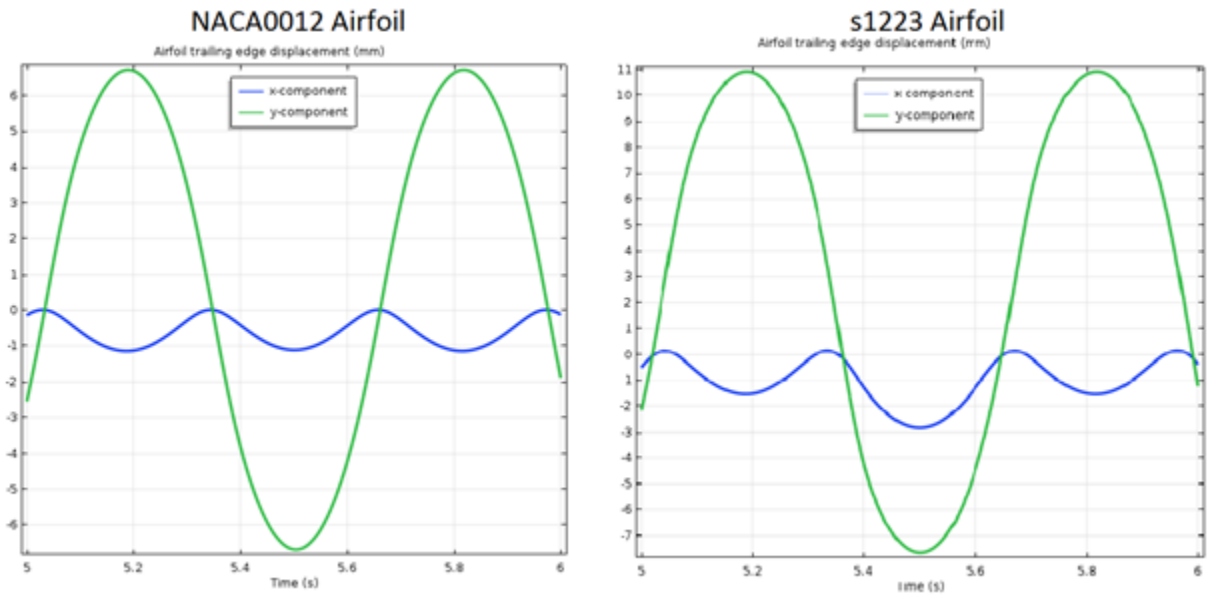

Figure 4.10: Trailing edge displacement of airfoil at Glycerin in x-direction and y-direction, A) NACA0012 B)s1223

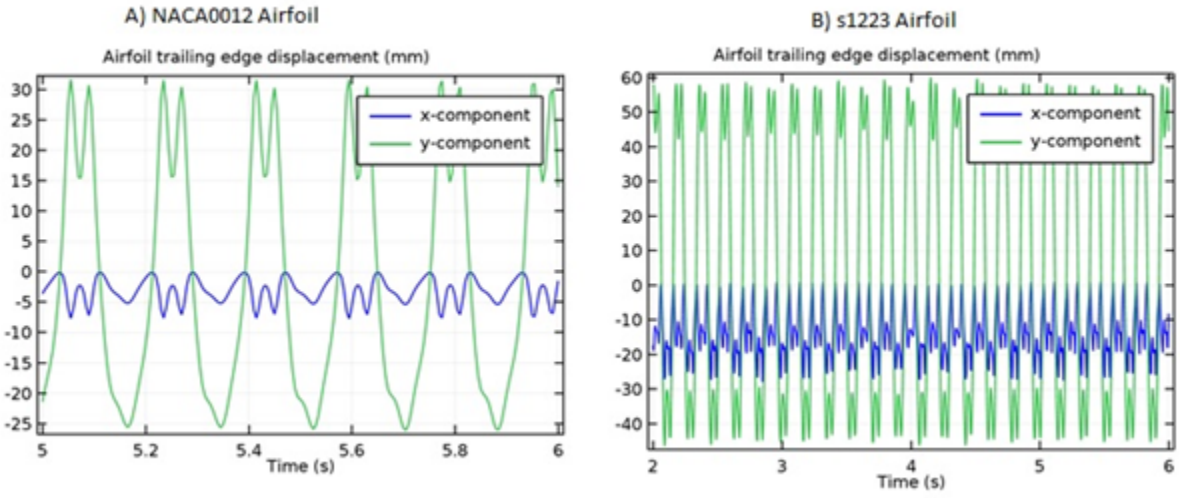

Figure 4.11: Trailing edge displacement of airfoil at Air in x-direction and y-direction, A) NACA0012 B)s1223

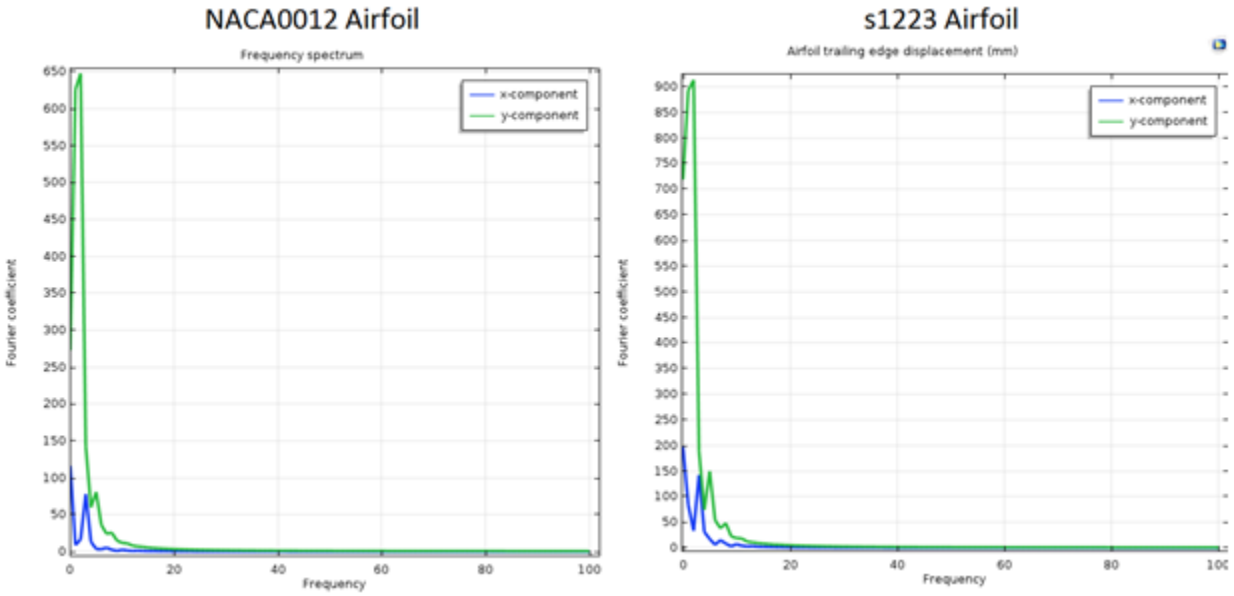

Figure 4.12: Frequency spectrum of trailing edge for airfoil Glycerin, A) NACA0012 B)s1223

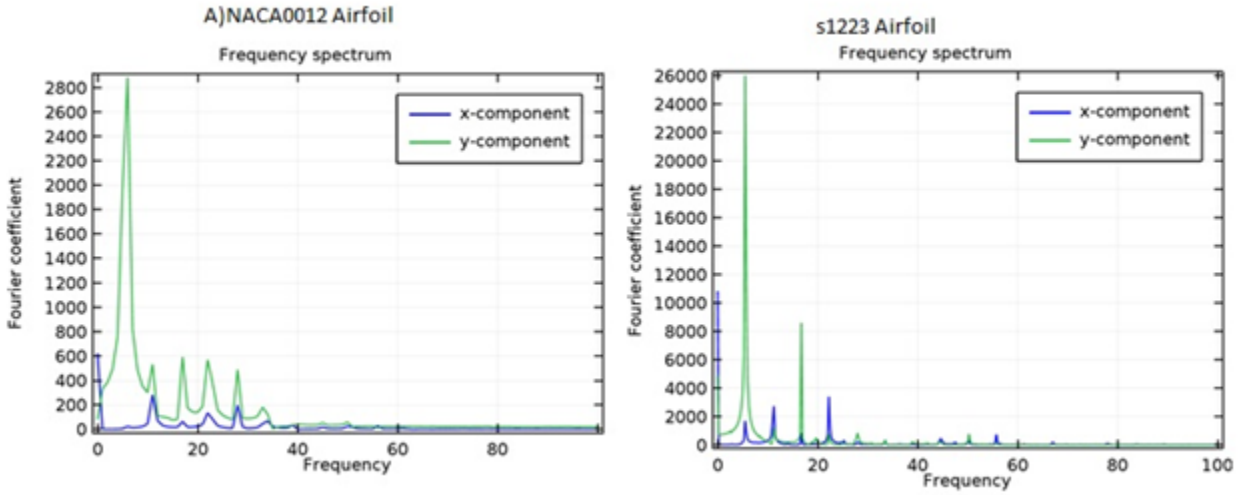

Figure 4.13: Frequency spectrum of trailing edge for airfoil at Air, A) NACA0012 B)s1223

Chapter 5

3D CM SCALE Flapping Wing of UAV at Very Low Reynolds Numbers Laminar Flow

5.1 Introduction

In this chapter, we present a new parametric approach for the development of flapping wing of Micro Aerial Vehicle by using new joint mechanism and two different airfoils. The approach is based on applying force at wing tip to produce flapping wing at low Reynolds number laminar flow regeme by using fluid structure intruction (FSI) which is a flow pattern is the von Karman vortex street that can form as fluid flows past a wing structure and monitoring the vortices which may induce vibrations in the flapping wing. The proposed research originated from previous studies on the response of nonlinear systems involves a fluid-structure interaction where the large deformation affect the flow path. The magnitude and the frequencies of the oscillation generated by the fluid around the structure is computed and compared with the values proposed by [64, 73]. Specifically, it was shown that, the magnitude and the frequencies of the oscillation generated by the fluid around the s1223 airfoil wing is better than NACA0012 airfoil wing.

5.2 Wing Design

Since this MAV is supposed to be nature inspired, the idea is that the best design basis for wings should be from real birds. The basis to start off with possible include in the design that depending on the location that the MAV will be used the body and wings could be painted to look like different birds. As a baseline the FWMAV is modeled after the Warbler bird. This research must also focus on the ratio of body length to wing length as well as weight. This section focuses on modeling part of the research work. First, an overview of the strategy used for airfoil geometry, then, using solid modeling to build the MAV body frame and particularly the flapping wing frame. Then, baseline finite element static analysis and laminar flow analysis around the flapping wing in the designs.

5.3 Design Concepts

The design made use of previously encountered studies involving aerodynamics of small vehicles. The small length scales and low speeds that the UAV will travel at are a great benefit because any flow information could be modeled using laminar potential flows. The entire project is modeled in Solidworks before being analyzed further in COMSOL. The Navier-Stokes equations are used to give a complete description of all possible flow situations. However, obtaining a numerical solution using them is time consuming, even for the case of a laminar flow field around a wing. The first was to design a wing that utilized the lift capabilities of an airfoil. Initial benchmarking for the airfoil used the research by Pelletier and Mueller. The two were able to quantify the aerodynamics of low Reynolds number aerodynamics airfoils. The lift, drag and pitching moment coefficients in addition to the endurance parameter determines the flight parameters that are associated with the flight characteristics that determine the performance of low Reynolds numbered wings. The physical constraints of the model were designed as bird wings and were either flat bottom or featured a 4% camber. The wings had a thickness to chord ratio of .0193 and were selected for the ability to glide at low Reynolds number. Each wing that Pelletier and Mueller studied was divided into 2D models and semispan aspect ratios, a dimensionless expression for relative length of the wing [41]. Notable trends were that when higher semispan aspect ratios having higher lift coefficients and pitching-moment coefficients while having relatively similar drag coefficients for angles of attack between 0 and 10 degrees. Lift to drag ratio was highest for the higher aspect ratios demonstrating that longer wings

will provide better aerodynamic properties. This observation was also consistent for the cambered wings that had higher lift coefficients despite also having higher drag ratios. The shape of the trailing edge was also examined as of whether a sharp trailing edge or elliptical trailing edge was better for performance. The only variable that was under the edge design was the pitching-moment coefficient, for the flat wings only. At an angle of attack of 0 degrees, there was a slight increase in positive pitching-moment from sharp trailing edges that was not well observed in the cambered models. For the purposes of gliding, the data shows that a cambered wing with a high semispan aspect ratio (i.e. large wing span with small chord length) will have the best performance [41]. Andro mentioned the importance of the low aspect ratio again by the work of and Jacquin who examined the flapping frequencys influence on the aerodynamics. Frequencies of the airfoils were compared using the Stroudal number as the primary dimensionless parameter. The study was conducted using a NACA airfoil at a Reynolds number of 1000 and the flow field was analyzed numerically to determine the behavior of the air around the wing. From the calculated force gradients, there were definite and visible differences in the distribution of the air as the wing flapped relating to vorticity of the air. The pressure gradients on the down stroke were much higher, but on the upstroke a vortex was present that reduced pressure throughout the entire upstroke.

Relevant numerical information used the Stroudal values within the range of a bird in flight. Those values were below St = 0.5. Relevant calculations that were used to arrive at this value are all dependent on flight parameters that vary through time. Kaplan, Altman and Ol explored vorticity was an important factor to flight even with the benefit of gliding. Wing shape with low aspect ratios are for their aerodynamics are directly related to the wings while gliding by. The selected shapes for analysis were a rectangle, elliptical and delta wing. The rectangular performed the best among the shapes in terms of generating the highest lift, but the delta wing had the strongest relative vortices. The movement of theses vortices change the pressure gradient across the wings. The airfoils movement generally changes with the vortices and the lift that is calculated is subject to those same vortices. Combining these analyzes isolates three main design principles *i*) A thin cambered wing *ii*) the largest forces experienced on the down stroke and *iii*) a wing that compromised between a delta angle and a rectangular profile. MATLAB R2014b is used to perform airfoil design as shown in Figure (2). The airfoil was designed using a standard Joukowski Transformation of a potential flow field using the equations shown below. Once the complex z was solved for, the x and y coordinates that corresponded to the airfoil were exported in a .txt file that was imported into Solidworks using

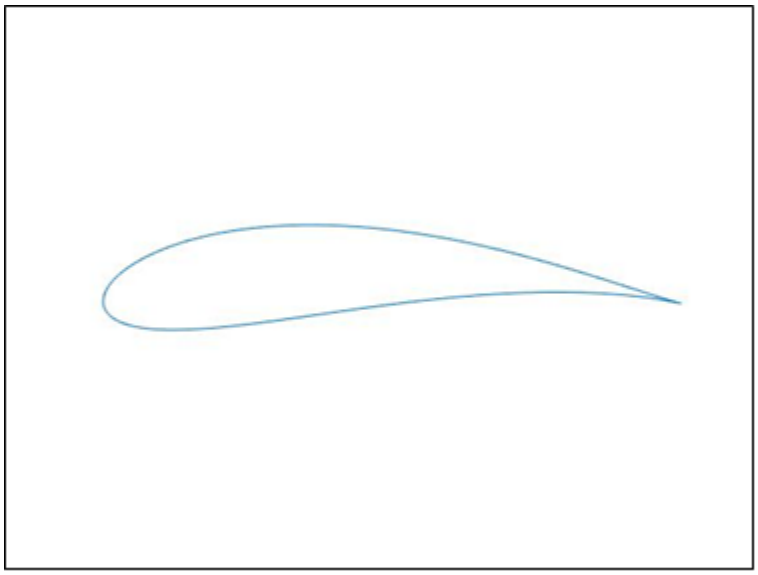

Figure 5.1: Airfoil

the Curves feature to create a workable sketch to generate an airfoil to use in the investigation.

$$\zeta = 1 + \frac{1}{z} \tag{5.1}$$

$$z = x + iy \tag{5.2}$$

Also, biological flapping wing flyers achieve flight maneuverability and efficiency in low speed flight regimes which have not perform again by human made flyers. Micro Aerial Vehicle (MAV) design goals are to develop flyers that maintain flight in regimes that biological flyers exceed in which includes low speeds, hovering, and urban settings. This flight is characterized by flow phenomena that are not well understood such as, flow separation and vortical flow. For the current study, two airfoils have been selected as shown in figure (3), $S1223$ airfoil designed in University of Illinois, Urbana Champaign and $NACA0012$ which is being used extensively for the wingtip in a lot of aerospace applications from the the tiny Cessna to the giant $C-5$ Galaxy and The wing model has been chosen based on a NACA 0012, as there is a strong base of historical data available to confirm the results of the CFD simulations. Laminar Regime has been considered because the low Reynolds number flight regime is characterized by complex flow phenomena such as: viscous flow, transition from laminar flow to turbulence, flow separation, vortical flow, etc. These flow phenomena are rarely

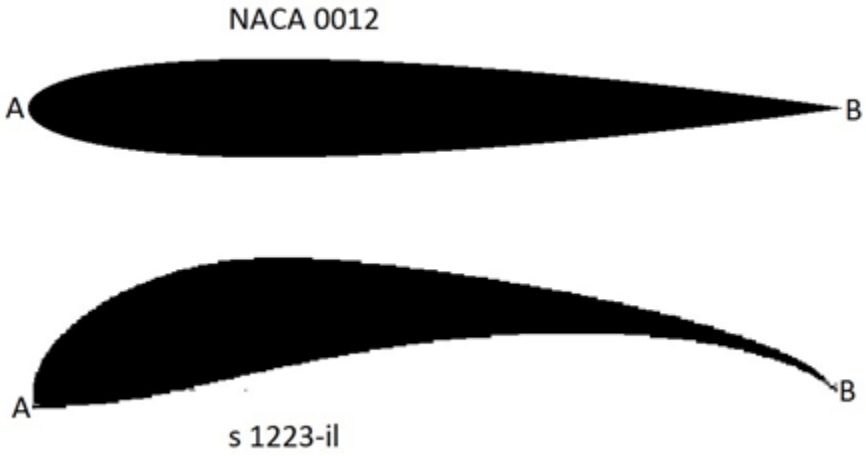

Figure 5.2: Two types of Airfoil

experienced in high Reynolds number conventional fixed wing flight and have not been extensively studied. Due to the complexities of flapping flight aerodynamics, the aerodynamics are not well understood.

5.4 Design Methodology

One of the aspects of the MAV design is that it utilizes flapping wings instead of fixed wings. This design is different from traditional plane wings; therefore, there are not many off the shelf devices that are usable. That left us with the option to design the mechanism to drive the wings and add the hinge mechanism to the wing. To increase the resemblance to natural flyers, a flapping MAV should include another mode of flight; gliding. This has proven to be a difficult objective to achieve for many researchers. A wing capable of gliding must be rigid enough to hold a steady angle of attack with a positive lift to drag ratio. This would mean locking a flapping wing in a specific place with a fixed pitch. In order to determine a possible pitch angle, an FEA analysis or wind tunnel test is needed going forward. The wing position, on the other hand, could simply be set to the top of the upstroke of the wing to prevent adding any extra weight in parts to hold the wing in place.

5.5 Wing Frame Design Methodology

Several aspects taken into consideration when designing the mechanism of flapping wing provided a robust foundation for design. First, it must be small and light weight that lends itself to a simple design. Then, the flap angle is assigned as a variable for optimum flight generation when creating the mechanism. Finally, the mechanism must be able to connect to gears mechanism and these mechanisms are connect to small DC motor. These three criteria provided guidelines for the design.

5.6 SIMULATION SOLUTION

To simulate the fluid structure interaction, it is necessary to install the physics for every steps of the structure in the simulation. So, the model geometry simulate a wing inside a wind tunnel as in figure 5.3 for more detail see [64]. The dimension of wind tunnel is (2.5 x1.88 x 1 m). the structure of flapping wing is composed of a fixed constraint (cylindrical domain) with 0.005 m radius, 0.02 m length and the center depend on the wing located and shape here centered at (0.03,0, 0.5). The length of the airfoil chord is 0.1 m, and the wingspan is 0.15 m. Both of wings and the cylinder made of elastic material as in Table 5.1. For both airfoils (s1223 and NACA 0012 airfoil) use the data file and the re-scale to appropriate position, Sometimes would require to increase the distance between the flapping wing structure and the channel inlet condition to prevent the effect of inlet velocity condition on the flow pattern before reaching the structure. The air enters the wind tunnel from the left side with mean velocity of 5 mile/hr (2.235 m/s) and assumed to be fully developed. The outflow condition set up in right side of the tunnel with zero pressure because is far away from the wing and there is no effect on the structure. Also, it is assumed there is no backflow in outflow to prevent the air from entering the domain through the boundary. Set no-slip condition on the all sides of the tunnel boundaries for the fluid. The properties of flapping wing and the air as in table below: In this paper we focus on fluid-structure interactions focuses on how the structural and fluid dynamics of and around a wing change with actuation frequency and airfoil flexibility. Through the development and analysis of a computational model of a two dimensional airfoil at laminar flow, we found that fluid forces do not dramatically change airfoils shape and thereby modify flight forces (i.e. the deformation in airfoil is dominated by the actuation of the airfoil structure, not the fluid loads imposed upon it). So, considering the fluid flow around the airfoils to be compressible, the

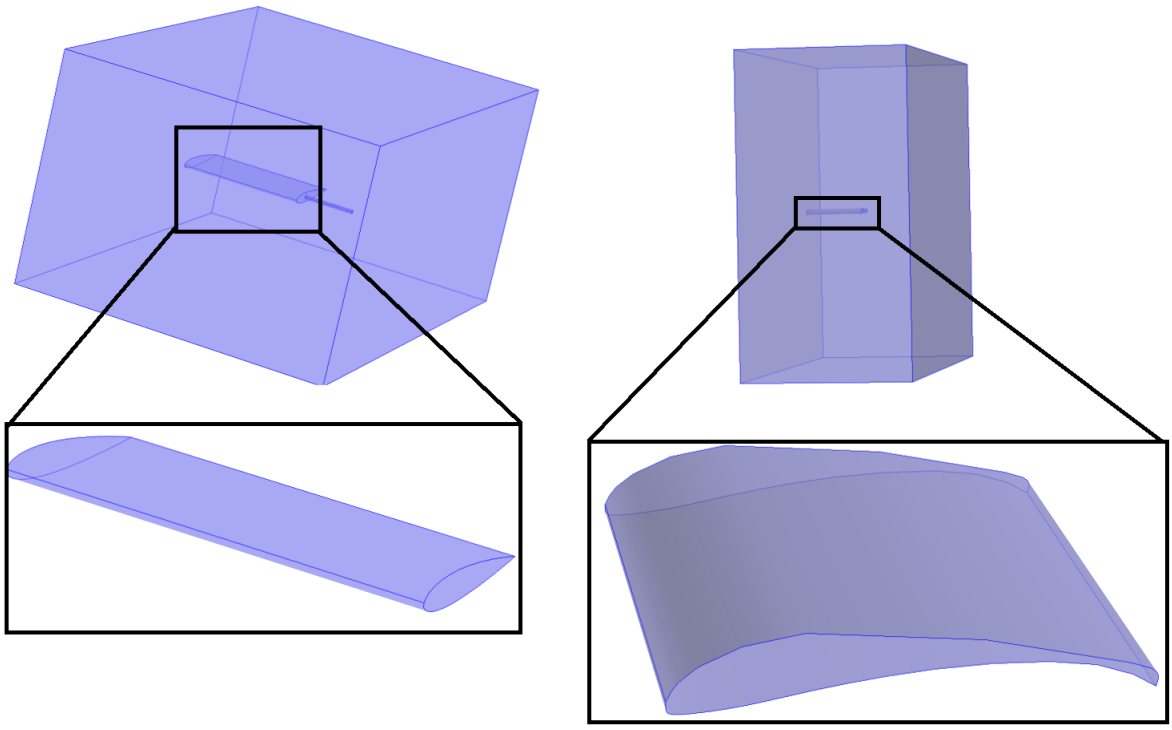

Figure 5.3: Model Geometry

equations used by the solver are Navier Stokes equations as shown below:

$$\rho(\frac{\partial u_{fluid}}{\partial t}) + \rho(u_{fluid} \cdot \nabla)u_{fluid} = \nabla \cdot \lceil -PI + \mu(\nabla u_{fluid} + (u_{fluid})^T) - 2/3\mu(\nabla \cdot u_{fluid})\rceil I + F \quad (5.3)$$

$$\frac{\partial \rho}{\partial t} + \nabla \cdot (\rho u_{fluid}) = 0 \quad (5.4)$$

$$\rho(\frac{\partial^2 u_{solid}}{\partial t^2}) - \nabla \cdot \sigma = Fv \quad (5.5)$$

Where, the velocity field components $u_{fluid} = (u_{fluid}, v_{fluid})$ and displacement field components $u_{solid} = (u_{solid}, v_{solid})$. In general there is no a specific known analytically solution for the Navier−Stokes equations, but by using the vicinity of critical points in the flow to derive the local solutions. In other hand, the flow is characterized by low Reynolds number which is given by:

$$R_e = \frac{\rho u_{fluid} L}{\mu} \quad (5.6)$$

	Physical properties	
Air	Fluid Density	1.123 K_g/m^3
	Dynamic viscosity	$1.8 * 10 - 3$ $Pa.s$
Rubber	Poisson ratio	0.4
	Young's modulus	5.6 MPa
	Material Density	1000 K_g/m^3
ABS	Young's modulus	2000 MPa
	Material Density	1110 K_g/m^3
	Poisson ratio	0.35

Table 5.1: Air and wing Properties.

5.7 Mesh Geometry

Meshing a geometry is an essential part of the simulation process, and can be crucial for obtaining the best results in the fastest manner. After creating a model in COMSOL Multiphysics, the mesh used for both wings (NACA 0012 airfoil wing and s1223 airfoil wing) to a Physics-controlled mesh. The mesh over the wing and the boundary layers are generated using fine mesh in both wings as shown in figure 5.5. A rectancular domain equal to 20 times the chord of the wing, as shown in Figure 5.4 is utilized in which the wing is allowed to flap according to the given kinematics. Unstructured meshes are generated on the faces of the solid wing shape. A Boundary layer with initial cell height equal to 0.0001c where c is the chord length is generated over the wing. Typically, the boundary layer is composed of 30 layers of cells. The mesh beyond the boundary layer is generated using the size function in Size and is unstructured in nature as is seen in Figure 5.4. The fluid dynamic mesh feature is used so as to account for changes in the mesh when the wing moves through the flapping cycle. As the wing flaps, the mesh is distorted. This may lead to intersections of nodes and/or negative volumes being created. The fluid dynamic mesh feature has a remeshing function that remeshes the grid as the wing moves through the flapping cycle after each time step. The range in which the dynamic meshing is used can be decided from the minimum and maximum size of the mesh as can be seen from the settings tab in the feature. Lowering the minimum element size in mesh that is computationally taxing. The mesh for every airfoil and the tunnel as below in table 5.2.

Validation and verification are two important processes that are carried out as part of the computational analysis. Validation of the computation means that the process or the equations that a particular code is utilizing is able to accurately capture the processes that are occurring in, for

	NACA0012 Airfoil	S1223 Airfoil
Triangular elements	1398	1398
Quadrilateral elements	202	202
Edge elements	131	131
Vertex elements	10	10
Number of elements	1600	1600
Minimum element quality	$2.502 * 10^{-4}$	$2.502 * 10^{-4}$
Average element quality	0.8135	0.8135
Element area ratio	$2.509 * 10^{-5}$	$2.509 * 10^{-5}$
Mesh area	$2.5m^2$	$2.5m^2$
Maximum growth rate	2.688	2.688
Average growth rate	1.523	1.523

Table 5.2: Mesh for wings and tunnel

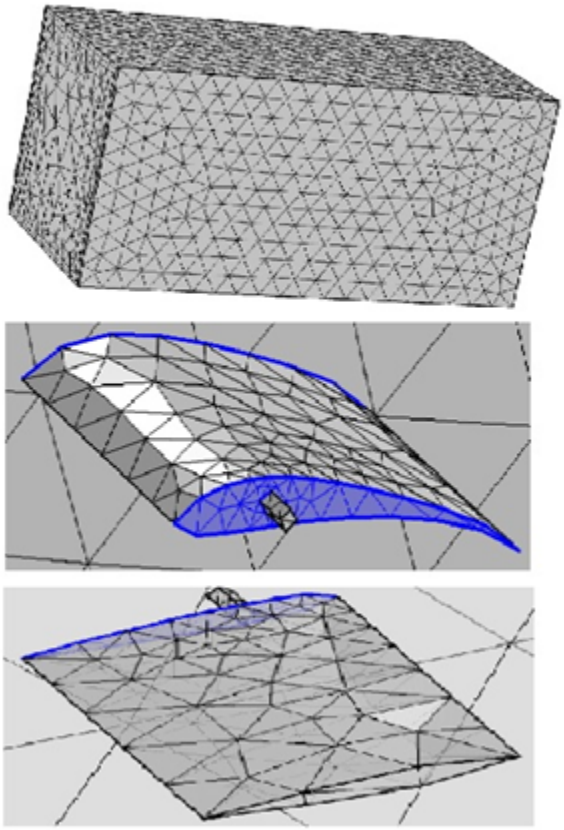

Figure 5.4: Mesh geometry

example the flapping cycle of a wing.

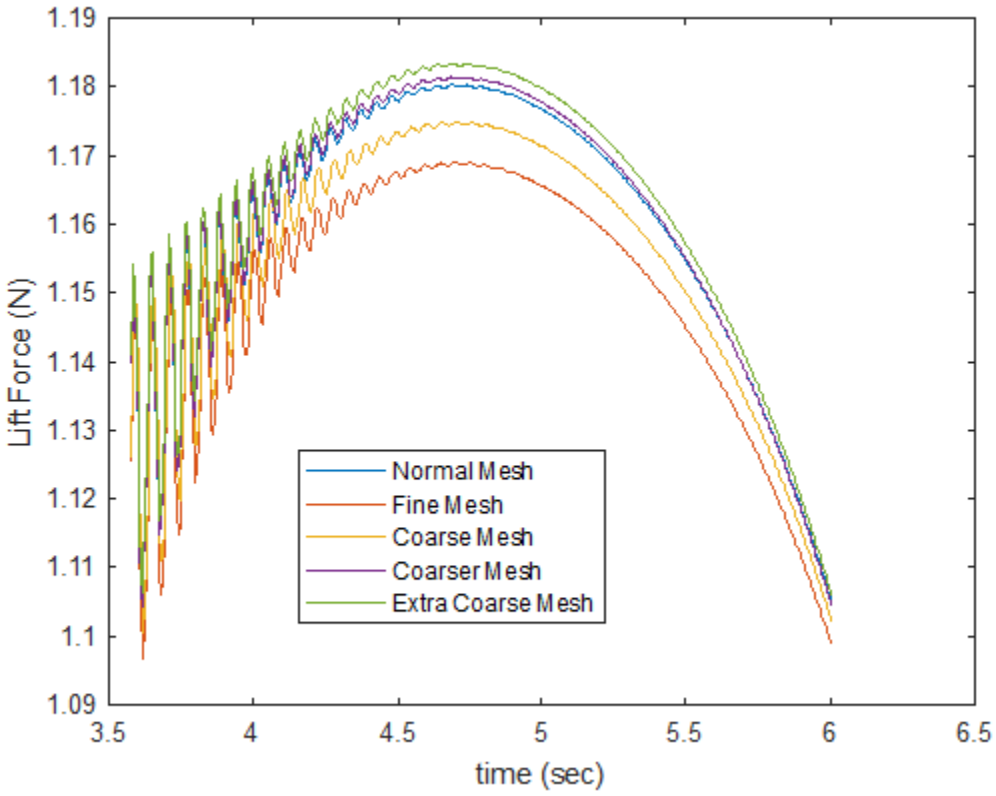

Figure 5.5: Mesh geometry

5.8 Results and Discussion

In the present analysis, the velocity field are analyzed at different angle of attacks (-2, 0, 2, 4, 6, 8, 10, 12, 14 and 16). In Figure 5.6 shows the von Mises stress in the NACA0012 flapping airfoil and the velocity field for angle of attack 0 at four different time. At time 2 sec the wingtip up so, the pressure on upper surface of the wing is higher than the lower surface of the wing that's mean the lowest lift produce at this position, another thing the leading edge at low position which help to push the fluid behind the wing. At time 3 sec second picture in figure 5.6 the trailing edge at low position down and wingtip at normal position, so the pressure at lower surface of the wing is higher than the pressure at upper surface of the wing of which mean high lift produce and the leading edge of the wing at high position up which help the more fluid move below the wing. Continue with third picture in figure 5.6 when the wingtip become at low position, the wing root at high position, the

air divide on the upper and lower sides of the wing to produce high lift because the pressure on upper surface higher than the pressure on lower surface. From Figure 5.6 note that the stagnation point obviously seen on the leading edge of the wing because the flapping, the location of stagnation point change when the location of leading edge change. Also, in laminar flow there are separation and contact points but in this study, note that there is no separation point around the flapping wings surfaces because the flapping for example if assume a separation point near leading edge when the wing moves upstroke the separation point disappear and if the wing moves down stroke the separation point become far away from surface. So, every separation point become a contact point thats mean the flow cover the wing and the von Karman vortex street past the wings, which will be essentially deformed and influences those stream field. The only separation point can clearly be seen in the trailing edge as shown in Figure 5.6. In additional, observed a vortex shedding around the trailing edge of both wings.

The FSI results were used to visualize flow features. Results obtained at 5 mph at 0 angle of attack were qualitatively similar to those for (2,4,6,8,10,12,14 and 16). In Figure 5.6, a series of helicity contours are shown for each flap studied at 5 mph (2.23 m/s). Helicity values were analyzed from the instantaneous flow field for the last time step computed in the FSI analysis. Planes within each of the four flap series were taken at 0 angle of attack along the wing field, and were continue to be displayed behind to the trailing edge of wing.

An angle of 0 degrees and small movement up and down represents the wing root of the wing, while wingtip represent the top and bottom of the wing, respectively. At this position, we observed a clockwise (as viewed from behind the wing) vortex coming off of the trailing edge of the wing, and a counterclockwise vortex coming off of the leading edge of the wing on flow field.

Both vortices, once separated were seen to move in a downstream direction, being carried along by the surrounding axial flow. In Figure 5.6, the flow field was moved forward to small degrees, closer to and above the leading edge of the wing. Again, a pair of counter rotating vortices were noted, coming off of the leading and trailing edges of the wing. These vortices were carried along with the forward flapping movements of the wing and were continually shed along the circumference of the wingtip as seen in Figure 5.6

In Figure 5.7, shows the change in lift and drag forces for both the flapping wings at 0 deg angle of attack. The change in pressure around the flapping wing produce a forces Lift and Drag. These forces evaluated by the difference between the upper surface pressure and the lower

surface pressure. As shown in Figure 5.7, the evolution of lift and drag forces for all time for both wings at 0 deg angle of attack. At time (t=1 sec) the oscillation of wing with NACA0012 airfoil are fully developed but wing with s1223 airfoil it is less than 1 sec. In other hand the change in lift force larger than in drag force because the oscillating in y direction is larger than x-direction. Also, when angle of attack increase both drag and lift force increase as shown in Figure 5.8 and Figure 5.9. In Figure 5.10 shows the oscillation magnitude of trailing edge for both direction x and y. for NACA0012 the x-displacement oscillation about 3.5 mm around the average 2.5 mm and the difference in y displacement 5 mm with oscillation around 30 mm. The trailing edge oscillation in s1223 airfoil completely difference because the oscillation magnitude in x displacement around 2 mm with average 1 mm. Also, the difference in y displacement around 20 mm with oscillation magnitude of 60 mm. The huge difference between oscillation magnitudes because the trailing edge in s1223 convex but the trailing edge of NACA0012 is straight. In addition, in Figure 5.11 the main harmonic oscillation frequencies. The frequency for the x displacement is 1.7 H_z but in y displacement is around 1.8 H_z in wing with NACA0012 airfoil. In wing with s1223 airfoil the frequency in x and y displacement around 8 H_z.

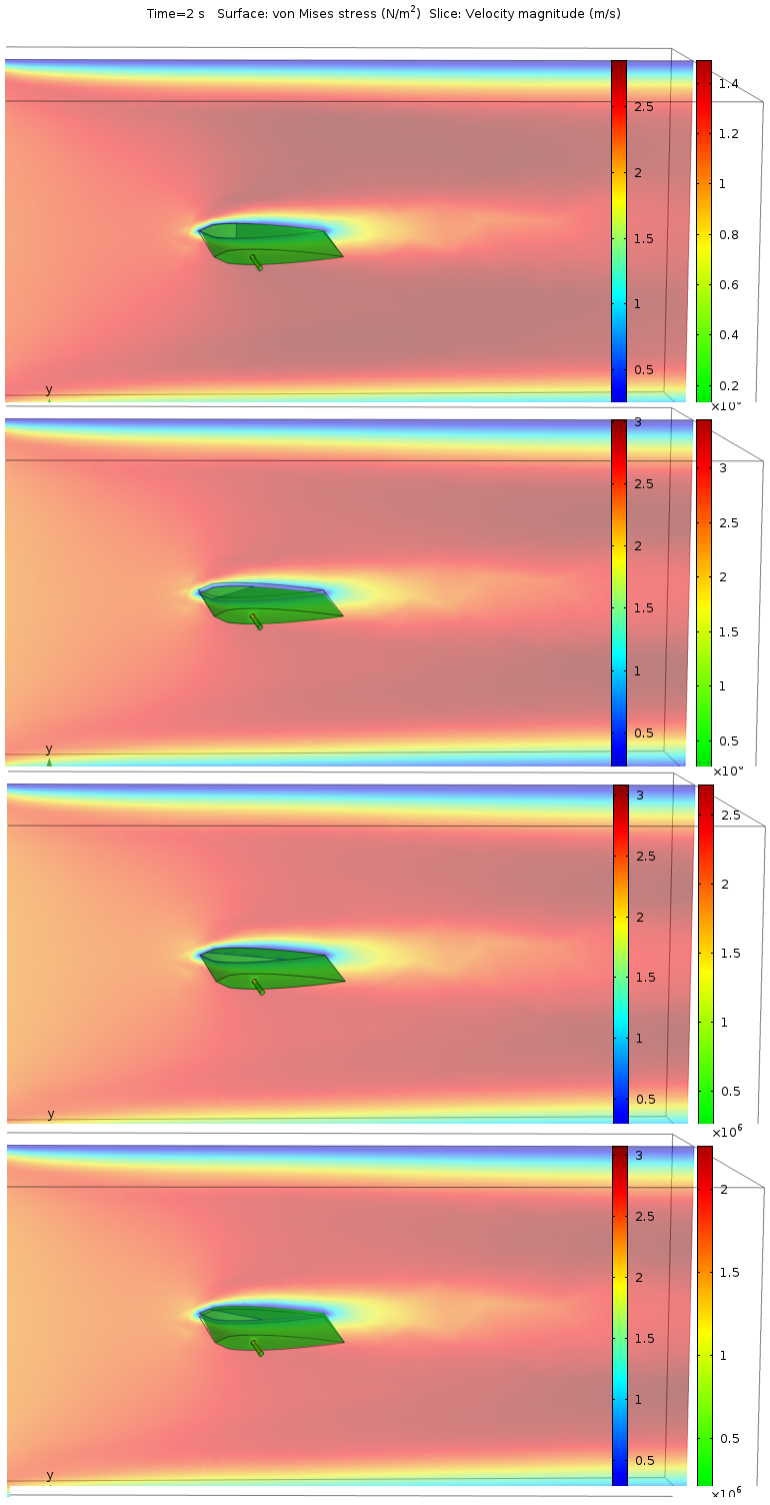

Figure 5.6: von Mises stress in structure and Velocity field in Air for four different time steps at angle of attack 0

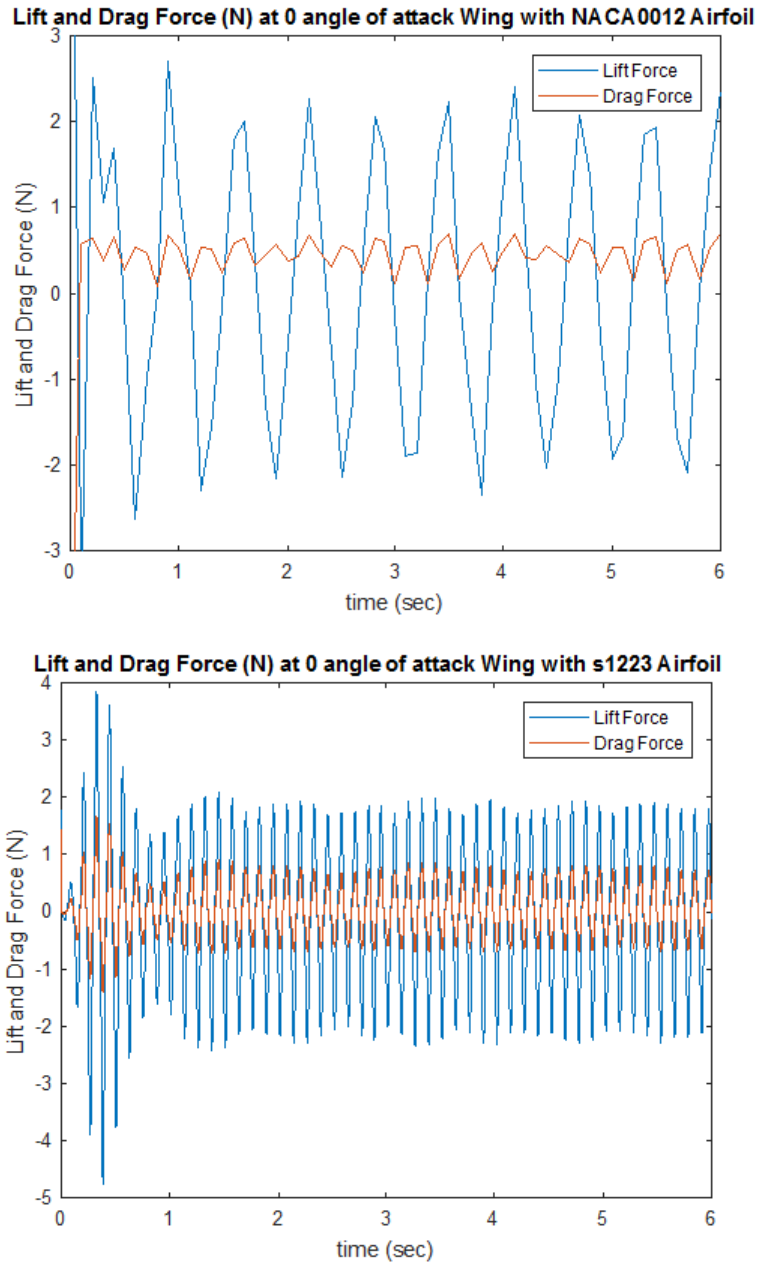

Figure 5.7: Lift and Drag forces for both wings at angle of attack 0

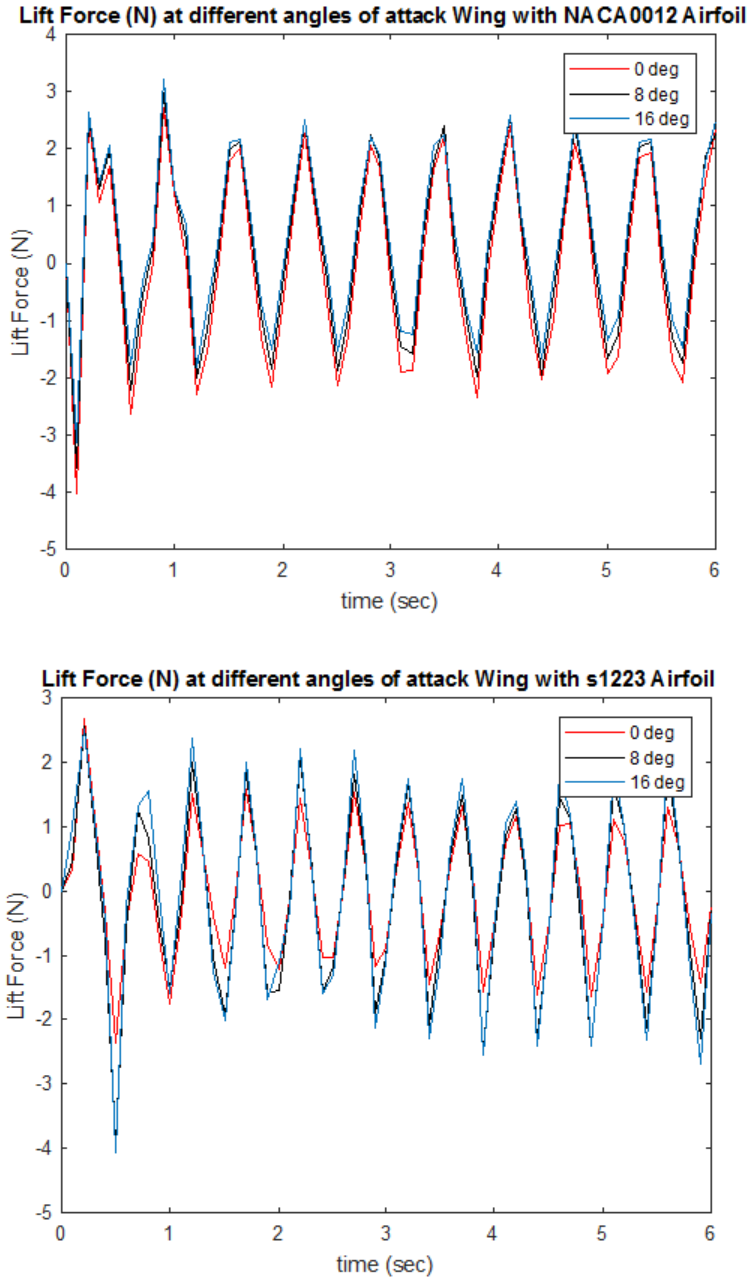

Figure 5.8: Lift forces for both wings at different angles of attack

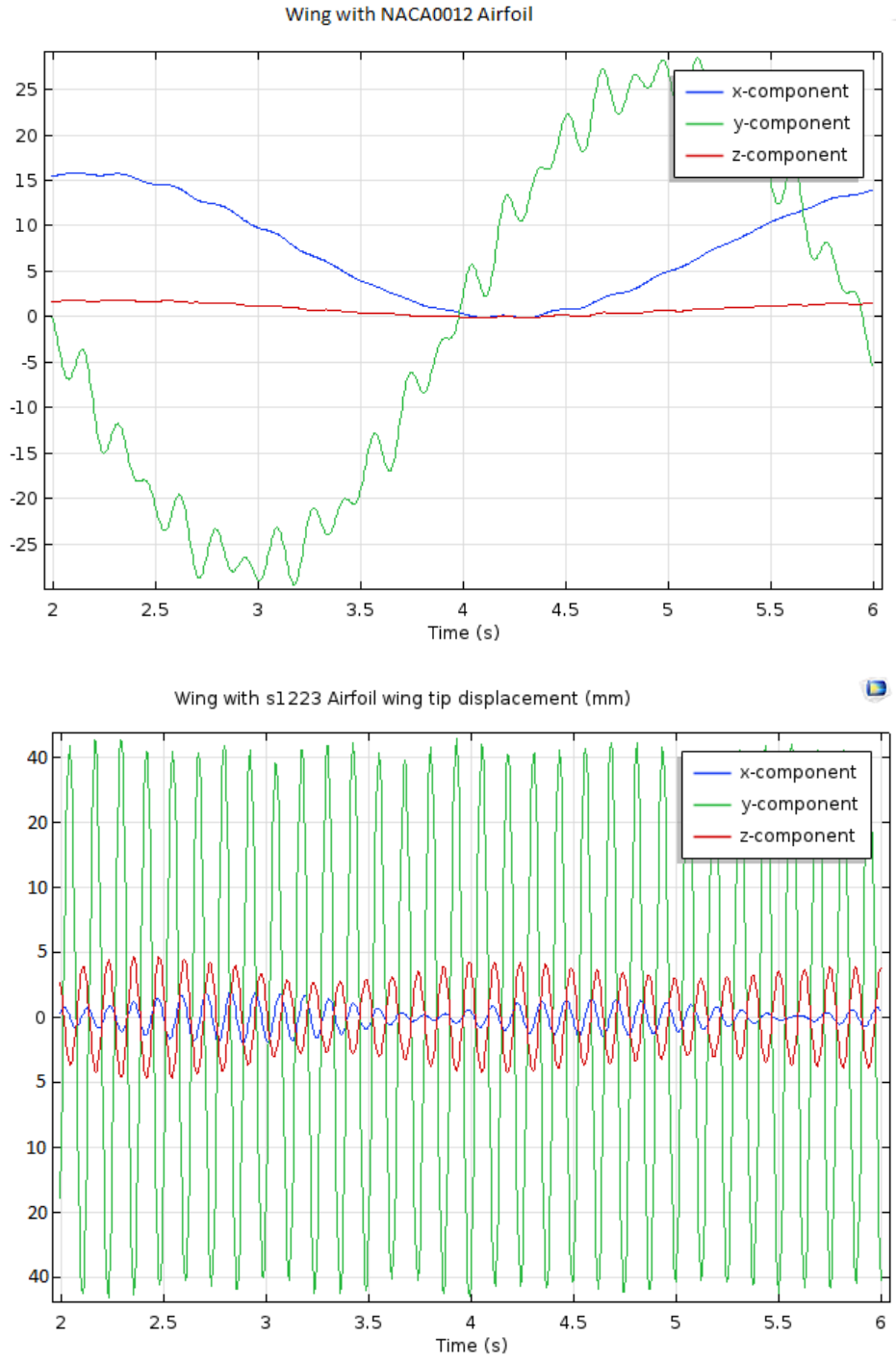

Figure 5.9: Wingtip displacement for both wings at 0 angle of attack

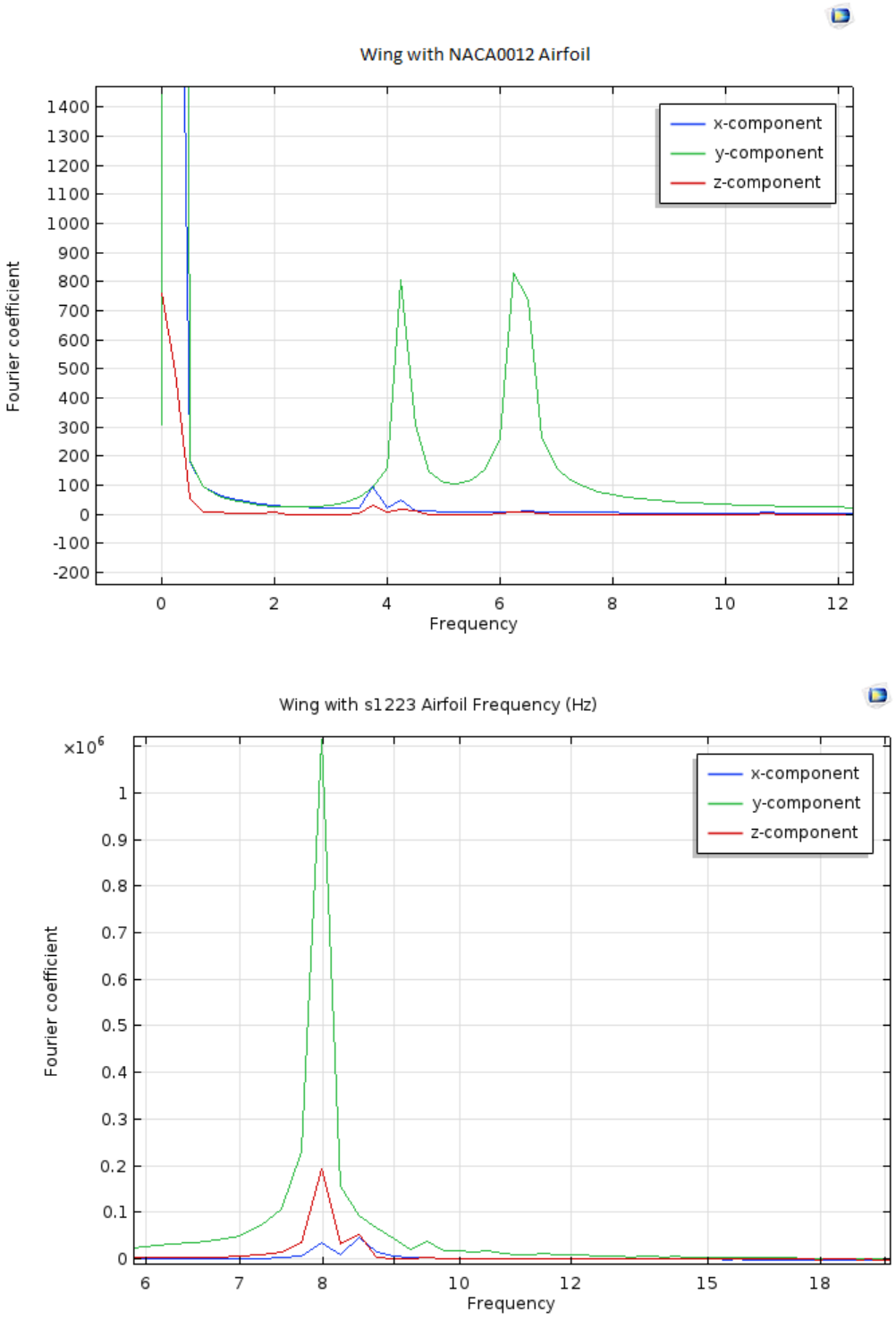

Figure 5.10: Frequency spectrum for both wings at 0 angle of attack

Chapter 6

Computational Fluid Dynamic Analysis for Flapping Wing of cm-Scale UAV at Very Low Reynolds Numbers Turbulent Flow

6.1 Introduction

This Chapter, presents the flapping airfoil and flapping wing at low Reynolds number with turbulent condition. The propulsive performance is one of the most important considerations for this kind of flapping wing. This chapter is aimed at providing a fluid structure interaction synthesis on the Lift and drag characteristics of two airfoils then flapping wings at turbulent flow configuration based on the computational fluid analysis approach. Firstly, set up the FSI model of the flapping airfoils and wings are present. Secondly, the effect of flapping motion of the airfoils and wings on lift and drag forces is illustrated. Finally, the quantification effects of the trailing edge displacement and frequency on the lift and drag characteristics of the flapping wing can be obtained. The analysis results in this study will provide additional useful guidelines to design an effectively flapping flight system applying for the flapping wing micro aerial vehicle or unmanned aerial vehicle.

6.2 Computational Fluid Dynamics SIMULATION

In this study, NACA0012 and s1223 were again adopted as straight and curve airfoils, respectively. These airfoil shapes are shown in Figure 5.1, respectively. The freestream Mach number M set to less than 0.3, the value at which compressibility can be ignored and computational efficiency can be improved. The Reynolds number Re was set to 23,000, which is the same as that in the previous experimental studies. The angles of attack were set to 0.0, 8.0, and 16.0 deg for computation, and note that turbulent flow computation is approximately 300 times more expensive than laminar computation. However, laminar computational are models unable to treat turbulent transitions.

First, we will go to describe the modeling and analysis process used to compare time-dependent air models to previously developed laminar simulation. The development of a time-varying wind model is the initial step in the construction of the flapping wing of UAV system. The flapping wing model have been based on a NACA0012, and s1223. The wing have been initially designed with a chord of 10 cm and span 15 cm, from which all wing flaps has been selected due to data being available for lift and drag respectively as shown in figure 6.1. This model is implemented in the COMSOL Multiphysics environment. The focus of this paper is orientated around the CFD and FSI capabilities. The important thing is to develop the system that measures the unsteady wing loadings being experienced during flapping process to determine the required payload effort to keep the UAV to its original flight path. To simulate the fluid structure interaction, need to install the physics for every steps of the structure in the simulation. Initially, simulations are performed using $k-\epsilon$ turbulence modeling under unsteady-state conditions in order to compare the results against laminar flow results. The simulations are performed at wind velocity 5 m/hr, angles of attack, and trailing edge deflections. So, the model geometry contain wing inside a wind tunnel as in figure 5.1 for more detail see Reference [64]. The turbulent models generated by simulations are presenting lift, and drag forces (L, and D) data that indicates that the boundary layer remains attached to the wing surface while at these angles of attack due to the flapping. From the historical data presented by Abbott et [67], boundary layer separation and wing stalling should begin around an angle of attack of 10. Consequently, because the flapping process, the results shows the separation vanish and we continue to resolve the cause of the variation. The CFD simulations have been set with a nominal speed of 2.23 m/s, giving a Reynolds number of 153000. Additionally, $k\epsilon$ turbulence

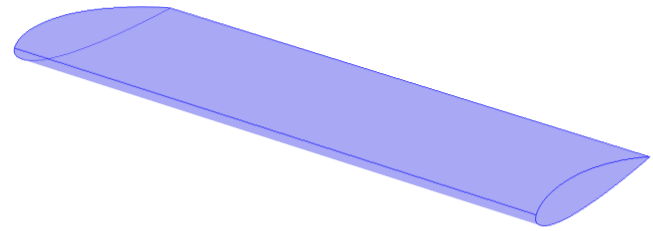

Wing with NACA0012 Airfoil

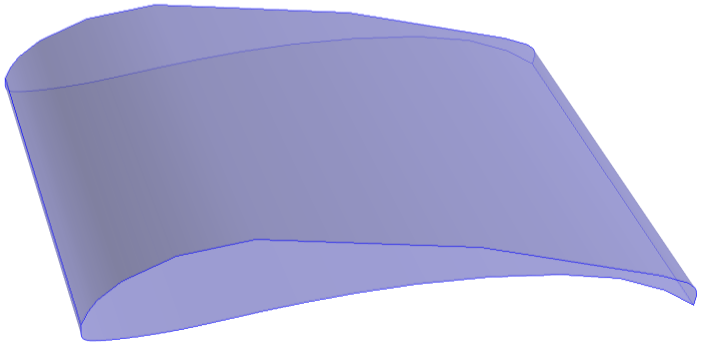

Wing with s1223 Airfoil

Figure 6.1: Wings

model parameters have been set to mimic the airflow characteristics within the wind tunnel used to generate the data in Reference [67]; these parameters are defined by the following equations:

$$k = \frac{3}{2}(U_0 * I_T)^2 \tag{6.1}$$

$$\epsilon = C_{\mu}^{\frac{3}{4}} \frac{k^{\frac{3}{2}}}{L_T} \tag{6.2}$$

where U_0 is the airspeed, I_T is the turbulent intensity, on COMSOL Multiphysics the values of I_T and C_μ are known, which on a low turbulence wind tunnel can be assumed to be 0.004 [74], L_T is the turbulent length scale, and C_μ is the model constant for a flow through a pipe, given by C_μ to be 0.09. The classical formulation for turbulent length scale profiles in a fully developed channel flows. gives a characteristic value at the core of L_T it is a measure of the size of the turbulent eddies that are not resolved. For fully developed channel flows, this parameter can be approximately derived as [75]

$$L_T = 0.007 * L \tag{6.3}$$

To simulate the fluid structure interaction, the models included the physics for every step of the structure in the simulation. Therefore, the model geometry contain airfoil inside control volume as in figure 6.3 [64].

The dimension of channel domain is (1 m height and 2.5 m long). the structure of flapping airfoil is composed of a fixed Roller (circular domain) inside the airfoil with 0.003 m radius and the center depend on the airfoil located and shape here centered at (0.42,0.5). The length of the airfoil chord is 0.1 m, both of airfoil and the roller made of elastic material as in figure 6.4.

For both airfoils s1223 and NACA 0012 airfoil use the data file and the re-scale to appropriate position. The air enter the wind tunnel as a parabolic velocity profile in the left side with mean velocity of 5 mile/hr (2.235 m/s) and assumed to be fully developed. Sometimes would require to increase the distance between the flapping wing structure and the channel inlet condition to prevent the effect of inlet velocity condition on the flow pattern before reaching the structure.

$$U = 1.5U_0 \frac{y(H - y^2}{\frac{H}{2}} \tag{6.4}$$

$$U = (1.5 * 2.23[m/s] * \frac{y * (1[m] - y)^2}{\frac{1[m]}{2}}) * step1(t) \tag{6.5}$$

The turbulent length scale $L_T = 0.007 * L$ where L is the height of the wind tunnel at the testing point; for this initial analysis the wind tunnel height has been defined as 1 m. This dimension

	Physical properties	
Air	Fluid Density	1.123 K_g/m^3
	Dynamic viscosity	$1.8 * 10 - 3$ $Pa.s$
Rubber	Poisson ratio	0.4
	Young's modulus	5.6 MPa
	Material Density	1000 K_g/m^3

Table 6.1: Air and Airfoil Properties.

	Physical properties	
Air	Fluid Density	1.123 K_g/m^3
	Dynamic viscosity	$1.8 * 10 - 3$ $Pa.s$
Rubber	Poisson ratio	0.4
	Young's modulus	5.6 MPa
	Material Density	1000 K_g/m^3
ABS	Young's modulus	2000 MPa
	Material Density	1110 K_g/m^3
	Poisson ratio	0.35

Table 6.2: Air and wing Properties.

is selected to ensure the simulations generate comparable data without risk of influence of the tunnel walls on the flow over the airfoil. In other hand the walls of the channel have been defined with slip condition for the fluid and far away from airfoil, thereby minimizing boundary layer development that may disturb the airflow around the airfoil profile.

The outflow condition set up in right side of the tunnel with zero pressure because is far away from the wing and there is no effect on the structure. Also, it is assumed there is no back flow in outflow to prevent the air from entering the domain through the boundary Figure 6.3 and figure 6.4.

Both of and the cylinder made of elastic material as in Table 6.1.

The outflow condition set up in right side of the tunnel with zero pressure because is far away from the wing and there is no effect on the structure. Also, it is assumed there is no backflow in outflow to prevent the air from entering the domain through the boundary. Set slip condition on the all sides of the tunnel boundaries for the fluid. The properties of flapping wing and the air as in table 6.2: In this paper we focus on fluid-structure interactions focuses on how the structural and fluid dynamics of and around a wing change with actuation frequency and airfoil flexibility. Through the development and analysis of a computational model of a two dimensional airfoil at Reynolds-Averaged NavierStokes ($RANS$) turbulent flow, we found that fluid forces do not dramatically

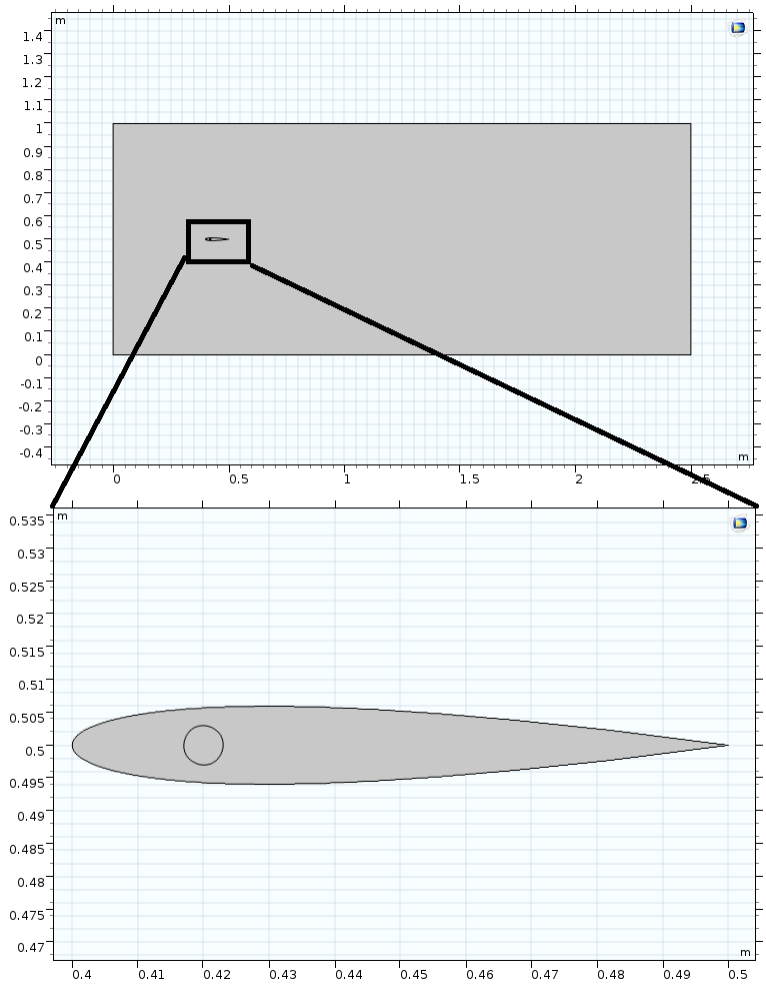

Figure 6.2: 2D Model Geometry

change airfoils shape and thereby modify flight forces (i.e. the deformation in airfoil is dominated by the actuation of the airfoil structure, not the fluid loads imposed upon it). So, considering the fluid flow around the airfoils to be compressible, the equations used by the solver are Navier Stokes equations as shown below:

$$\rho(\frac{\partial u_{fluid}}{\partial t}) + \rho(u_{fluid} \cdot \nabla)u_{fluid} = \nabla \cdot \lceil -PI + \mu(\nabla u_{fluid} + (u_{fluid})^T) - 2/3\mu(\nabla \cdot u_{fluid})\rceil I + F \quad (6.6)$$

$$\frac{\partial \rho}{\partial t} + \nabla \cdot (\rho u_{fluid}) = 0 \quad (6.7)$$

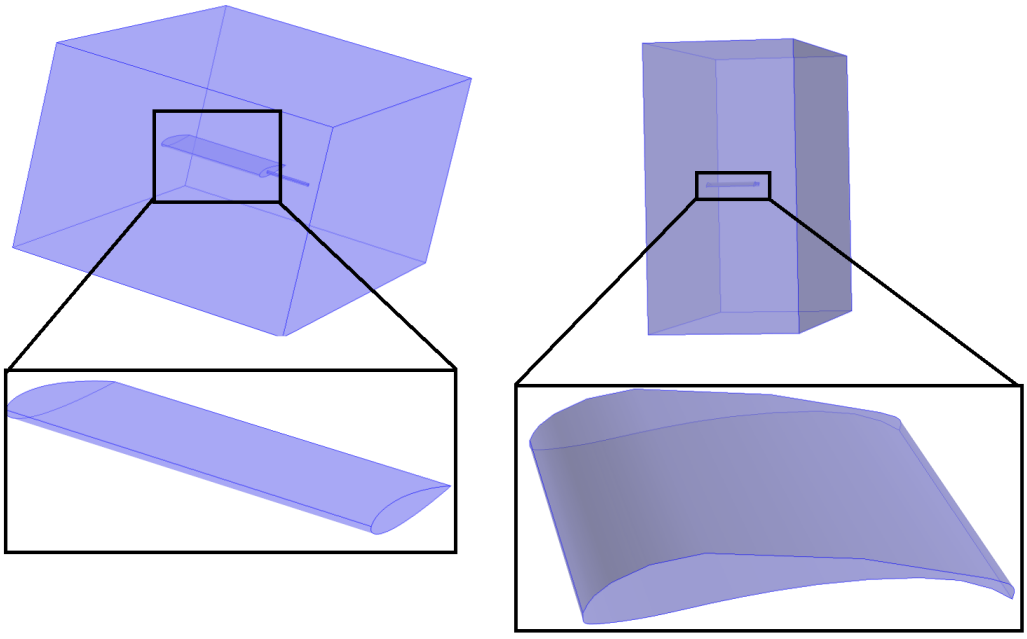

Figure 6.3: 3D Model Geometry

$$\rho(\frac{\partial^2 u_{solid}}{\partial t^2}) - \nabla \cdot \sigma = Fv \tag{6.8}$$

Where, the velocity field components $u_{fluid} = (u_{fluid}, v_{fluid})$ and displacement field components $u_{solid} = (u_{solid}, v_{solid})$. In general there is no a specific known analytically solution for the Navier−Stokes equations, but by using the vicinity of critical points in the flow to derive the local solutions. In other hand, the flow is characterized by low Reynolds number which is given by:

$$R_e = \frac{\rho u_{fluid} L}{\mu} \tag{6.9}$$

6.3 Mesh Geometry

Accuracy and solution time are two of the most critical concerns in computational fluid dynamics (CFD) simulation, and both are highly dependent on the characteristics of the mesh. Different types of meshing elements are needed to deliver optimal performance in resolving different geometries and flow regimes. But transitioning between varying types of elements has long been a challenge.

	NACA 0012 Airfoil	S1223 Airfoil
Triangular elements	1398	1398
Quadrilateral elements	202	202
Edge elements	131	131
Vertex elements	10	10
Number of elements	1600	1600
Minimum element quality	$2.502 * 10^{-4}$	$2.502 * 10^{-4}$
Average element quality	0.8135	0.8135
Element area ratio	$2.509 * 10^{-5}$	$2.509 * 10^{-5}$
Mesh area	$2.5m^2$	$2.5m^2$
Maximum growth rate	2.688	2.688
Average growth rate	1.523	1.523

Table 6.3: Mesh for wings and tunnel

Meshing a geometry is an essential part of the simulation process, and can be crucial for obtaining the best results in the fastest manner. After creating a model in COMSOL Multiphysics, the mesh used for both airfoils and wings (NACA 0012 airfoil wing and s1223 airfoil wing) to a Physics-controlled mesh with a normal element size. Lowering the minimum element size in mesh that is computationally taxing, to resolve the flow in the wake. To achieve this, additional mesh control entities are introduced in the geometry. These entities are advantageous to normal geometrical entities since they are removed whence they are completely meshed. A smoothing algorithm then smooths the mesh locally in order to minimize gradients in the mesh size. Also, it is easier to introduce a boundary layer mesh when the control entities are removed. Therefore the mesh needs to be quite fine on the airfoils or wing interface so that the fluid motion remains continuous. The mesh used in this model is plotted in Figure The mesh for every airfoil and the tunnel as below in table 2.

6.4 Results and Discussion

In the present analysis, the velocity field are analyzed. In Figure 5.7 shows the von Mises stress in the NACA0012 flapping airfoil and the velocity field for angle of attack 0 at four different time. From Figure 5.7 note that,at all steady flapping oscilating, the wake retained approximately the same form. The wake contains lateral jets of fluid, alternating in direction, separated by one or more vortices or a shear layer figure 7. Each time the trailing edge changes direction, it sheds a stopstart vortex. As the trailing edge moves to the other side, a low pressure region develops in the

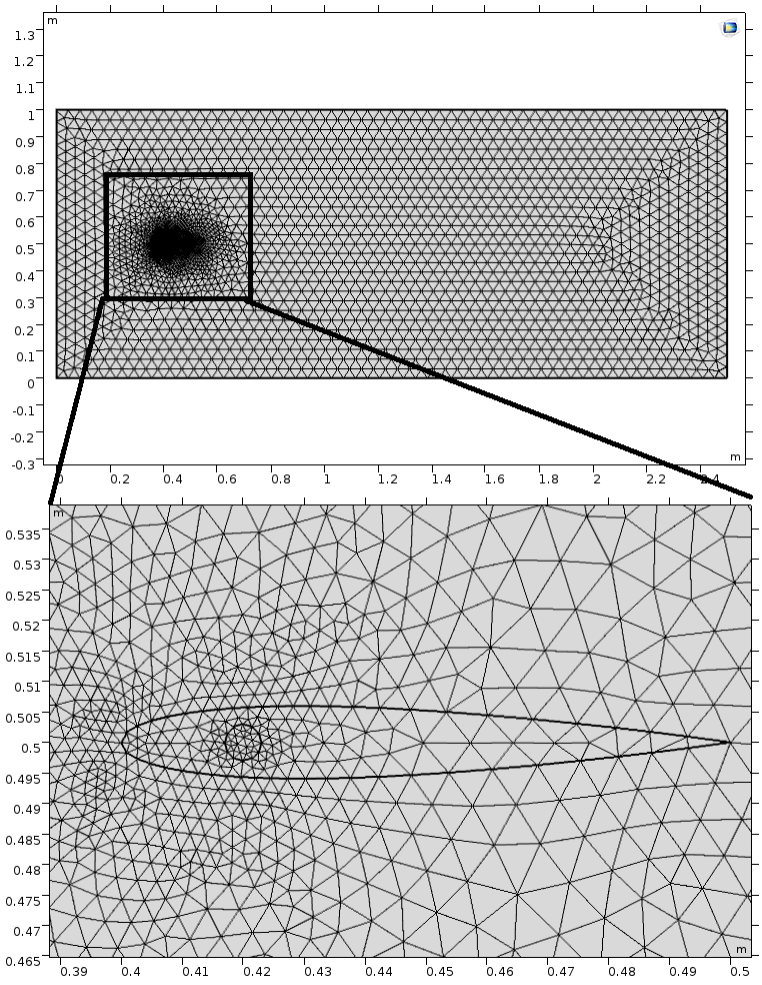

Figure 6.4: 2D Mesh geometry

posterior quarter of the body, sucking a bolus of fluid laterally. The bolus is shed off the trailing edge, stretching the stopstart vortex into an unstable shear layer, which eventually rolls up into two or more separate, same-sign vortices. This pattern was consistent at all speeds, even though the strength of the lateral jet increased at higher speeds figure 7.. Also, Wake flow at different speeds and different phases (different colors) during the trailing edge beat cycle. Black arrows represent flow velocity magnitude and direction. Vorticity is shown in color in the background. The flow around the airfoil is in blue because the low fluid speed. So, every separation point become a contact point thats mean the flow cover the wing and the von Karman vortex street past the airfoils, which will be essentially deformed and influences those stream field. The only separation point can clearly be

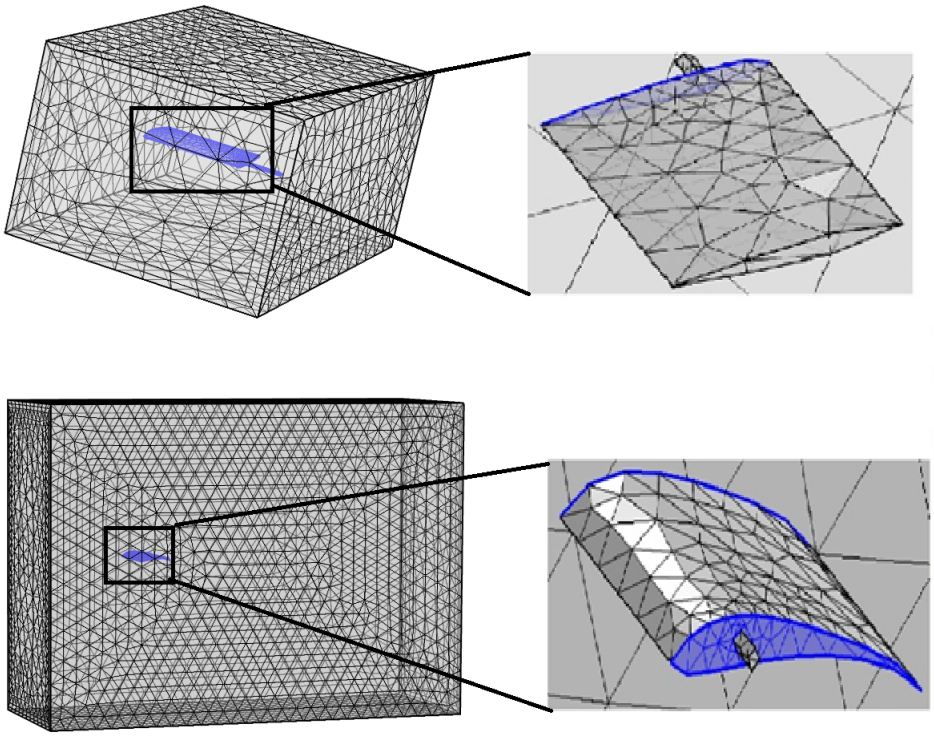

Figure 6.5: 3D Mesh geometry

seen in the trailing edge as shown in Figure 5.7. In additional, observed a vortex shedding around the trailing edge of both airfoils. In Figure 5.8, shows the change in lift and drag forces for both the flapping wings. The change in pressure around the flapping wing produce a forces Lift and Drag. These forces evaluated by the difference between the upper surface pressure and the lower surface pressure. As shown in Figure 5.8, the evolution of lift and drag forces for all time for both wings at 0 deg angle of attack. At time (t=1 sec) the oscillation of wing with NACA0012 airfoil are fully developed but wing with s1223 airfoil it is less than 1 sec. In other hand the change in lift force larger than in drag force because the oscillating in y direction is larger than x-direction. Also, when angle of attack increase both drag and lift force increase as shown in Figure (10) and Figure (11). In Figure (12) shows the oscillation magnitude of trailing edge for both direction x and y. for NACA0012 the $x$displacement oscillation about 3.5 mm around the average 2.5 mm and

the difference in y displacement 5 mm with oscillation around 30 mm. The trailing edge oscillation in s1223 airfoil completely difference because the oscillation magnitude in x displacement around 2 mm with average 1 mm. Also, the difference in y displacement around 20 mm with oscillation magnitude of 60 mm. The huge difference between oscillation magnitudes because the trailing edge in s1223 convex but the trailing edge of NACA0012 is straight. In addition, in Figure (13) the main harmonic oscillation frequencies. The frequency for the x displacement is 1.7 H_z but in y displacement is around 1.8 H_z in wing with NACA0012 airfoil. In wing with s1223 airfoil the frequency in x and y displacement around 8 H_z.

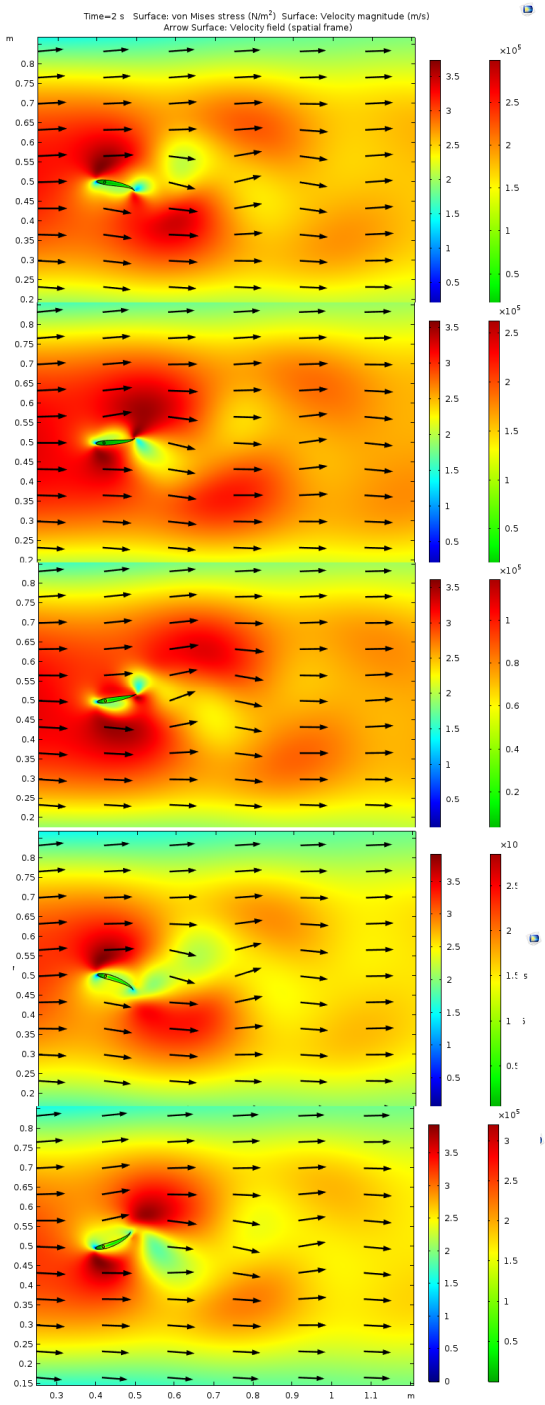

Figure 6.6: von Mises stress in structure and Velocity field in Air for four different time steps at angle of attack 0

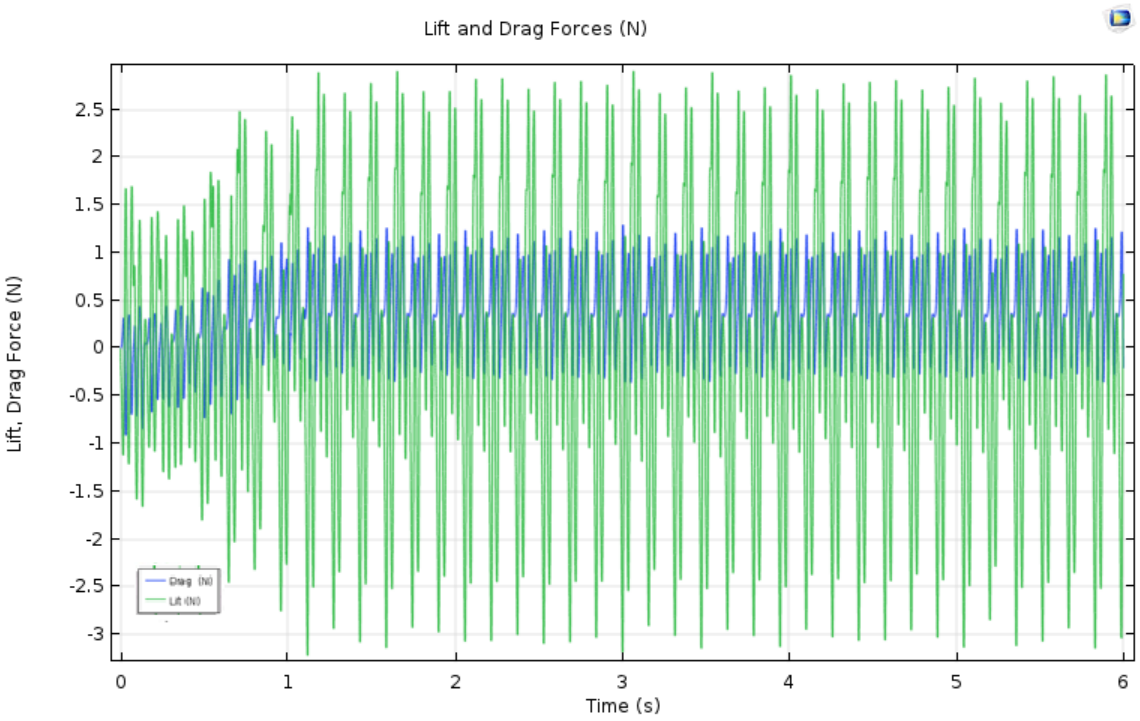

Figure 6.7: Lift and Drag forces for NACA0012 airfoil at angle of attack 0

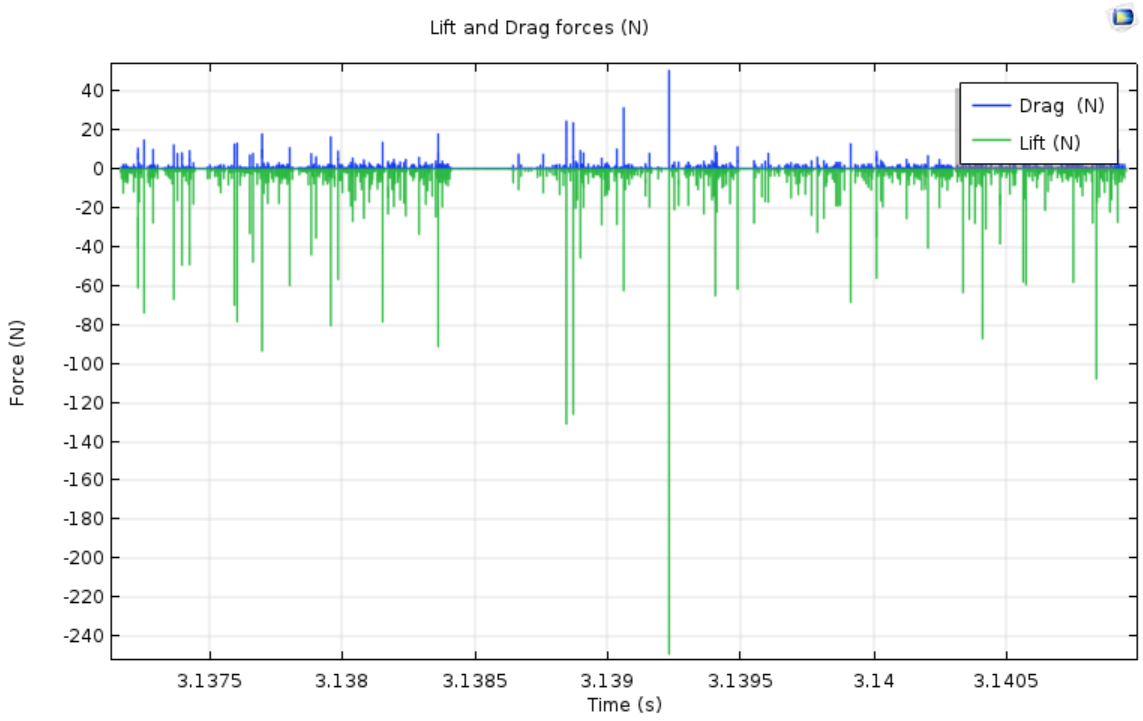

Figure 6.8: Lift and Drag forces for s1223 airfoil at angle of attack 0

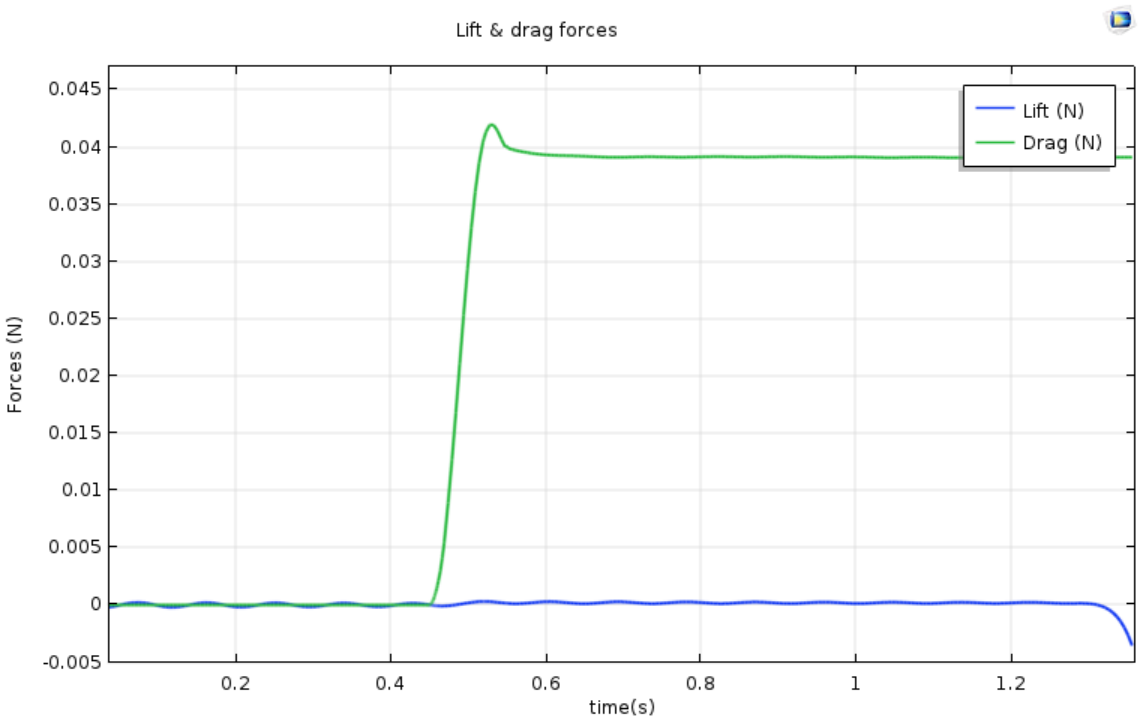

Figure 6.9: Lift and Drag forces for wing with NACA0012 airfoil at angle of attack 0

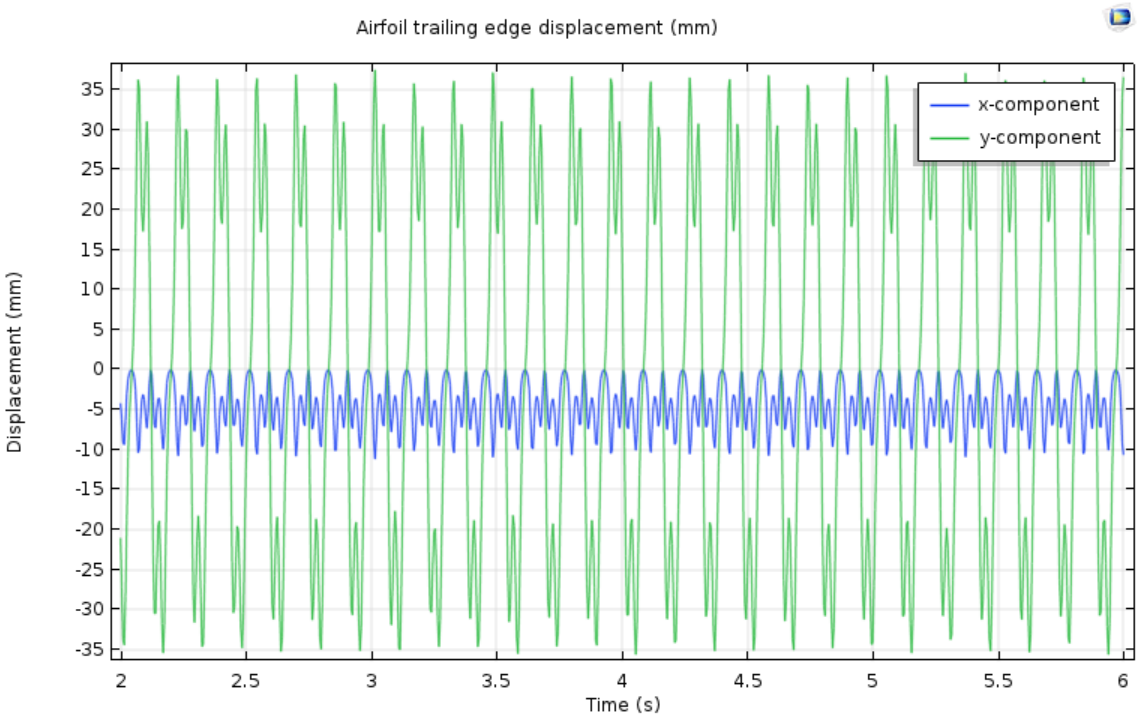

Figure 6.10: NACA0012 airfoil Trailing edge displacement at 0 angles of attack

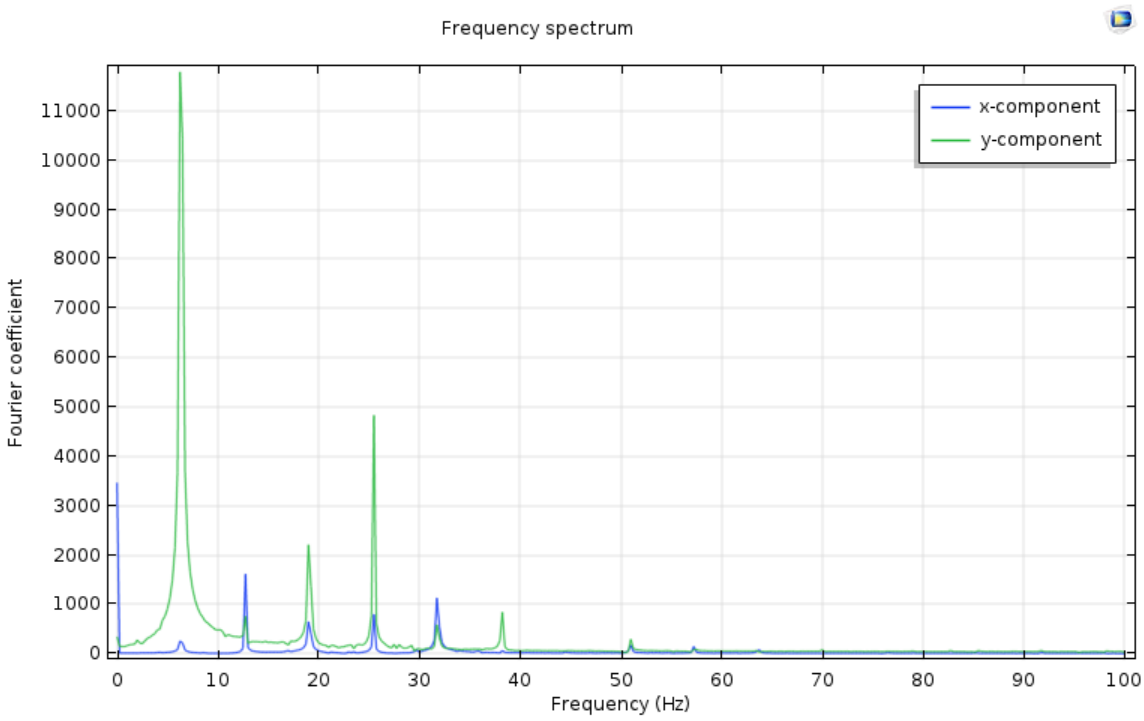

Figure 6.11: NACA0012 Trailing edge frequency spectrum at 0 angles of attack

Chapter 7

Conclusions

This dissertation investigated the feasibility of analysis a flapping wing for a biologically inspired cm-scale unmanned aerial vehicle. This analysis uses a fluid structure interaction for flapping wing in laminar flow and turbulent flow.To this end,the dissertation used biological inspiration design, numerical simulations, and an specially designed modules to detail the influence of aerodynamical forces on the flapping wing for cm-scale unmanned air vehicle at different flow and different conditions.

In chapter **??**, we proposed and initiated a new parametric approach for the development of flapping wing models inspired from birds. The body of the apparatus was designed to be aerodynamic for more precise and efficient maneuvering during operation. The wings were designed strong enough to support the weight of the bird when it was being flown. The apparatus was designed to be lightweight and durable while the manufacturing process remained a top priority. This would require choosing a definite material for the wing frame and foil in order to obtain the required constants needed for the flapping wing formulas.

As mentioned in chapter 2 and 3 improvements on wing analysis and design would need to be coupled with a finalized design of a wing mechanism. The spatial constraints currently prevent many driving mechanisms from being used. The current design uses the simplest method of connection and driving force by interlocking the wings together and driving them directly with the motor. In order to produce the required torque from a high rpm motor, a gearbox needs to be created. This would convert the high rpms into a higher torque, but requires multiple gears. If it is possible to create a gearbox within the required space of the body, a multi gear driven system could be used to

drive the wings consistently, producing symmetrical force from each wing. Again this would not only require the creation of a gearbox to fit inside the body, but also a redesign of the wing attachment points. The interlocking arms would be replaced with a symmetrical arm to lock onto the gears used.

In the course of this research, 2D CFD/FSI was utilized to examine the cm-scale flapping mechanics with variations in size, weight and speed, the kinematics and dynamics to gain insight into lift and drag ; flow characteristics surrounding a low Reynolds number wing and resulting criteria for selecting appropriate airfoil shapes, and flapping wing concepts for lift-to-drag ratio and aerodynamic performance. The flapping flight of an airfoil fly shows two aerodynamic force peaks in each flapping stroke. The research shows that the first peak is due to rapid vorticity increase as the airfoil experiences fast pitching-up rotation, while the second peak is likely to be associated with wake-capturing. Overall, these two peaks account for a large portion of the total lift. While similar results are noted, our results are for a cm-scale application instead of a mm-scale application. The comparison in the results between both airfoils shows the s1223 airfoil is better than NACA0012 in laminar flow at room conditions. Our understanding of flapping wing dynamics and many aspects of low Reynolds number flight involve large-scale vortical motion flows, and requires Navier Stokes and/or Turbulent models to understand many the issues.

Gear trains need to be redesigned or specialized for the size and wing beat frequency required for future operation. Simulations show that the aerodynamic forces have affected in each flapping stroke in upstroke and down stroke. It was seen that the peak of lift force in the wing with s1223 airfoil is higher than with NACA0012 airfoil peak due to the increasing curvature in trailing edge in wing with s1223 airfoil. Also, it has been found out that the results of different angle of attacks increase the lift and drag forces in both wings experiences fast pitching-up rotation, while the second effect in aerodynamic forces is likely to be associated with wake-capturing. Overall, these two effects account for a large portion of the total lift.

Currently there is no comprehensive and accepted theory of transverse turbulent mixing and the prediction of its rate is mainly based upon the results of experimental works carried on in laboratory channels or in streams and rivers. Flapping wing simulations for unmanned air vehicle model were been developed using an approach based on the Reynolds Averaged NavierStokes equations (RANS) was applied, where the closure problem was solved by using a time-dependent $k - \epsilon$ turbulence model in two dimensional and three dimensional, where the wind speed flow inter the

channel from right side and becomes a fully developed flow. One objective of this research was to present the preliminary results of a numerical study of the time-varying simulations performed are shown to be closely correlated to the laminar flow simulations developed previously but in three dimensional just reach the steady state. These simulations enable the progression of the turbulent air flow model to be extended to allow flapping wing to be improved. The basic sinusoidal wave load process model has been implemented to create multiple velocity magnitude jet flow over a period of 6 seconds. The simulations performed include several flapping beats within this time frame of which the data at each time step closely follow the data gathered from the laminar flow and time-varying turbulence flow models. A second objective was to assess the effect on turbulent mixing of a grid formed by traingular elements with differen mesh sizes. A comparison between the numerical results with the change in grid size demonstrated that the lowering the minimum element size in mesh that is computationally taxing. Further research will be addressed to extend to 3D case this analysis based on the RANS

Chapter 8

Future Work

The work done up to this point has been preliminary design and analysis work. The next step is to conduct a gear analysis on the gearing system using to ensure that there will be no failure in the current design. In the case of failure, the gear housing system will have to be redesigned. The redesign process is anticipated to be minimal because only one compartment needs be changed instead of the entire frame.

Another major area of the research that needs to be completed is the final wing design. The design ideas of turbulators and air channels will be explored in an attempt to decrease the drag coefficient. By solving the issue of the drag coefficient on the upstroke, flight will be easier to achieve. With the simple flapping motion of the FWUAV, it is paramount to minimize the factors working against its flight.

The next step is to have all of the manufactured components and hardware in place for the assembly of the FWUAV. With the design work completed, the manufacture of the parts is the limiting factor. In the event of ineffective parts, the design will be explored again to reinforce the weak points to keep from failure.

Once all of the parts are in place, the design will then be tested. Benchtop tests will be conducted to determine the lift created by the wings and the actual flight time with the given battery. If determined that the lift and thrust are not sufficient to sustain flight, redesign work will be conducted to improve the flight characteristics. The redesign will take a top to bottom look of the design to determine the flaws in the design of each and every component and characteristic. If successful, the benchtop tests will move to tests in the field to test the FWUAV in the air. From

there, the design can be refined to improve the actual flight characteristics.

Include defining the finalize tail design to improve flight and observing the vehicles handling qualities in roll, pitch, and yaw. Once familiarization with the air vehicle is complete, further flight testing can take place to document the flying qualities of the baseline UAV configuration. Data from these flight tests will act as the control point to which modified versions of the cm-scale UAV can be compared.

It is recommended that extensive tests be made to determine the characteristics of flapping wings in order to form a comparison between different types of flapping wings. Also, tests should be made to find the optimum airfoil shapes for flapping flight, such airfoils in addition having excelent low speed characteristics.

Include the investigation of how to shield onboard sensors from the UAVs electronic interference, the development of area coverage flight missions, the effects of interior components weight like motor or camera, the real-time data processing system, and the integration of UAVs systems.

Appendices

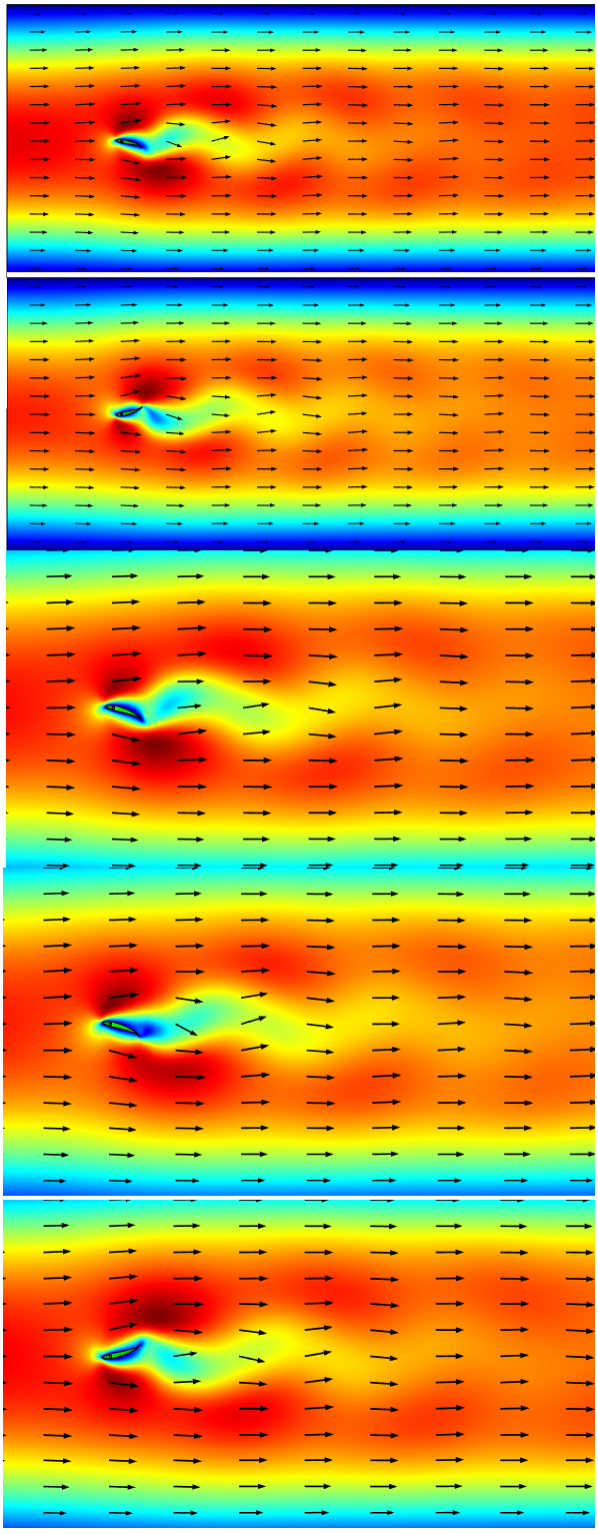

Figure 1: von Mises stress in structure and Velocity field in Air for four different time steps at angle of attack 0 NACA0012 Airfoil

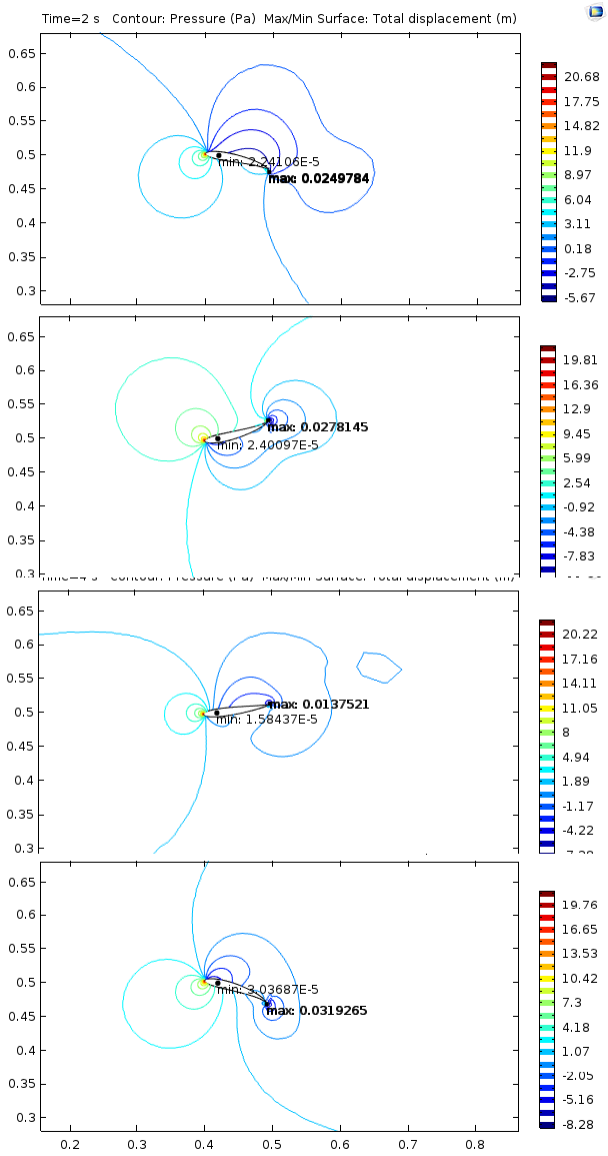

Figure 2: Pressure field in Air for four different time steps at angle of attack 0 NACA0012 Airfoil

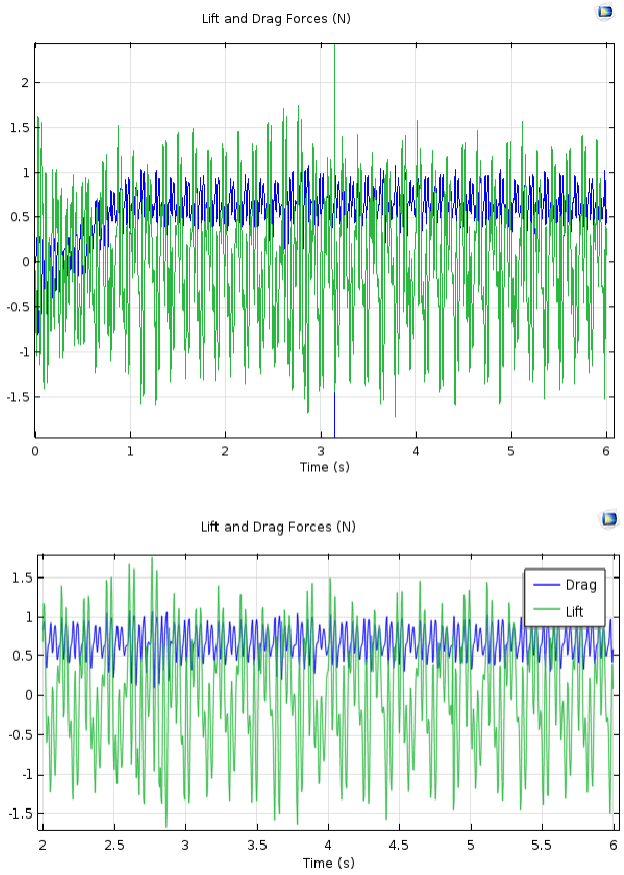

Figure 3: Lift and Drag Forces (N) in Air at angle of attack 0 NACA0012 Airfoil

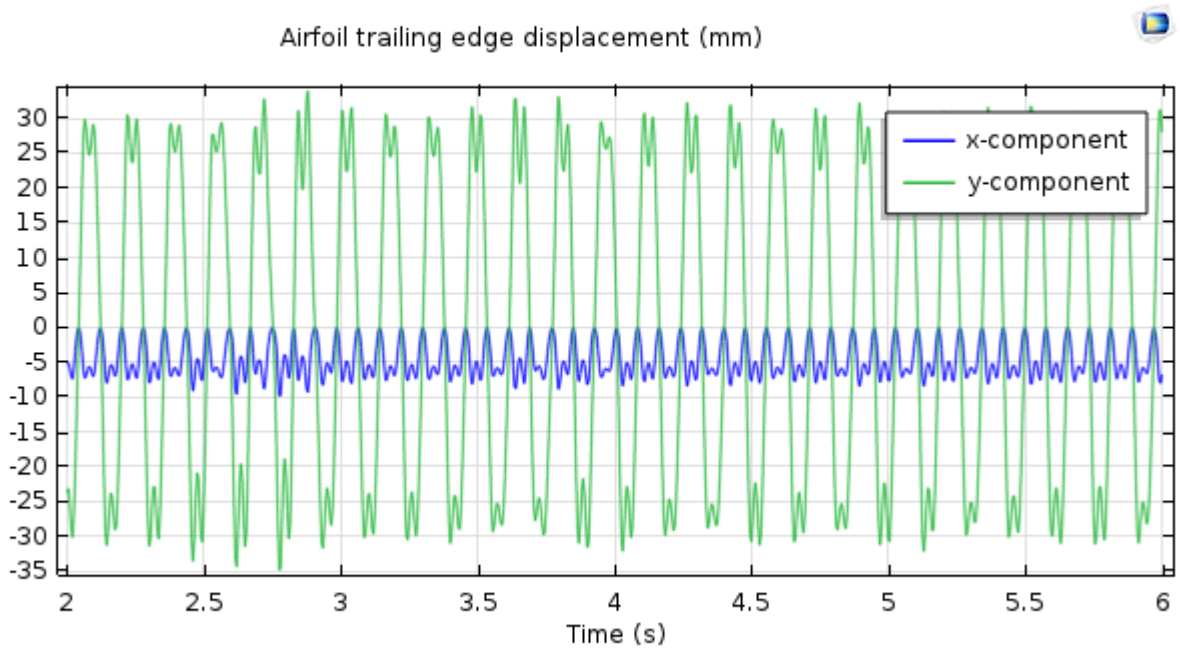

Figure 4: Trailing edge displacement of airfoil in Air at angle of attack 0 NACA0012 Airfoil

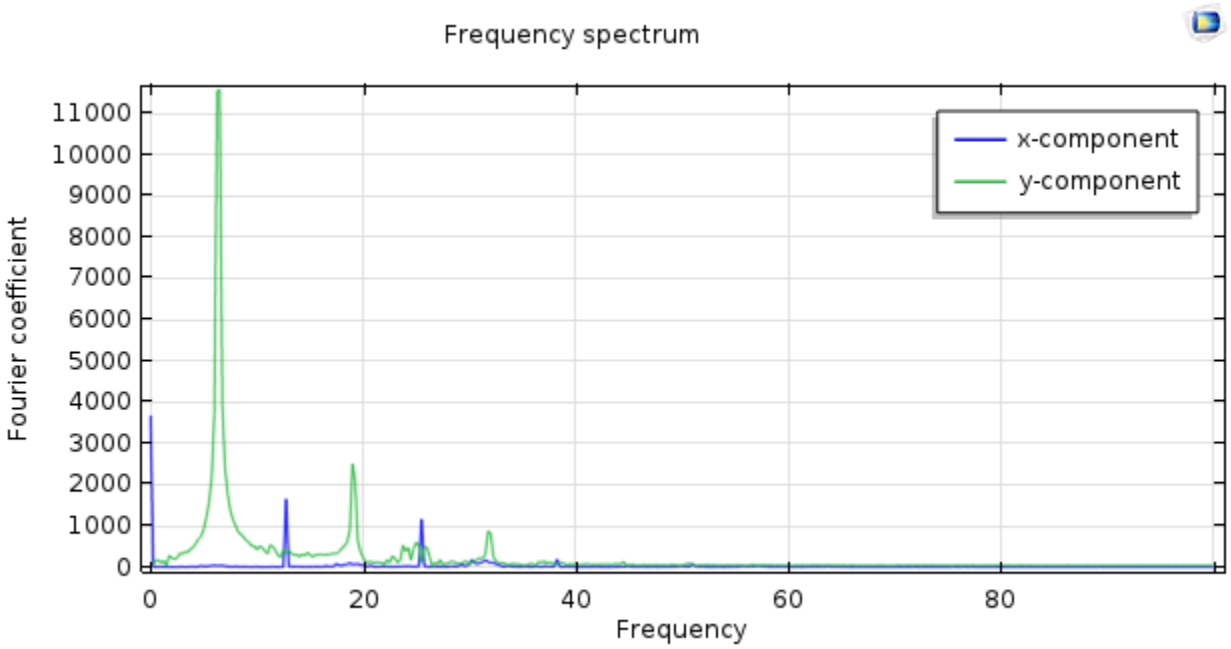

Figure 5: Frequency spectrum of trailing edge in Air at angle of attack 0 NACA0012 Airfoil

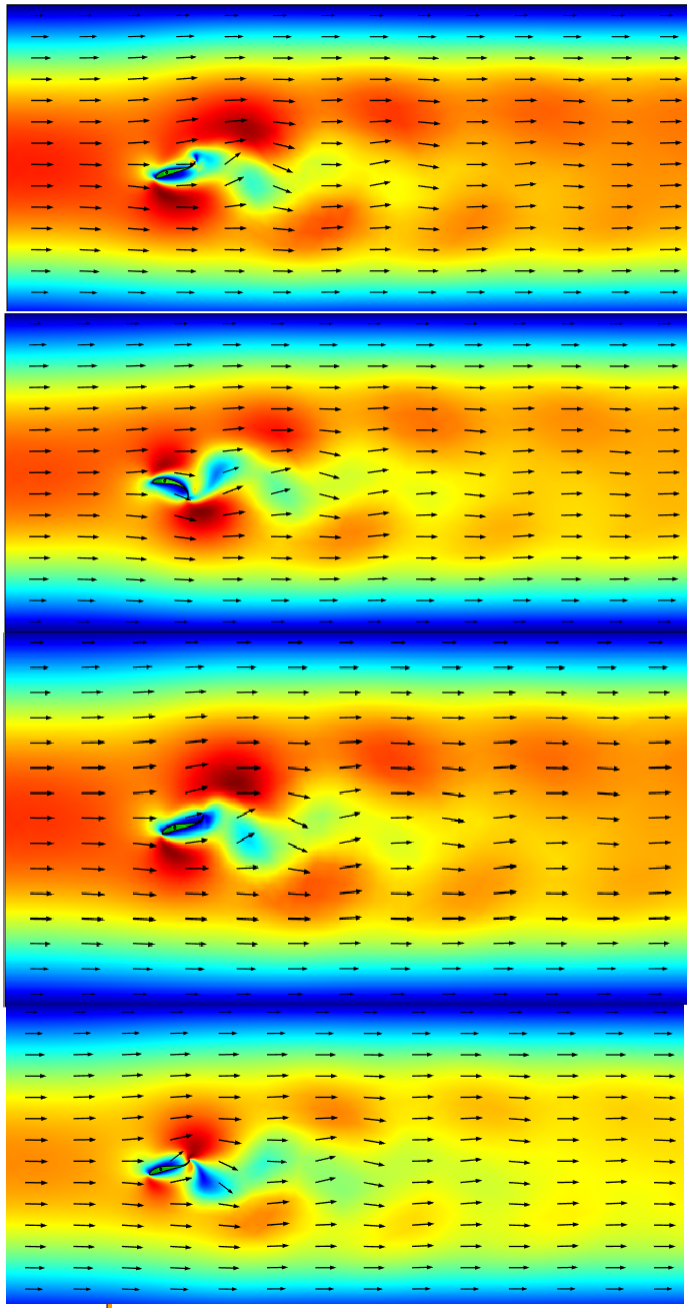

Figure 6: von Mises stress in structure and Velocity field in Air for four different time steps at angle of attack 0 s1223 Airfoil

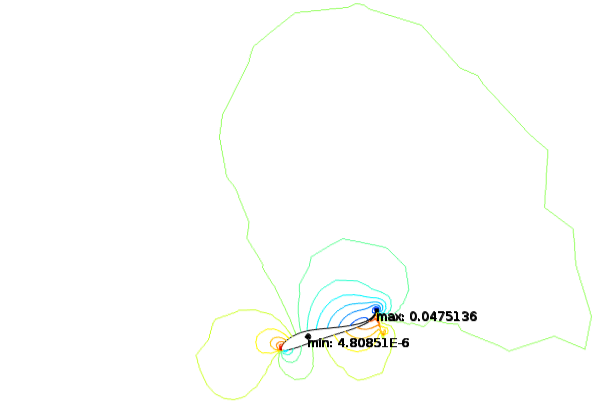
max: 0.0475136
min: 4.80851E-6

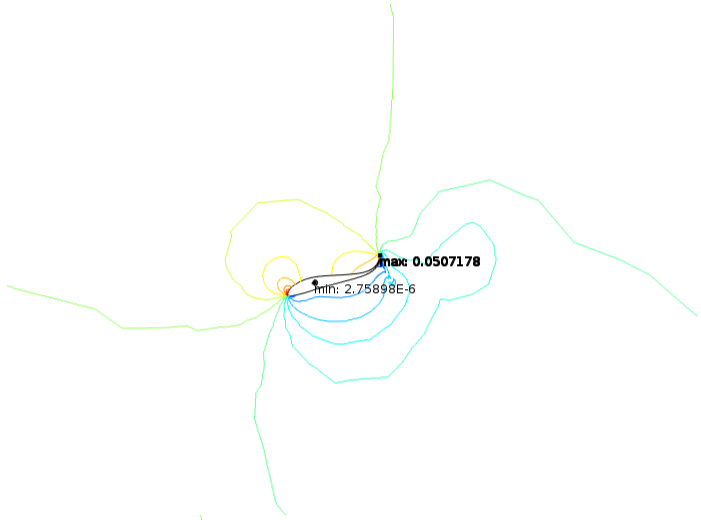
max: 0.0507178
min: 2.75898E-6

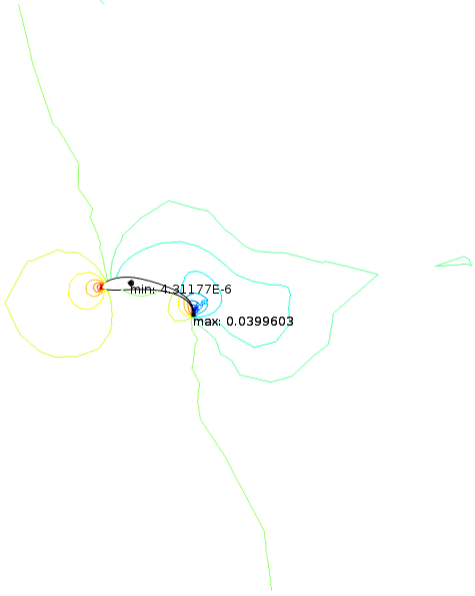
min: 4.31177E-6
max: 0.0399603

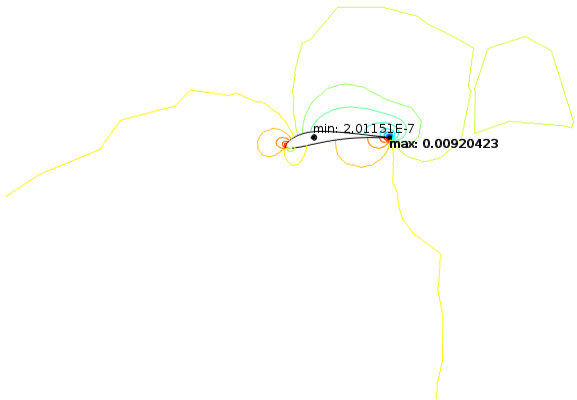
min: 2.01151E-7
max: 0.00920423

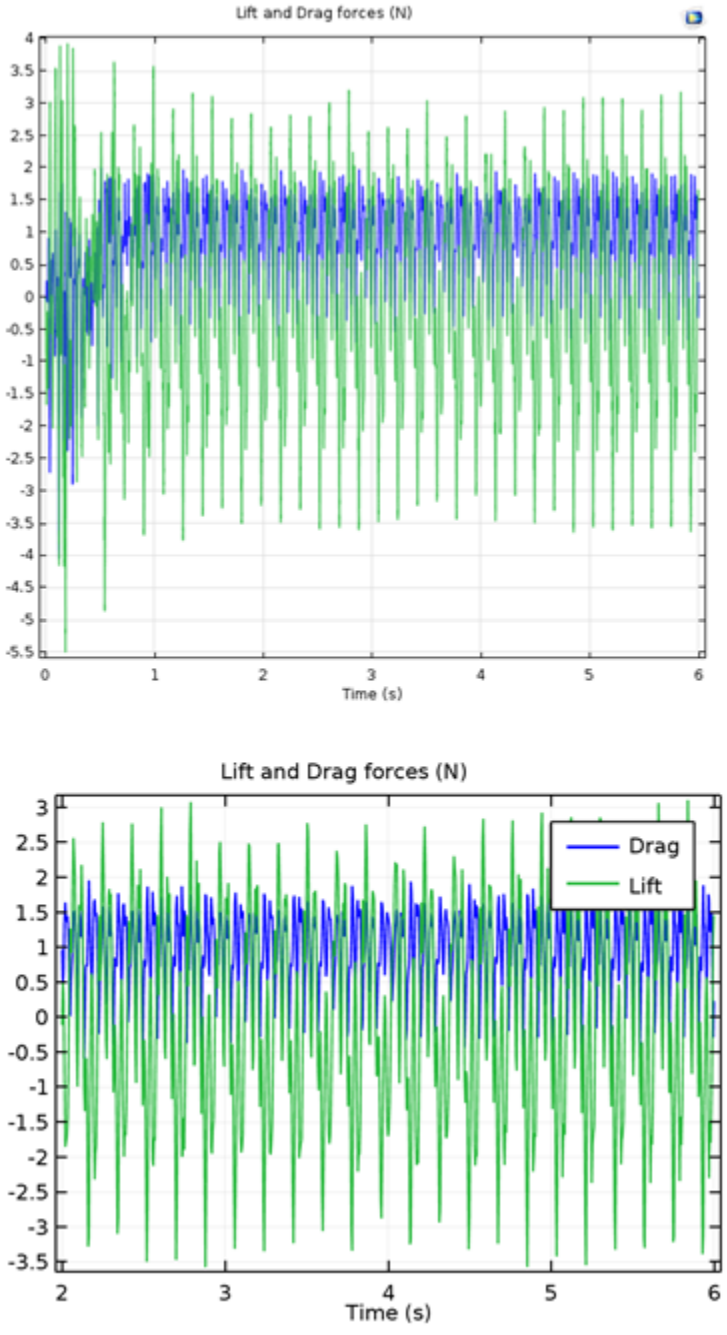

Figure 8: Lift and Drag Forces (N) in Air at angle of attack 0 s1223 Airfoil

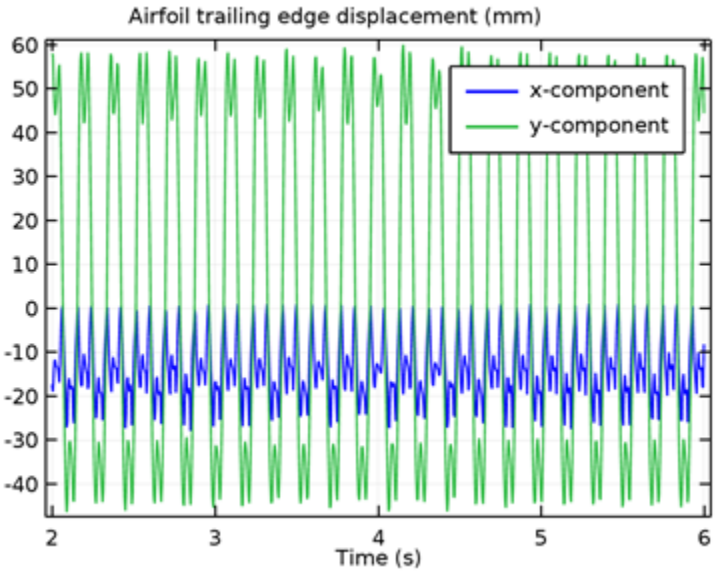

Figure 9: Trailing edge displacement of airfoil in Air at angle of attack 0 s1223 Airfoil

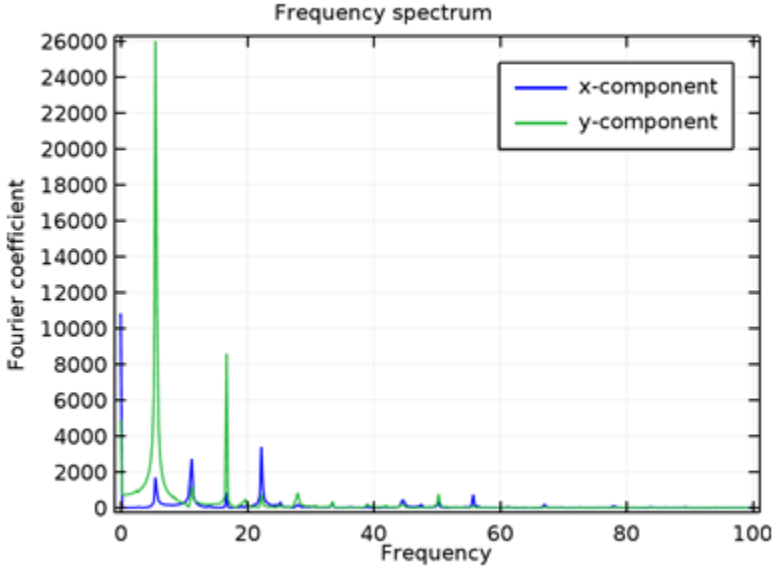

Figure 10: Frequency spectrum of trailing edge in Air at angle of attack 0 s1223 Airfoil

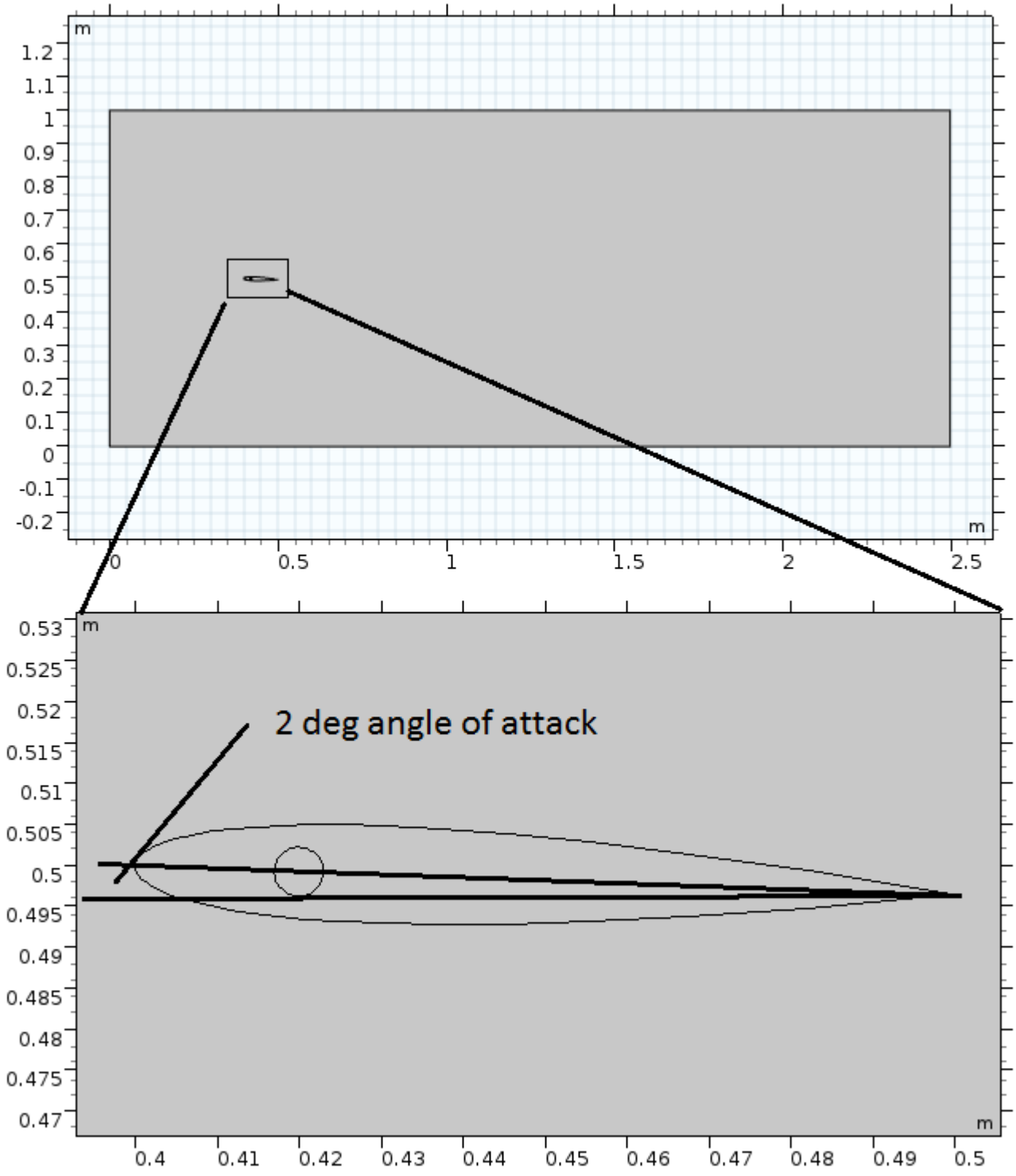

Figure 11: Model geometry and Detail of the structure part NACA0012 Airfoil

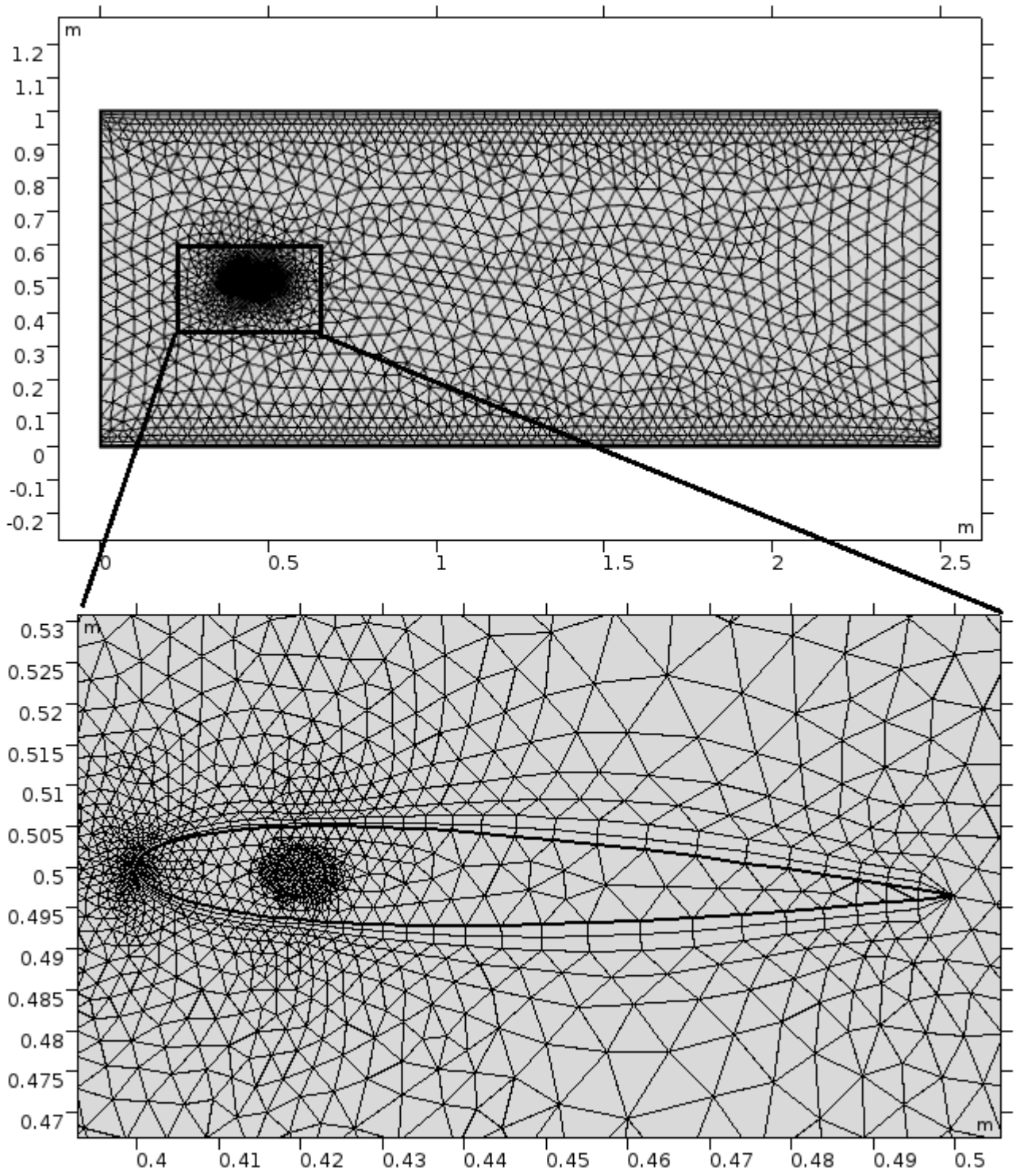

Figure 12: Mesh geometry around NACA0012 Airfoil

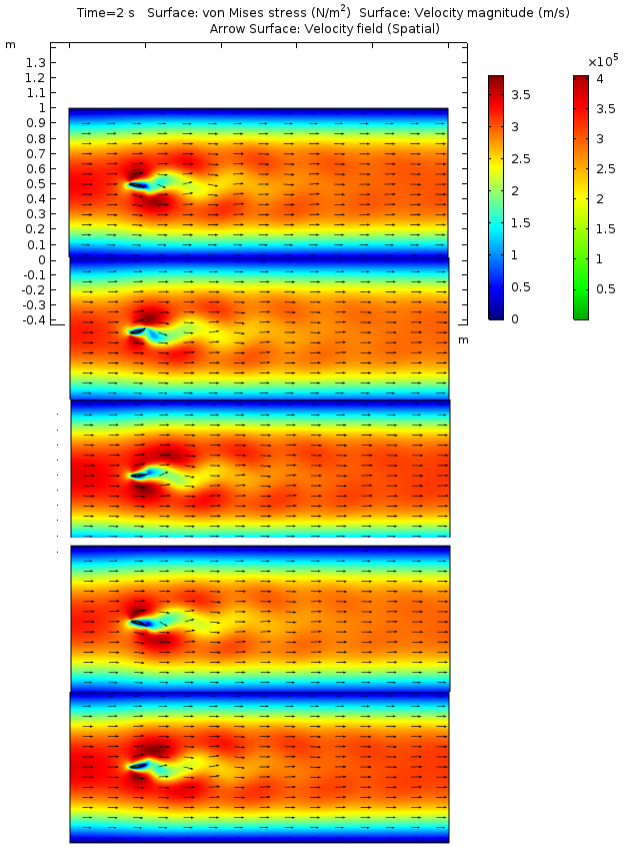

Figure 13: von Mises stress in structure and Velocity field in Air for four different time steps at angle of attack 2 NACA0012 Airfoil

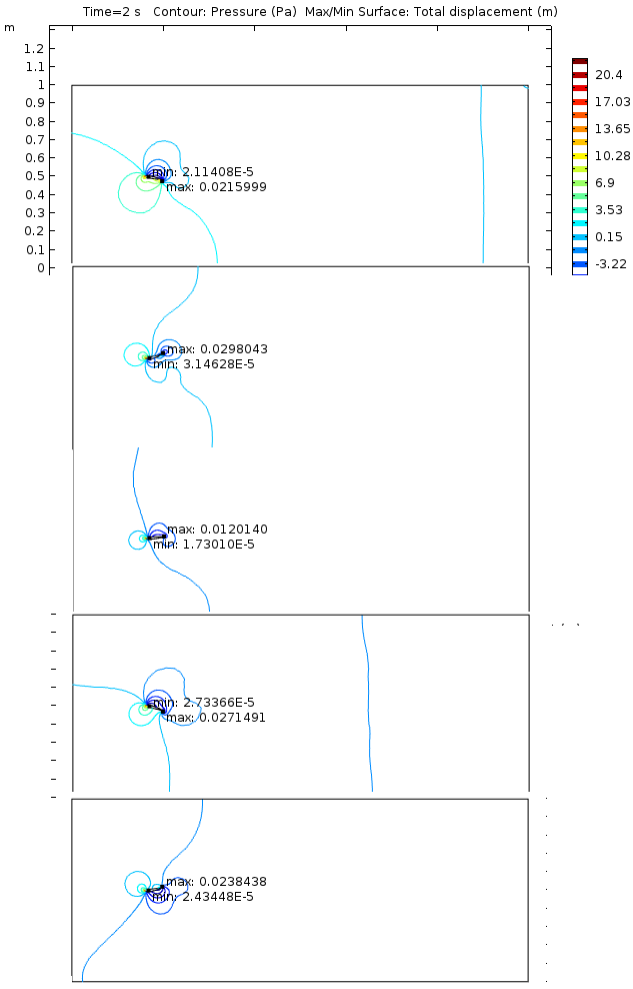

Figure 14: Pressure field in Air for four different time steps at angle of attack 2 NACA0012 Airfoil

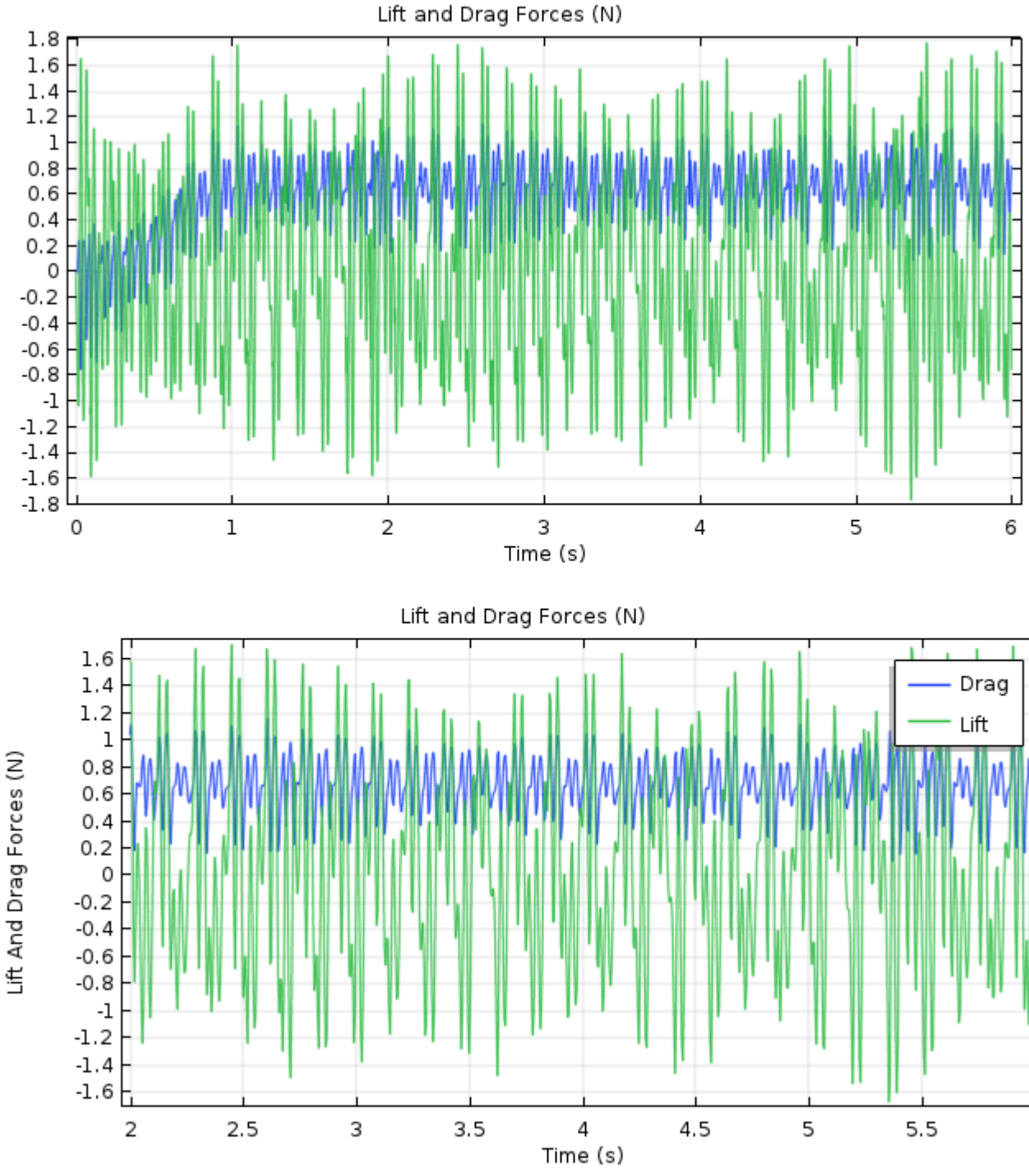

Figure 15: Lift and Drag Forces (N) in Air at angle of attack 2 NACA0012 Airfoil

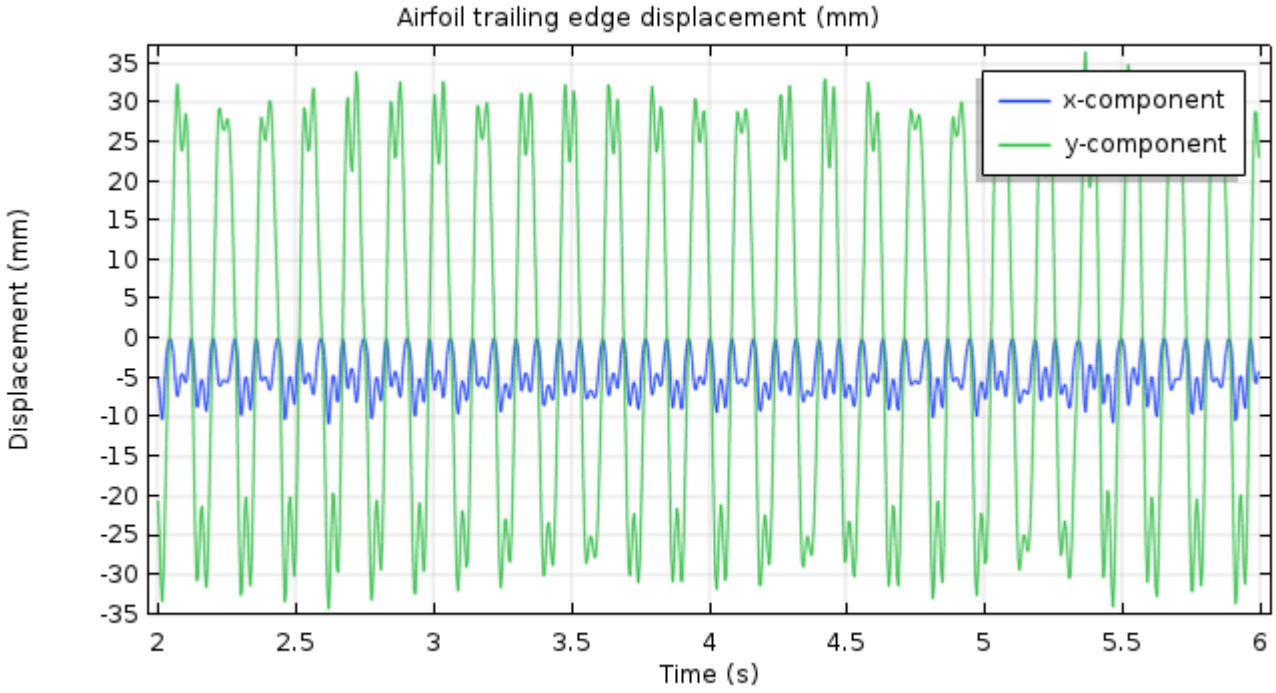

Figure 16: Trailing edge displacement of airfoil in Air at angle of attack 2 NACA0012 Airfoil

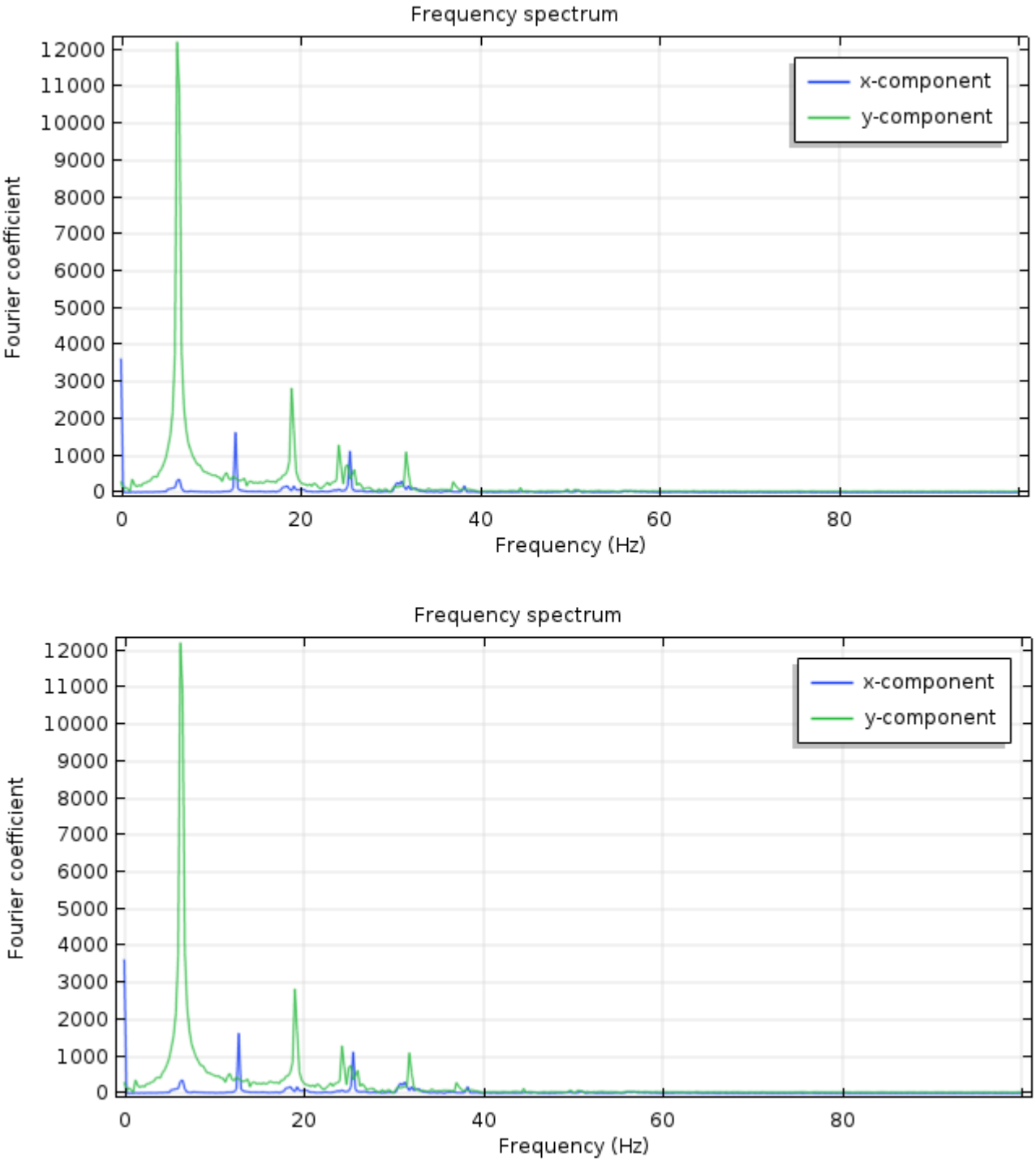

Figure 17: Frequency Spectrum of airfoil in Air at angle of attack 2 NACA0012 Airfoil

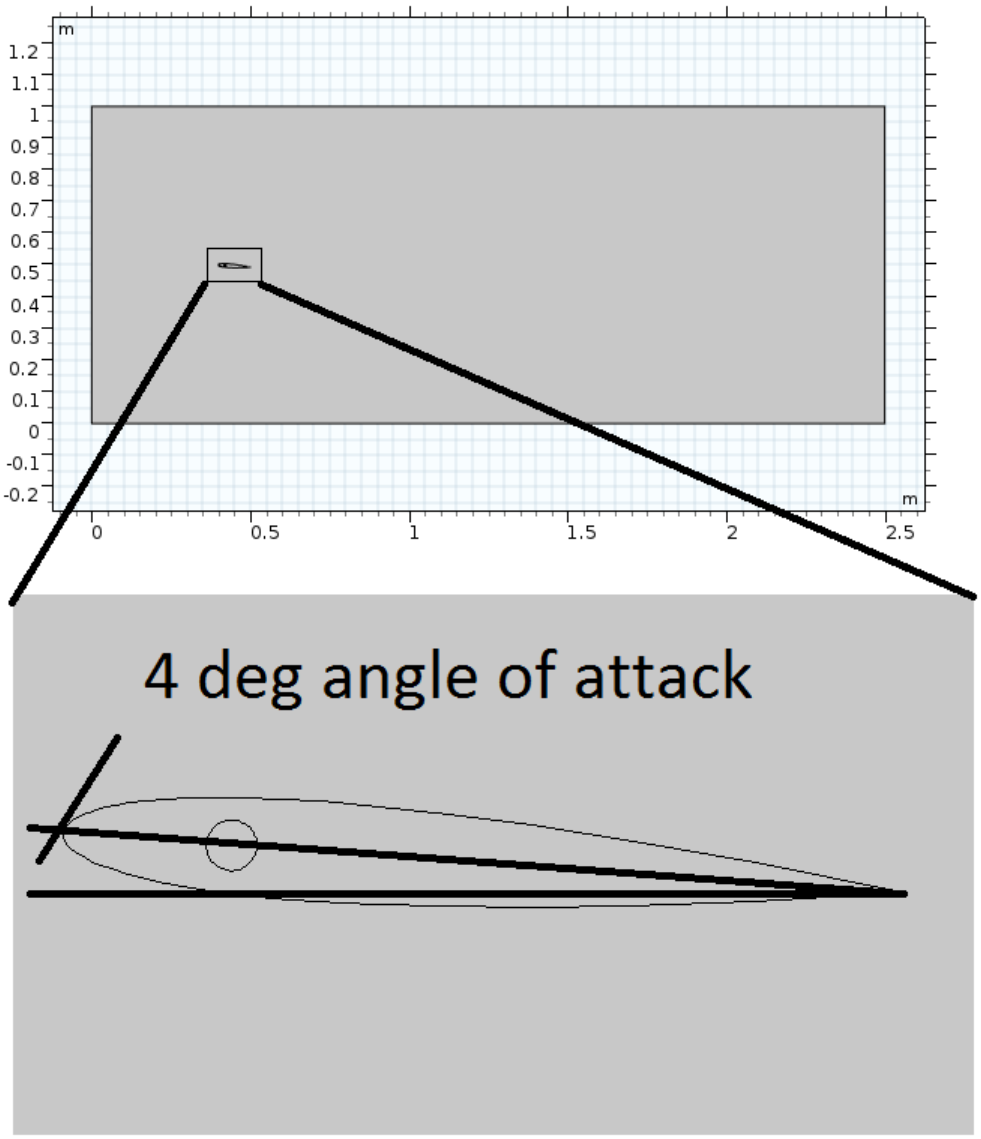

Figure 18: Model geometry and Detail of the structure part NACA0012 Airfoil in Air at 4 angle of attack

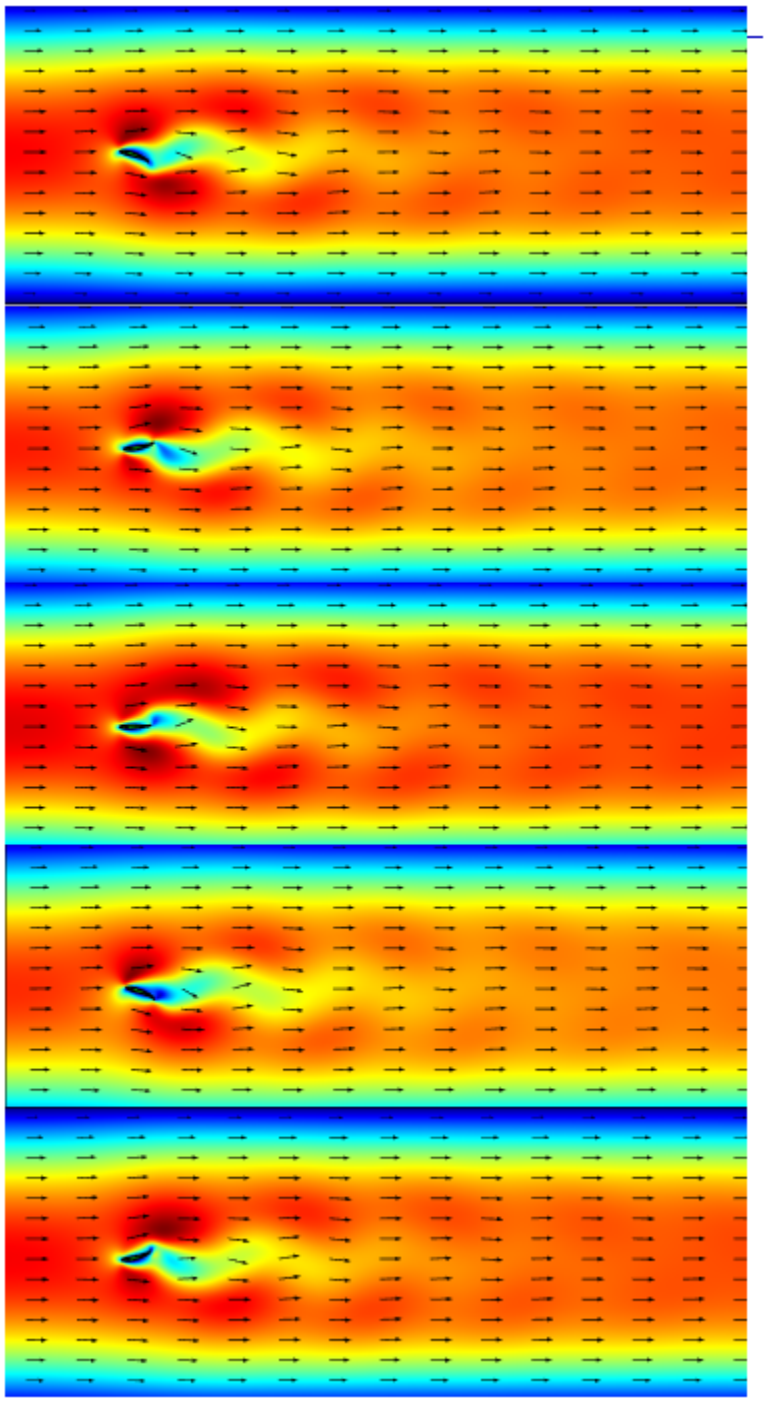

Figure 19: von Mises stress in structure and Velocity field for NACA0012 Airfoil in Air at 4 angle of attack

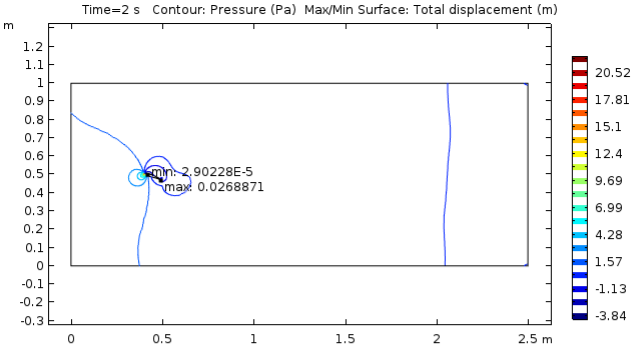
Time=2 s Contour: Pressure (Pa) Max/Min Surface: Total displacement (m)
m
min: 2.90228E-5
max: 0.0268871
20.52
17.81
15.1
12.4
9.69
6.99
4.28
1.57
-1.13
-3.84
0 0.5 1 1.5 2 2.5 m

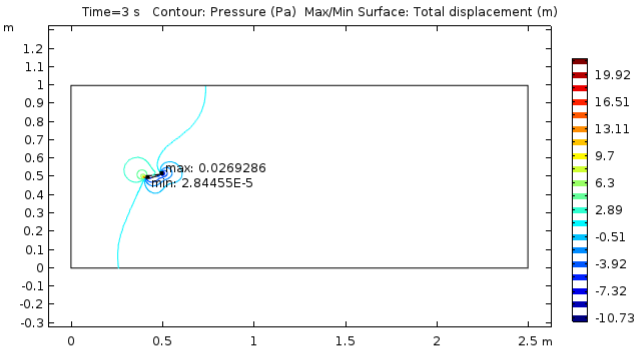
Time=3 s Contour: Pressure (Pa) Max/Min Surface: Total displacement (m)
m
max: 0.0269286
min: 2.84455E-5
19.92
16.51
13.11
9.7
6.3
2.89
-0.51
-3.92
-7.32
-10.73
0 0.5 1 1.5 2 2.5 m

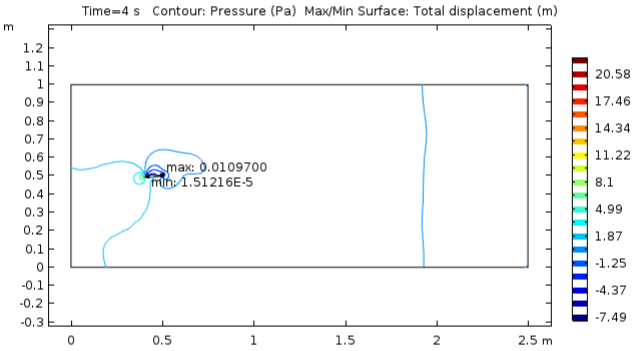
Time=4 s Contour: Pressure (Pa) Max/Min Surface: Total displacement (m)
m
max: 0.0109700
min: 1.51216E-5
20.58
17.46
14.34
11.22
8.1
4.99
1.87
-1.25
-4.37
-7.49
0 0.5 1 1.5 2 2.5 m

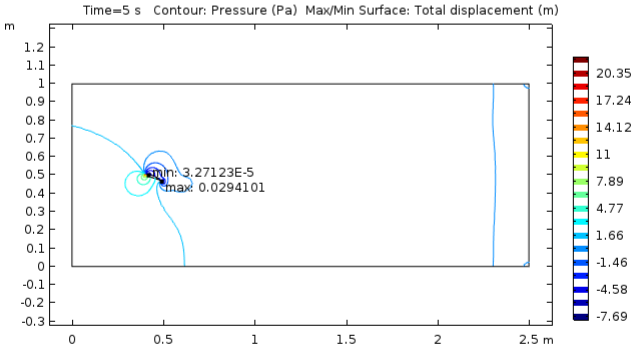
Time=5 s Contour: Pressure (Pa) Max/Min Surface: Total displacement (m)
m
min: 3.27123E-5
max: 0.0294101
20.35
17.24
14.12
11
7.89
4.77
1.66
-1.46
-4.58
-7.69
0 0.5 1 1.5 2 2.5 m

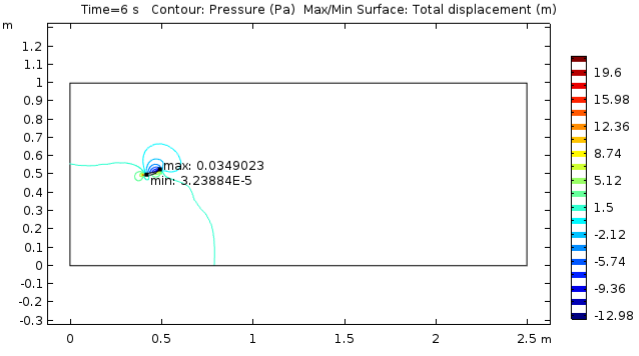
Time=6 s Contour: Pressure (Pa) Max/Min Surface: Total displacement (m)
m
max: 0.0349023
min: 3.23884E-5
19.6
15.98
12.36
8.74
5.12
1.5
-2.12
-5.74
-9.36
-12.98
0 0.5 1 1.5 2 2.5 m

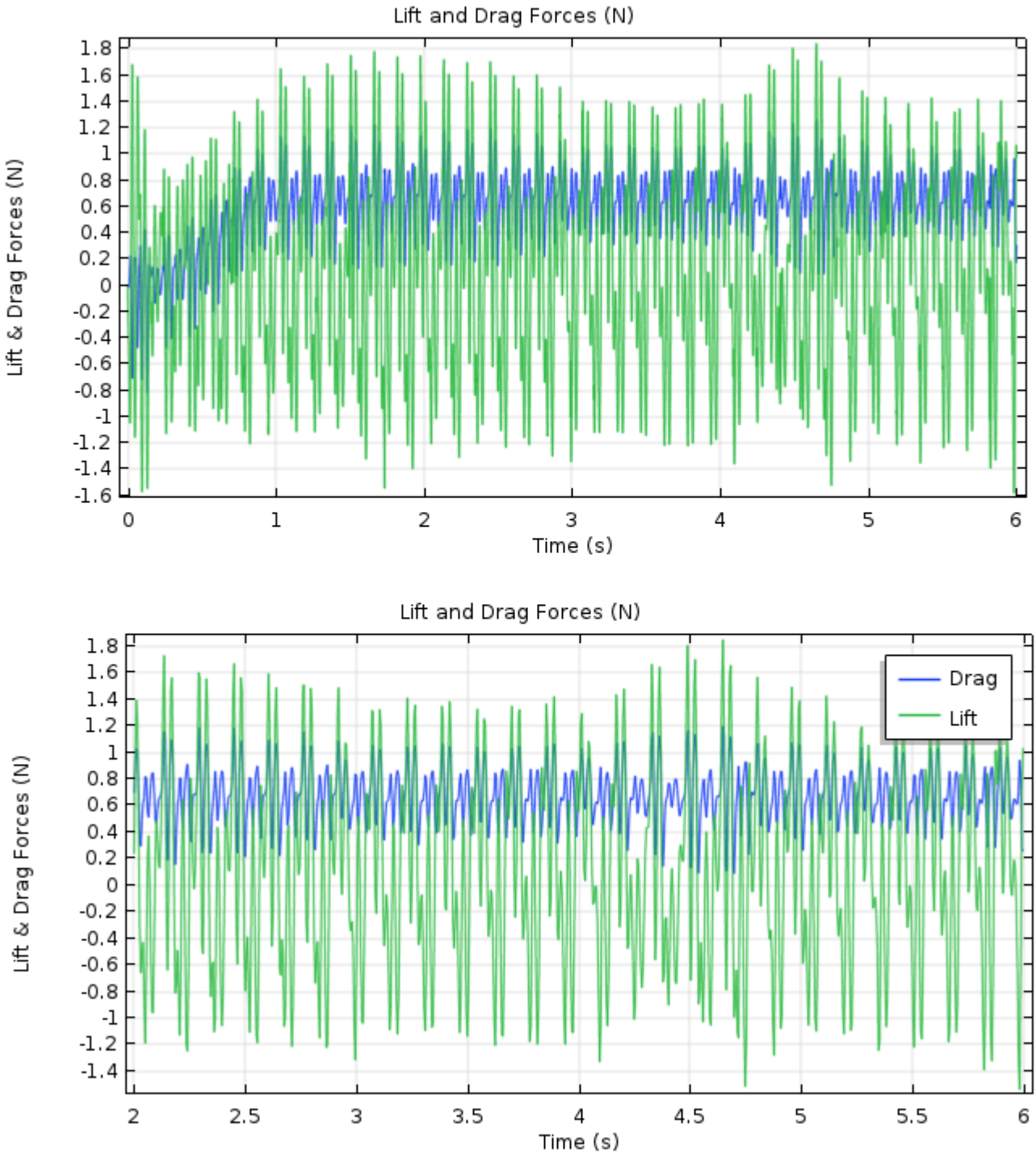

Figure 21: Lift and Drag Forces (N) in Air at 4 angle of attack NACA0012 Airfoil

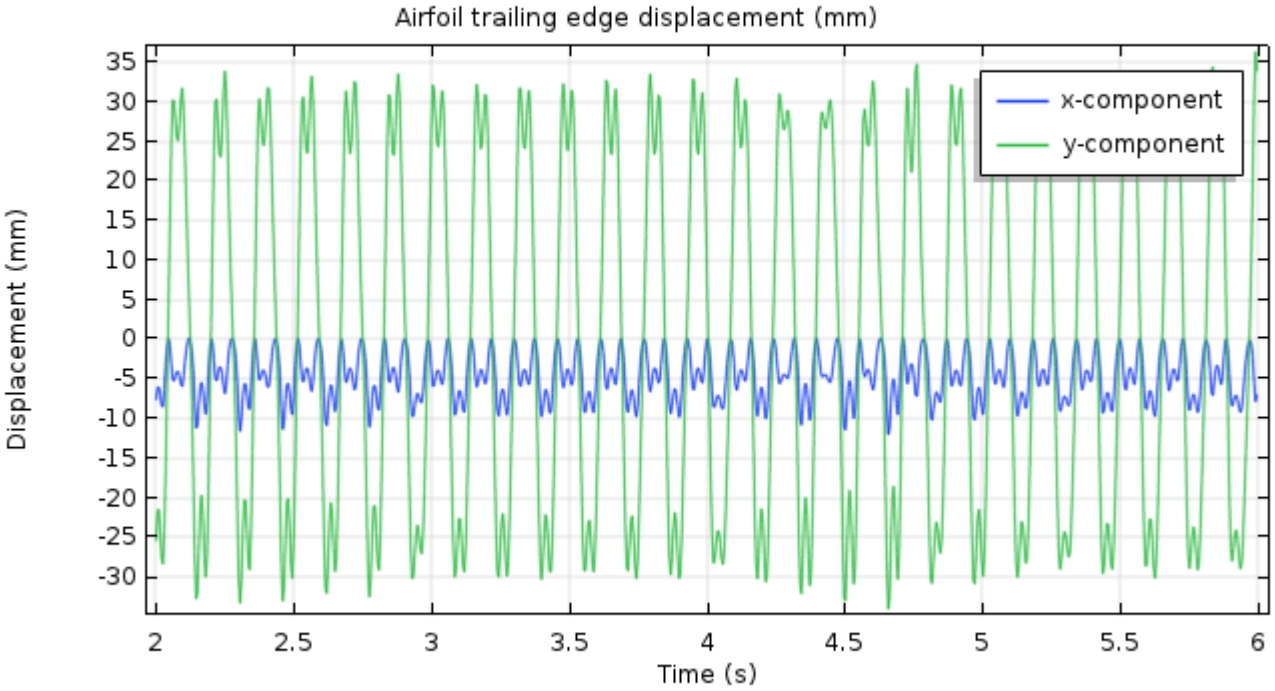

Figure 22: Trailing edge displacement of airfoil in Air at angle of attack 2 NACA0012 Airfoil

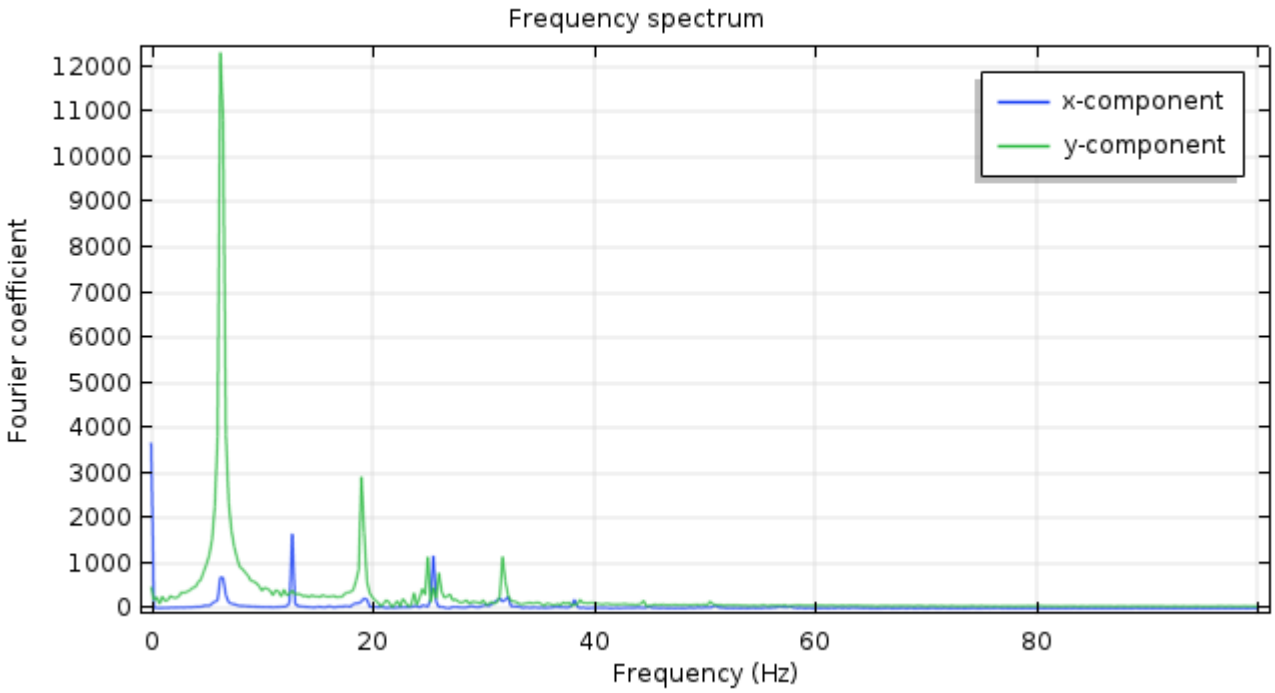

Figure 23: Frequency Spectrum of airfoil in Air at 4 angle of attack NACA0012 Airfoil

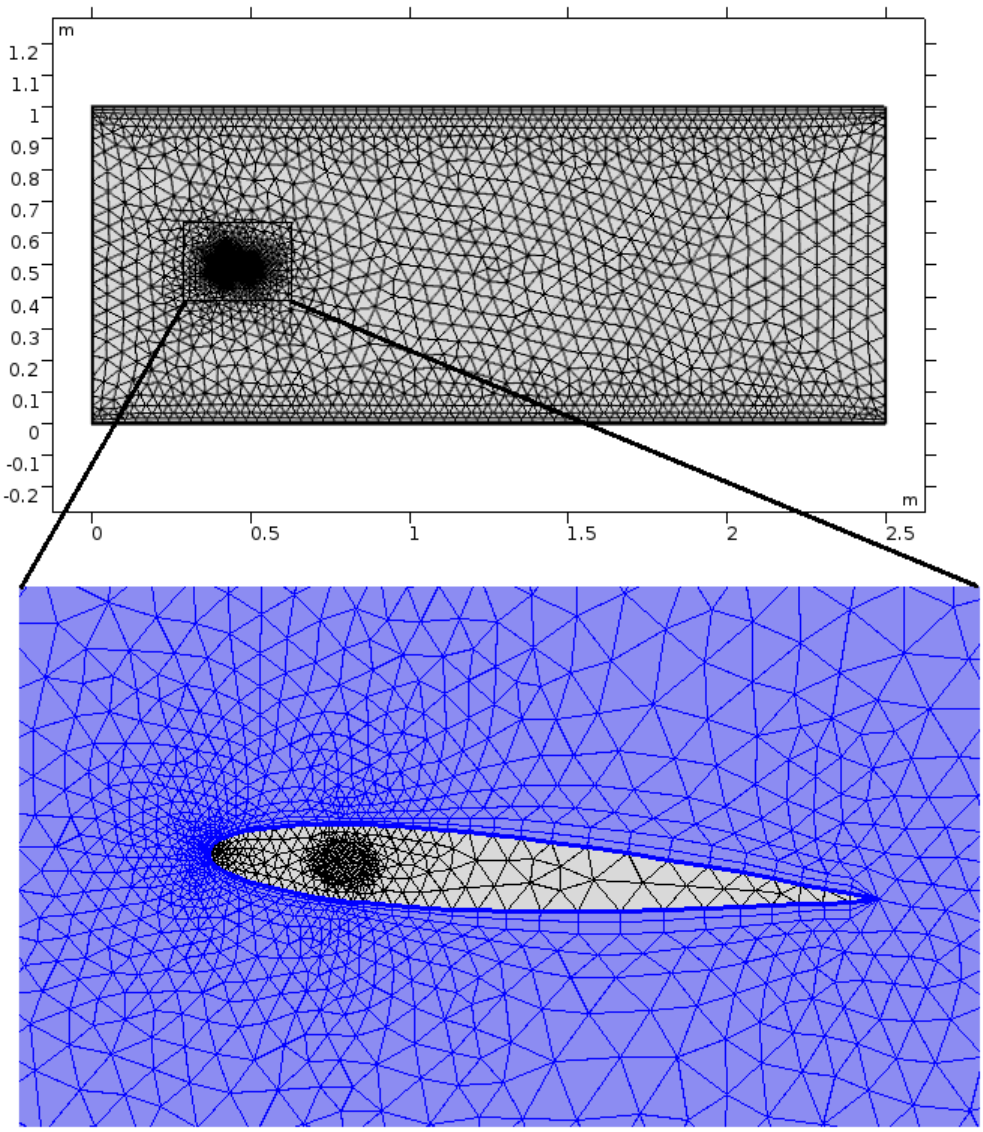

Figure 24: Mesh geometry around NACA0012 Airfoil

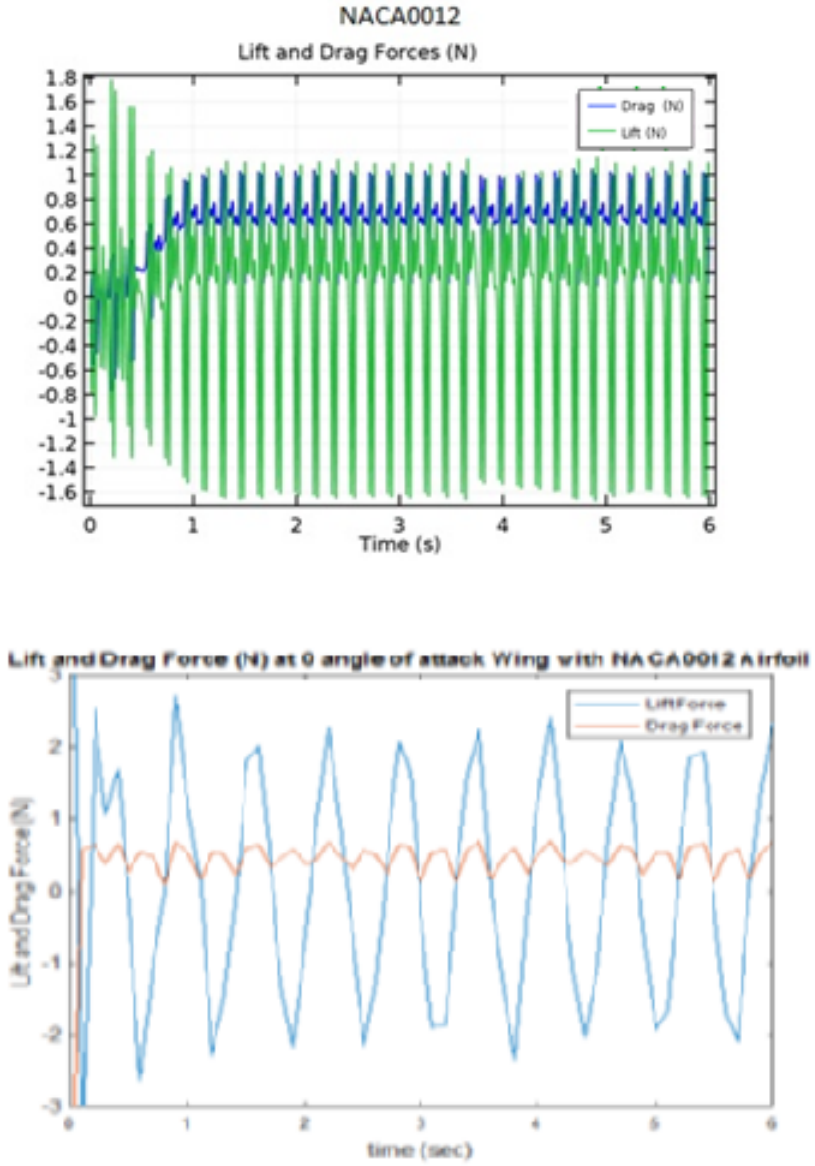

Figure 25: Comparison Lift and Drag Forces (N) in Air between NACA0012 Airfoil and wing with NACA0012 Airfoil at angle of attack 0

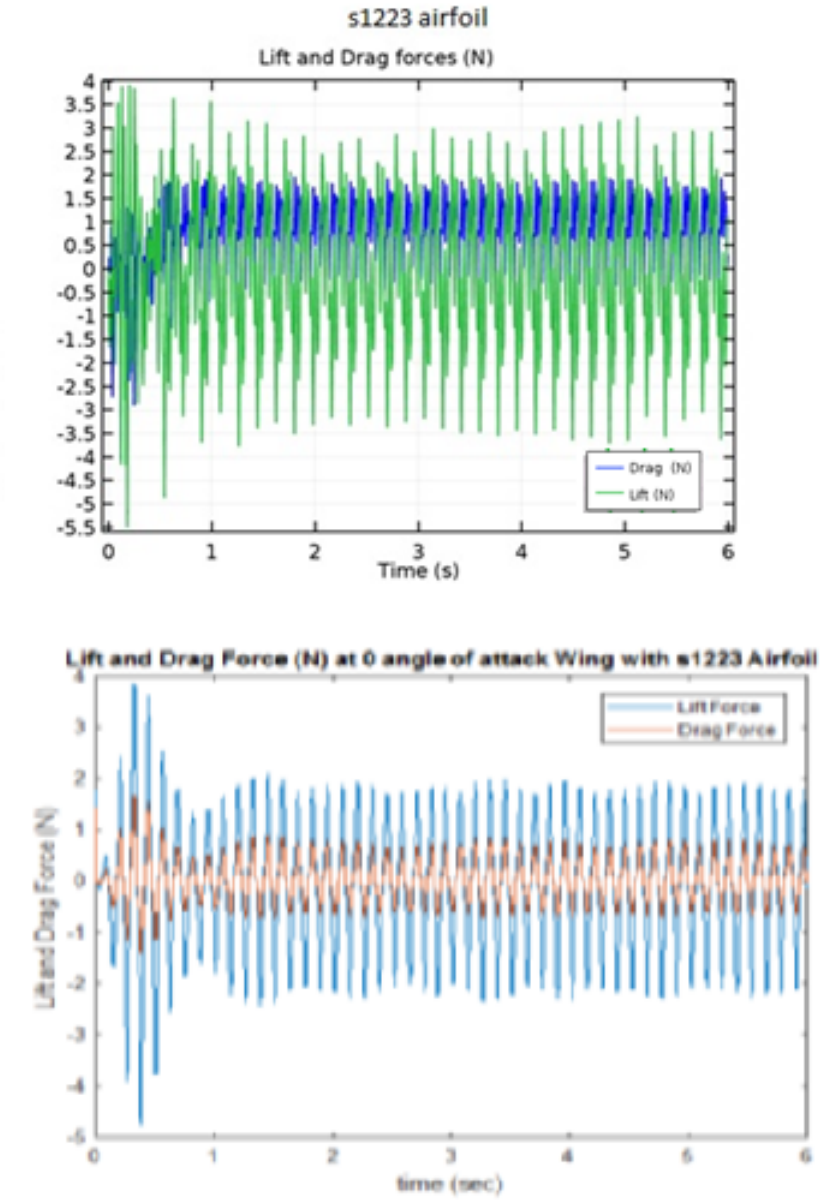

Figure 26: Comparison Lift and Drag Forces (N) in Air between s1223 Airfoil and wing with s1223 Airfoil at angle of attack 0

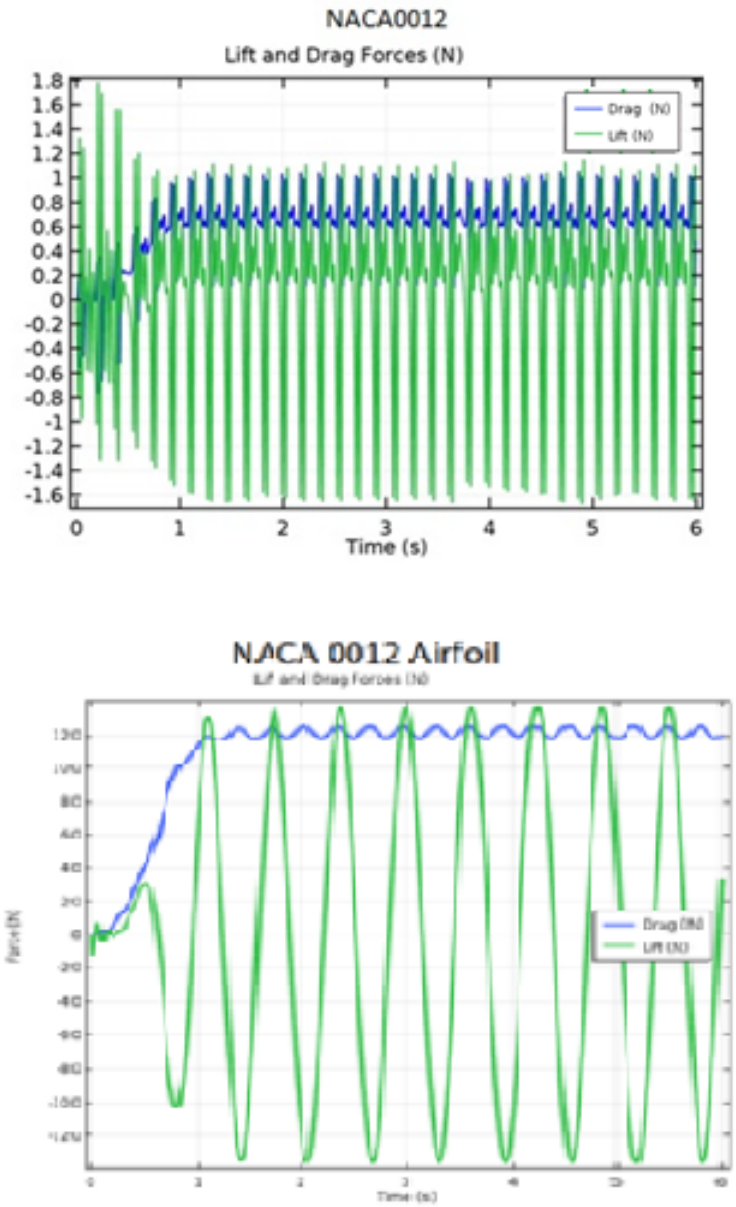

Figure 27: Comparison Lift and Drag Forces (N) between Air and Glycerin for NACA0012 Airfoil at angle of attack 0

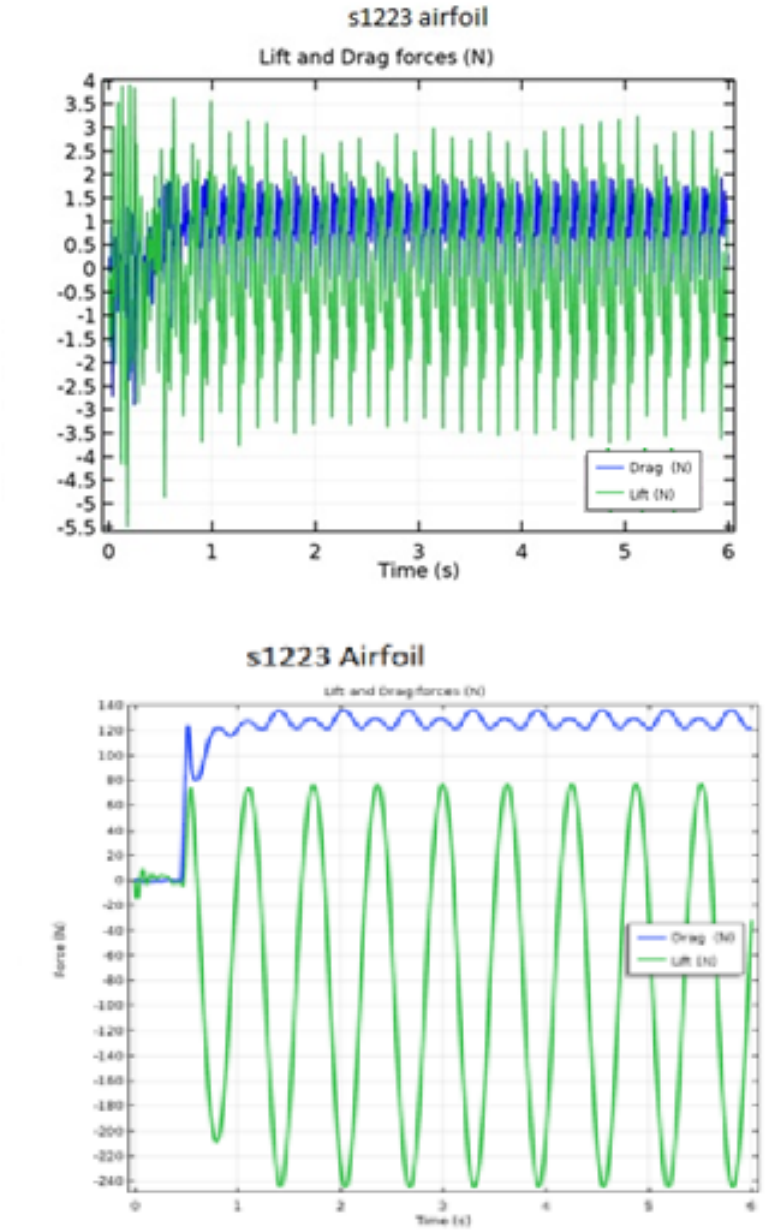

Figure 28: Comparison Lift and Drag Forces (N) between Air and Glycerin for s1223 Airfoil at angle of attack 0

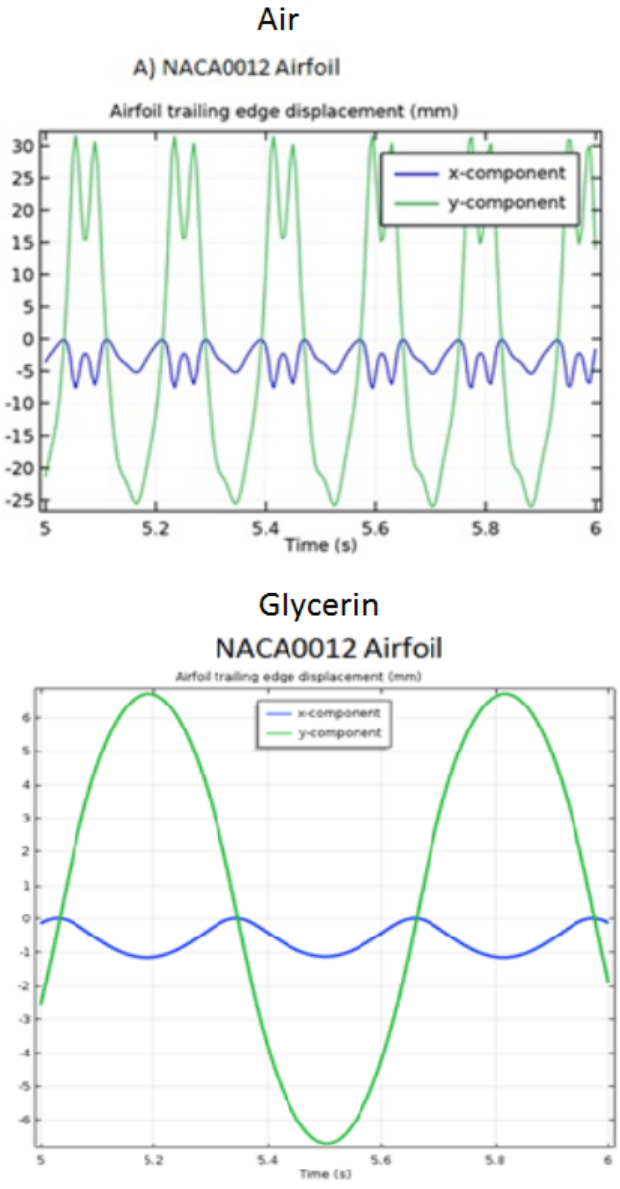

Figure 29: Comparison Trailing edge displacement (mm) between Air and Glycerin for NACA0012 Airfoil at angle of attack 0

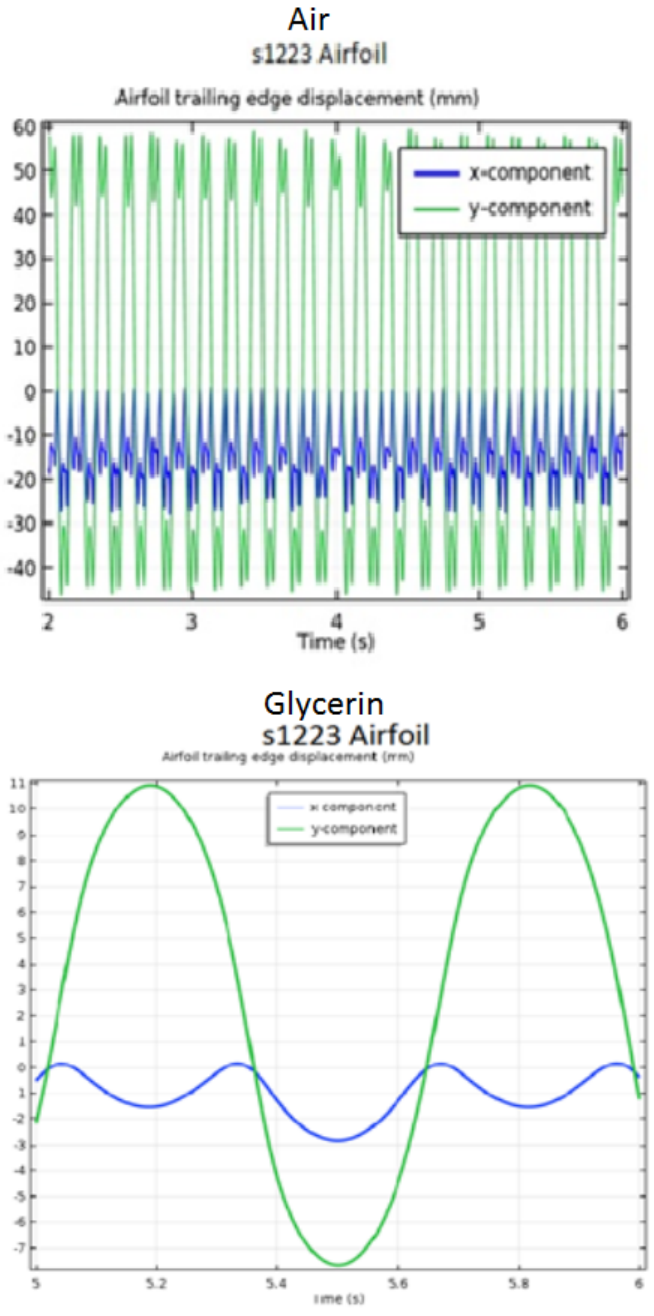

Figure 30: Comparison Trailing edge displacement (mm) between Air and Glycerin for s1223 Airfoil at angle of attack 0

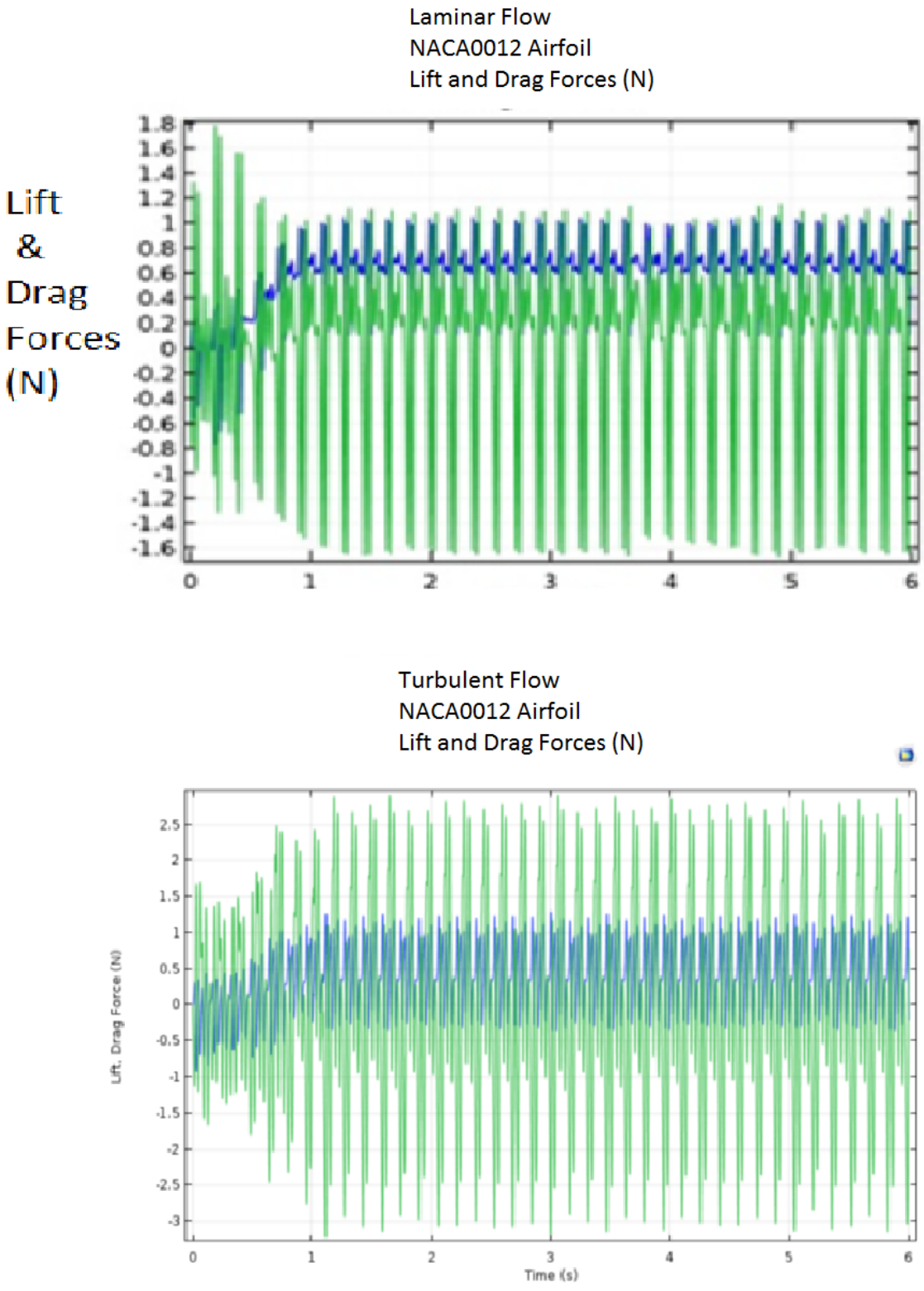

Figure 31: Comparison Lift and Drag Forces (N) between Laminar flow and Turbulent flow for NACA0012 Airfoil at angle of attack 0

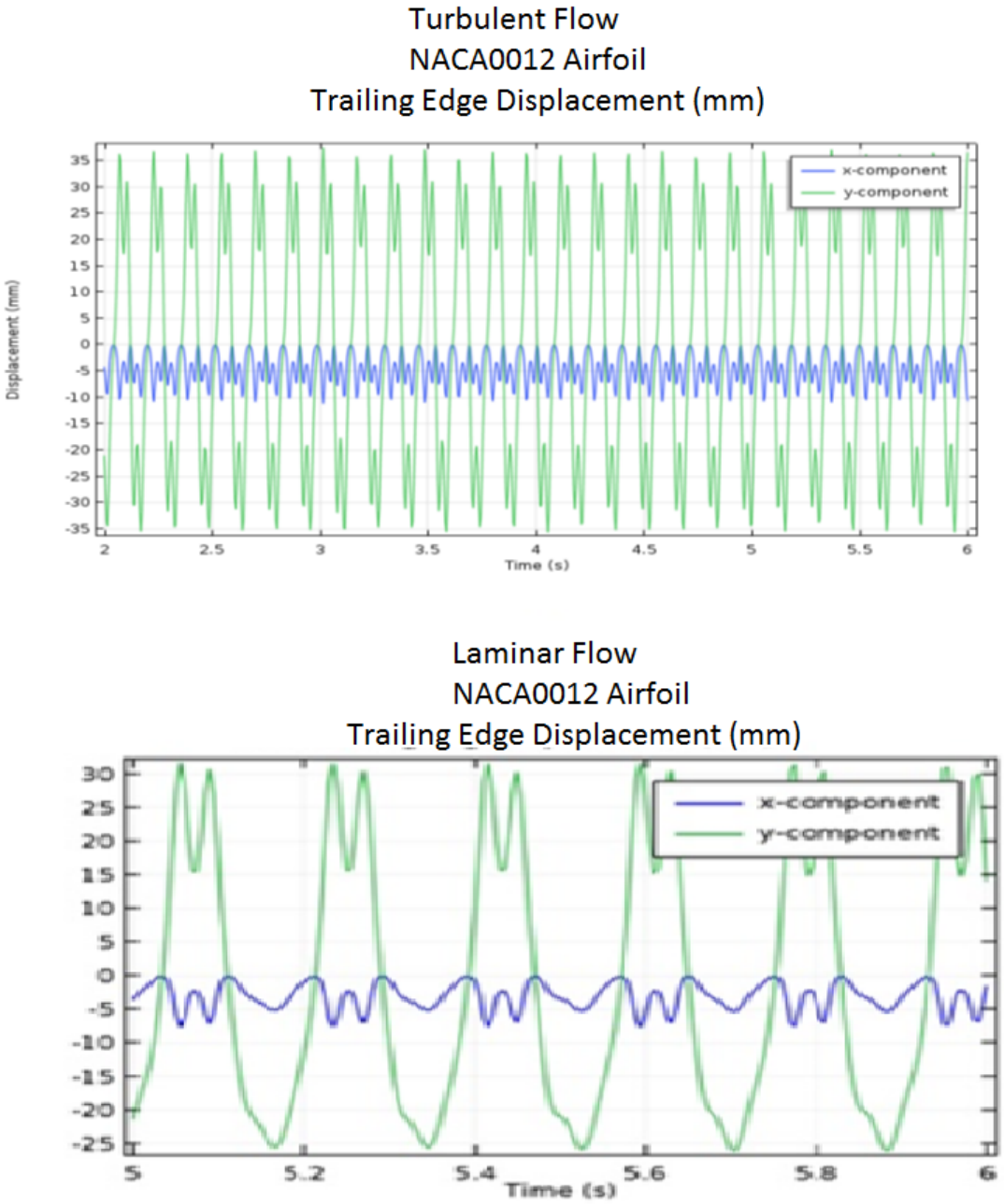

Figure 32: Comparison Trailing edge displacement (mm) between Laminar flow and Turbulent flow for NACA0012 Airfoil at angle of attack 0

Bibliography

[1] NOVA Science Programming of Air and Online, "Spies that Fly", November (2011), publisher (http://www.pbs.org/wgbh/nova/spiesfly/uavs.html)

[2] Hiong Go, Tiauw, and Wang Hao. "Investigation on propulsion of flapping wing with modified pitch motion." Aircraft Engineering and Aerospace Technology 82, no. 4 (2010): 217-224

[3] Gutierrez, Eric, Daniel B. Quinn, Diana D. Chin, and David Lentink. "Lift calculations based on accepted wake models for animal flight are inconsistent and sensitive to vortex dynamics." Bioinspiration & biomimetics 12, no. 1 (2016): 016004

[4] Curtis, David H., Mark F. Reeder, Craig E. Svanberg, Richard G. Cobb, and Gregory H. Parker. "Flapping Wing Micro Air Vehicle Bench Test Setup." International Journal of Micro Air Vehicles 4, no. 1 (2012): 51-77.

[5] J.D. DeLaurier, "An aerodynamic model for flapping-wing flight", Aeronautical Journal of the Royal Aeronautical Society, volume(97), Issue(964), pages(125–130), April (1993), publisher (Cambridge Core)

[6] Chirarattananon, Pakpong, Yufeng Chen, E. Farrell Helbling, Kevin Y. Ma, Richard Cheng, and Robert J. Wood, "Dynamics and flight control of a flapping-wing robotic insect in the presence of wind gusts", Interface focus 7, no. 1, February (2017), p.20160080

[7] Floreano, Dario, and Robert J. Wood. "Science, technology and the future of small autonomous drones." Nature 521, no. 7553 (2015): 460

[8] J.D. DeLaurier, "The development of an efficient ornithopter wing", Aeronautical Journal of the Royal Aeronautical Society, volume(97), Issue(965), pages (153–162), May (1993), publisher (Cambridge Core)

[9] Craparo E and Ingram B, "A micro-sized ornithopter wing design", January (2003), In41st aerospace sciences meeting and exhibit, p. 108

[10] Menter, F. R., "Two-Equation Eddy Viscosity Models for Engineering Applications", AIAA Journal, Volume(32), No. 8, 1994, pp. 1598-1605

[11] T.Theodorsen, "General Theory of Aerodynamic Instability and the mechanism of Flutter", January (1934), publisher (NACA Report No. R/496)

[12] Han, J., Lee, J., and Kim,D., "Bio-inspired UAV Design", A University Perspective. Proc. Of SPIE Vol. 7295,729511, 2009.

[13] Kessler, S. and Speering, S., "Design of a High-g Unmanned Aerial Vehicle Structure", SAE international, and American Institute of Aeronautics and Astronautics, 2000.

[14] Hall, K. C., Pigott, S. A. and Hall, S. R., "Power Requirements for Large - Amplitude Flapping Flight", AIAA Paper 97-0827, January 1997.

[15] Hansen. J.R., "The Bird is on the Wing: Aerodynamics and the Progress of the American Airplane", 2004, Texas: A& M University Press.

[16] Videler, J.J., 2006. Aviation Flight. Oxford: Oxford University Press.

[17] Scholz, M.P., "Advanced NXT: The Da Vinci Inventions Book", 2007, New York: Apress

[18] Yang, Lung-Jieh, Balasubramanian Esakki, Udayagiri Chandrasekhar, Kuan-Cheng Hung, and Chieh-Ming Cheng. "Practical flapping mechanisms for 20 cm-span micro air vehicles." International Journal of Micro Air Vehicles 7, no. 2 (2015): 181-202.

[19] Burgess, S. C., R. J. Lock, J. Wang, G. D. Sattler, and J. D. Oliver. "The energy benefits of the pantograph wing mechanism in flapping flight: case study of a gull." International Journal of Micro Air Vehicles 7, no. 3 (2015): 275-283.

[20] Nakata, Toshiyuki, and Hao Liu. "Aerodynamic performance of a hovering hawkmoth with flexible wings: a computational approach." Proc. R. Soc. B 279.1729 (2012): 722-731

[21] Mountcastle, A. M., and Daniel, T. L. (2010). Aerodynamic and functional consequences of wing compliance. In Animal Locomotion (pp. 311-320). Springer, Berlin, Heidelberg

[22] Barannyk O, Buckham B J and Oshkai P 2012 On performance of an oscillating plate underwater propulsion system with variable chordwise flexibility at different depths of submergence Journal of Fluids and Structures 28 152-66

[23] Lienhard , John H., "Abbas Ibn Firnas, The Engines of Our Ingenuity", NPR. KUHF-FM Houston. 2004. No. 1910. Transcript (http:// www.uh.edu/engines/epi1910.htm).

[24] Old, W., "To Fly: The History of Wright Brothers", 2002, New York: Clarion Books.

[25] , Maxworthy, Tony. "Experiments on the Weis-Fogh mechanism of lift generation by insects in hovering flight. Part 1. Dynamics of the fling." Journal of Fluid Mechanics 93, no. 1 (1979): 47-63.

[26] Ellington, Charles Porter. "The aerodynamics of hovering insect flight. IV. Aerodynamic mechanisms." Philosophical Transactions of the Royal Society of London. B, Biological Sciences 305, no. 1122 (1984): 79-113.

[27] , Shyy, Wei, Peter Ifju, and Dragos Viieru. "Membrane wing-based micro air vehicles." Applied mechanics reviews 58, no. 4 (2005): 283-301.

[28] Jones, KD and Lund, TC and Platzer, MF, "Experimental and computational investigation of flapping wing propulsion for micro air vehicles", Journal of Fixed and Flapping Wing Aerodynamics for Micro Air Vehicle Applications, volume (195), Issue(964), pages (307–339), 2000

[29] Jones, KD and Bradshaw, CJ and Papadopoulos, J and Platzer, MF, "Bio-inspired design of flapping-wing micro air vehicles", The Aeronautical Journal, volume (109), Number(1098), pages (385–393), 2005, publisher (Cambridge University Press)

[30] Ho, Steven and Nassef, Hany and Pornsinsirirak, Nick and Tai, Yu-Chong and Ho, Chih-Ming, "Unsteady aerodynamics and flow control for flapping wing flyers", Journal of Progress in Aerospace Sciences, volume (39), Number(8), pages (635–681), 2003, publisher (Elsevier)

[31] Raney, David L and Slominski, Eric C, "Mechanization and control concepts for biologically inspired micro air vehicles", Journal of Aircraft, volume (41), Number(6), pages (1257–1265), 2004

[32] Deal, Christopher and Huang, Po-Hao, "Remote Control Hovering Ornithopter", 46th AIAA Aerospace Sciences Meeting and Exhibit, pages (1421), 2008

[33] Lin, Che-Shu and Hwu, Chyanbin and Young, Wen-Bin, "The Thrust and Lift of an Ornithopter's Membrane Wings With Simple Flapping Motion", Aerospace Science and Technology - AEROSP SCI TECHNOL, volume (10), pages (111-119), March 2006

[34] Mau, Sandra, "Ornithopter Wing Optimization", Unpublished personal notes, August 2003

[35] , Jones, A. R., N. M. Bakhtian, and H. Babinsky. "Low Reynolds number aerodynamics of leading-edge flaps." Journal of Aircraft 45, no. 1 (2008): 342-345.

[36] Yang, S. L., and G. R. Spedding. "Passive separation control by acoustic resonance." Experiments in fluids 54, no. 10 (2013): 1603.

[37] Etkin, Bernard and Reid, Lloyd Duff, "Dynamics of flight: stability and control", volume (3), 1996, publisher (Wiley New York)

[38] Khan, Zaeem A and Agrawal, Sunil K, "Modeling and simulation of flapping wing micro air vehicles", ASME 2005 International Design Engineering Technical Conferences and Computers and Information in Engineering Conference, pages (871–879), 2005, publisher (American Society of Mechanical Engineers)

[39] Sane, Sanjay P and Dickinson, Michael H, "The control of flight force by a flapping wing: lift and drag production", Journal of experimental biology, volume (204), Number(15), pages (2607–2626), 2001, publisher (The Company of Biologists Ltd)

[40] Duan, Hongjun and Li, Qingwei, "Dynamic model and attitude control of flapping wing micro aerial vehicle", Robotics and Biomimetics (ROBIO), 2009 IEEE International Conference on, pages (451–456), 2009, publisher (IEEE organization)

[41] Pelletier, Alain and Mueller, Thomas J, "Low Reynolds number aerodynamics of low-aspect-ratio, thin/flat/cambered-plate wings", Journal of Aircraft, volume (37), Number(5), pages (825–832), 2000

[42] Calogero J, Frecker M, Wissa A, Hubbard JE. Optimization of a bend-twist-and-sweep compliant mechanism. InASME 2014 Conference on Smart Materials, Adaptive Structures and Intelligent Systems 2014 Sep 8 (pp. V002T06A004-V002T06A004). American Society of Mechanical Engineers

[43] Zhang, Zhen, Pu Xie, and Ou Ma. "Bio-inspired trajectory generation for UAV perching movement based on tau theory." International Journal of Advanced Robotic Systems 11, no. 9 (2014): 141

[44] Tummala, Yashwanth, Aimy Wissa, Mary Frecker, and James E. Hubbard. "Design and optimization of a contact-aided compliant mechanism for passive bending." Journal of Mechanisms and Robotics 6, no. 3 (2014): 031013.

[45] Liani, Evandro, Shijun Guo, and Giuliano Allegri. "Aeroelastic effect on flapping wing performance." In 48th AIAA/ASME/ASCE/AHS/ASC Structures, Structural Dynamics, and Materials Conference, p. 2412. 2007.

[46] Clemons, Lucas, Hirofumi Igarashi, and Hui Hu. "An experimental study of unsteady vortex structures in the wake of a piezoelectric flapping wing." In 48th AIAA aerospace sciences meeting including the new horizons forum and aerospace exposition, p. 1025. 2010.

[47] Lin, Che-Shu, Chyanbin Hwu, and Wen-Bin Young. "The thrust and lift of an ornithopter's membrane wings with simple flapping motion." Aerospace Science and Technology 10, no. 2 (2006): 111-119.

[48] Olson, D. H., Dmytro Silin, Motoyuki Aki, Creighton Murrieta, Jeremy Tyler, Anton Kochevar, Alex Jehle, and Sergey Shkarayev. "Wind tunnel testing and design of fixed and flapping wing micro air vehicles at the university of Arizona." International Micro Air Vehicle Competition, Seoul, South Korea (2005).

[49] Prempraneerach, P., F. S. Hover, and Michael S. Triantafyllou. "The effect of chordwise flexibility on the thrust and efficiency of a flapping foil." In Proc. 13th Int. Symp. on Unmanned Untethered Submersible Technology: special session on bioengineering research related to autonomous underwater vehicles, New Hampshire, vol. 152, pp. 152-170. 2003.

[50] Ebrahimi, Abbas, and Karim Mazaheri. "Aerodynamic Performance of the Flapping Wing." In Applied Aerodynamics. InTech, 2012.

[51] Shkarayev, Sergey, and Dmitro Silin. "Aerodynamics of flapping-wing micro air vehicles." In 47th AIAA Aerospace Sciences Meeting Including the New Horizons Forum and Aerospace Exposition, p. 878. 2009.

[52] Thomson, Scott, Christopher Mattson, Mark Colton, Stephen Harston, Daniel Carlson, and Mark Cutler. "Experiment-based optimization of flapping wing kinematics." In 47th AIAA Aerospace Sciences Meeting including The New Horizons Forum and Aerospace Exposition, p. 874. 2009.

[53] Warkentin, Jonathan, and James DeLaurier. "Experimental aerodynamic study of tandem flapping membrane wings." Journal of Aircraft 44, no. 5 (2007): 1653-1661

[54] Norizham, Abdul Razak, Jos Ignacio Rothkegel Ide, and Grigorios Dimitriadis. "Experiments on a 3-D flapping and pitching mechanical model." In Proceedings of the 2009 International Forum on Aeroelasticity and Structural Dynamics, pp. Paper-IFASD. Azimuth Corporation, 2009.

[55] Yafeng, Zhang, Li Zhanke, Song Wenping, and Song Bifeng. "Lift and thrust characteristics of the flapping wing micro air vehicle." In 27th International Congress of the Aeronautical Sciences. 2010.

[56] Jones, A. R., and H. Babinsky. "Unsteady lift generation on rotating wings at low Reynolds numbers." Journal of Aircraft 47, no. 3 (2010): 1013-1021.

[57] Kulfan, Brenda M., "A paleo-aerodynamic exploration of the evolution of nature's flyers, man's aircraft, and the needs and options for future technology innovations", Proceedings of the SPIE, Volume 7288, id. 728803 (2009). (SPIE Homepage)

[58] Pennycuick, C.J., "Modelling the Flying Bird", Elsevier: Amsterdam, The Netherlands, 2008.

[59] Hummel, D., "Aerodynamic investigations on tail effects in birds," Zeitschrift fr Flugwissenschaften und Weltraumforschung, 16, 159-168 (1992).

[60] Thomas, A. L. R. (1993). "On the aerodynamics of birds tails", Philos. Trans. R. Soc. Lond. B Biol. Sci. 340, 361-380.

[61] Maybury, W. J. and Rayner, J. M. V. (2001), "The avian tail reduces body parasite drag by controlling flow separation and vortex shedding", Proc. R. Soc. Lond. B Biol. Sci. 268, 1405-1410.

[62] Thomas, A. L. R. and Taylor, G. K. (2001), "Animal flight dynamics. I. Stability in gliding fight", J. Theor. Biol. 212, 399-424.

[63] M. Islam, M. R. Amin and Y. M. Shariff, Computational Analysis Of A High-Lift And Low Reynolds Number Airfoil At Turbulent Atmospheric Conditions, IMECE2009, Florida, USA.

[64] Turek, Stefan and Hron, Jaroslav, "Proposal for numerical benchmarking of fluid-structure interaction between an elastic object and laminar incompressible flow", Fluid-structure interaction, pages (371–385), 2006, publisher (Springer)

[65] Bisplinghoff R L, Ashley H, and Halfman R L 1996 Aeroelasticity (New York: Dover)

[66] Kamalluddien Parker, Julio Soria, Karl von Ellenrieder. 2006. Characteristics of the Vortex Street Behind a Finite Aspect-Ratio Flapping Wing. 44th AIAA Aerospace Sciences Meeting and Exhibit

[67] Abbott, I.H., and Doenhoff, A.E.V., "Theory of Wing Sections", Dover Publications, New York, (1959).

[68] Eleni, Douvi C., Tsavalos I. Athanasios, and Margaris P. Dionissios. "Evaluation of the turbulence models for the simulation of the flow over a National Advisory Committee for Aeronautics (NACA) 0012 airfoil." Journal of Mechanical Engineering Research 4.3 (2012): 100-111.

[69] Hanjalic, K., Launder, B. (1972). "A Reynolds stress model of turbulence and its application to thin shear flows". Journal of Fluid Mechanics.

[70] McMichael, J. M. and Francis, M. S., "Micro Air Vehicles - Toward a New Dimension in Flight", DARPA, USA, 1997

[71] Shariff Ammoo, Mohd and Dahalan, Md. Nizam, "Micro Air Vehicle: Technology Review and Design Study", Proceedings of the 1st Regional Conference on Vehicle Engineering & Technology, Kuala Lumpur, Malaysia, August, 2006

[72] Muller, D., Bruck, H.A. and Gupta, S.K. (2009) Measurement of Thrust and Lift Forces Associated with Drag of Compliant Flapping Wing for Micro Air Vehicles using a New Test Stand Design. Experimental Mechanics, 50, 725-735.

[73] Wissa, Aimy and Grauer, Jared and Guerreiro, Nelson and Hubbard Jr, James and Altenbuchner, Cornelia and Tummala, Yashwanth and Frecker, Mary and Roberts, Richard, "Free flight testing and performance evaluation of a passively morphing ornithopter", International Journal of Micro Air Vehicles, volume (7), Number(1), pages (21–40), 2015, publisher (SAGE Publications Sage UK: London, England)

[74] Nader, Gilder, Claudia Dos Santos, P. Jabardo, Monica Cardoso, N. Taira, and M. Pereira. "Characterization of low turbulence wind tunnel", In Proceedings of XVIII IMEKO World Congress, Rio De Janeiro, Brazil, pp. 17-22, (2006).

[75] Freels, James D., Isaac T. Bodey, Rao V. Arimilli, Franklin G. Curtis, Kivanc Ekici, and Prashant K. Jain. "Preliminary Multiphysics Analyses of HFIR LEU Fuel Conversion using COMSOL", ORNL/TM-2011/07, Oak Ridge National Laboratory (2011).